RADIANT SMOLDERING IGNITION OF PLYWOOD

By

Mark T. Gratkowski

A Thesis

Submitted to the Faculty

Of the

WORCESTER POLYTECHNIC INSTITUTE

In partial fulfillment of the requirements for the

Degree of Master of Science

In

Fire Protection Engineering

By

_____

August 2004

APPROVED:

_____

Professor Nicholas A. Dembsey, Major Advisor

_____

Dr. Craig L. Beyler, Co-Advisor
Hughes Associates, Inc.

_____

Dr. Kathy A. Notarianni, Head of Department

ABSTRACT

This paper investigates the thermal conditions at the surface and at depth of 1.8 cm (3/4-inch) maple plywood exposed to heat fluxes between 6 and 15 kW/m^2 in the cone calorimeter for up to 8 hours. The minimum heat flux for unpiloted smoldering ignition was 7.5 kW/m^2 and compared favorably to classical self-heating theory. The role of self-heating was explored via temperature measurements distributed within the specimens. Elevated subsurface temperature profiles indicated self-heating was an important ignition factor resulting in ignition at depth with smolder propagation to the surface and into the material. The ignition depth was shown to be a function of the heat flux with the depth moving towards the surface as the heat flux increased.

Supporting work included sensor calibration testing, mass loss rate analysis, char depth testing and computer modeling. The calibration testing showed optical pyrometer temperature measurements compare favorably to those of surface mounted thermocouples. Mass loss rate analysis was found to be a lagging indicator of smoldering ignition. The char depth tests showed that the rate of change of the temperatures recorded at depth increased around the time the derived char front passed. Computer modeling (HEATING) of a heat flux applied to the plywood for conditions similar to the performed ignition tests compared favorably to experimental data for sub-critical incident heat flux temperature profiles, excepting surface temperatures. For heat fluxes near critical, the model correctly predicted thermal runaway below the sample surface. At higher heat fluxes simulation results indicated surface ignition at times significantly earlier than experimental results.

ACKNOWLEDGEMENTS

I would like to thank two individuals and several organizations for their contributions in getting me to where I am today. The first is Dr. Craig Beyler of Hughes Associates, Inc. Craig provided the impetus for this original work as well as the day-to-day oversight and review. Our discussions of the theoretical and experimental results helped crystallize the direction of the thesis. The second person I wish to thank is my thesis advisor at WPI, Professor Nicholas Dembsey. He had the unenviable task of trying to understand my work as conveyed primarily through email correspondence. The fact that he was able to understand the work and provide valuable direction is a testament to his dedication to his students.

This research would not have been possible without the support of Hughes Associates, Inc., who provided financial support, testing facilities and invaluable technical resources. I would also extend thanks to WPI for providing a solid foundation in fire protection engineering, and allowing me to pursue this research opportunity and to apply it towards the requirements for graduation.

Finally, none of the above would have ever happened if not for the opportunity provided by the Nassau Bay Volunteer Fire Department in my old hometown of Nassau Bay, Texas. It was during my service with the NBVFD that I discovered the field of fire protection engineering, WPI and a new career.

TABLE OF CONTENTS

LIST OF FIGURES

Appendix A

Appendix B

Appendix C

Appendix D

Appendix E

Appendix F

Appendix G

Appendix H

LIST OF TABLES

Appendix A

Appendix B-H

DOCUMENT ORGANIZATION

The text of this document is divided into two sections. The first section briefly describes the contents of the appendices. The second section is an overview of the work performed and conclusions drawn.

GUIDE TO APPENDICES

Appendix A contains the manuscript for a paper to be submitted to a peer review journal. It is the distillation of the work covered by this text in whole. The other appendices provide supporting data and rough drafts of work that was removed from the paper. They are included for completeness and for potential use in future research.

Appendix A – Radiant Smoldering Ignition of Plywood

This appendix begins by setting the context for the investigation of radiant smoldering ignition of plywood. The current work is defined in relation to prior work. The experimental setup is described along with the criteria for determining if smoldering ignition occurred. From this the minimum heat flux for smoldering ignition was determined.

Existing self-heating theory in the current context is presented and applied. The predicted minimum heat flux is compared to the experimental results with good agreement.

Thermal profiles were investigated for insight into the ignition process. Ignition was shown to occur at depth with smoldering propagating towards the surface and through the sample. Depth of ignition location was shown to move from in depth towards the surface at higher heat fluxes.

Appendix B – Time-Temperature Profiles

This appendix presents the time-temperature history for each of the specimen. A description of the noise reductions techniques is included.

Appendix C – Time-Rate of Change Profiles

This appendix presents the time-rate of temperature change history for each of the specimen. A description of the data processing and noise reductions techniques is included.

Appendix D – Ignition Thermal Profiles

This appendix presents the temperature profiles through the thickness of the specimen for select times and conditions. The non-dimensional temperature excess for the same select times and conditions is also presented. Representative average profiles for each heat flux as well as individual specimen profiles are included.

Appendix E – Mass Loss Rate Analysis

This appendix is a rough draft of the mass loss rate testing performed. Analysis techniques and results are presented along with comparison to literature data.

Appendix F – Char Depth Analysis

This appendix is a rough draft of the char depth testing performed. Test procedures, analysis techniques and results are presented. Char depth results were compared to in-depth temperature measurements for similar heat flux exposures.

Appendix G – Calibration Tests

This appendix presents the rough draft of testing methods and results for comparison of optical pyrometer temperature data to thermocouple data. Additional tests showed the variability of the heating of the wood surface with position and between samples.

Appendix H – Computer Modeling with HEATING

The computer model HEATING [1] was used to model the heating of wood samples subjected to a uniform heat flux similar to that from the cone calorimeter. A rough draft of the development of the model inputs is presented along with the results for sub-critical, near critical and super-critical heat flux exposures.

THESIS OVERVIEW

Self-heating theory has been applied to a wide range of smoldering ignition [2] scenarios including elevated ambient temperature piles, hot surface conduction, radiant exposure and hot spot ignition within a pile. While there has been extensive experimental study of self-heating for piles exposed to an elevated temperature, there are very few experimental studies of other applications of self-heating theory. The smoldering ignition of three quarter inch (1.8 cm) maple plywood from self-heating as a result of exposure to a low level radiant flux was investigated.

A review of literature showed that there has been little research performed on low heat flux radiant smoldering ignition of wood products at time scales above tens of minutes.

Plywood samples were instrumented with thermocouples mounted at several depths. Care was taken to ensure thermocouples were mounted at the correct depths. The samples were then tested at heat fluxes between 6 and 15 kW/m^2 for periods up to eight hours in a cone calorimeter [3]. Four criteria were established for determining if smoldering ignition occurred. They include: 1) observed glowing of the sample, 2) presence of elevated temperatures over 400 °C either at the surface or at depth, 3) evidence of a smolder propagation wave and 4) post-test observation of decomposition of the sample and residual white ash. From these criteria, the minimum heat flux to ignite the samples was determined.

Existing self-heating theory was investigated for application to plywood samples exposed to a heat flux in the cone calorimeter. An approach used by Bowes [2] was found that allowed the transient ignition of a cellulosic material to be analyzed through a

two-step steady state approach. The first step utilizes a self-heating theory model of a slab exposed to a high temperature on only one face. From this theory, the temperature at the hot face may be determined that would be sufficient to lead to a runaway self-heating reaction within the material. The second step is to determine the incident heat flux that raises the surface temperature of a non-reactive slab to the previously determined critical surface temperature for the runaway self-heating reaction. A simple energy balance at the sample surface determines this heat flux. The predicted surface temperatures and minimum heat flux was compared to experimental results.

Evaluation of the thermal conditions leading up to ignition provided insight into the behavior of plywood subject to radiant heat. The changes in the thermal profiles over time showed the dynamic nature of the ignition process. Three significant events were identified during analysis. They were the time to self-heating becoming the predominant heating mechanism within the sample, the time at which the temperatures at a depth below the surface surpassed the temperatures at the surface and the time of observed glowing either at the surface or within a crack. From analysis of these events, the ignition was shown to have occurred at a depth dependent on the applied heat flux.

The remainder of the work performed included calibration tests, mass loss rate analysis, char depth analysis and computer modeling of the heating of the samples up to the point of ignition. Calibration tests were performed to show that optical pyrometer data might properly be compared to thermocouple data. The calibration tests also showed the variability of the surface-heating rate of the wood samples. The mass loss rate analysis was performed to determine if mass loss rate was a viable method of determining if and when ignition occurred. Char depth analysis was performed for a series of samples

subjected to a 9 kW/m^2 heat flux for set periods of time to link the progression of char formation with the changes in the temperatures within the sample. The results were to be analyzed for use in computer modeling. The computer model HEATING [1] was used to simulate the heating of the plywood samples. Self-heating of the wood was approximated with an Arrhenius type reaction dependent on temperature. Several literature values of the kinetic parameters were employed with limited success [2,4].

CONCLUSIONS

The unpiloted response of 1.8 cm maple plywood to radiant heat fluxes from 6 to 15 kW/m^2 in the cone calorimeter was investigated. The minimum heat flux for smoldering ignition was determined to be 7.5 kW/m^2 and compared favorably to a predicted minimum heat flux of 7.2 kW/m^2.

As expected, times to significant thermal events (minimum heating rate, subsurface temperature crossover and observed glowing) decreased with higher applied heat fluxes. The times ranged from several hundred seconds to many thousands of seconds. The minimum heating rate increased from zero for low heat flux inert heating to 0.23 °C/sec at 15 kW/m^2, the highest heat flux applied.

Evaluation of the thermal profiles showed that self-heating becomes an important mechanism for ignition as the incident heat flux decreases to a critical minimum. Ignition occurs below the surface and smolder propagates from the ignition depth towards the surface and into the specimen. The ignition depth was shown to vary with the applied heat flux. At high heat fluxes, ignition occurs at or near the surface. As the applied heat flux approaches the minimum for smoldering ignition, the ignition location was shown to move between 31 and 50% into the depth of the wood.

Calibration tests showed that while individual thermocouples do not necessarily match each other, across the surface the average temperatures match those of the optical pyrometer.

Mass loss rate tests showed that the difference in mass loss rates was an order of magnitude between the 8 and 15 kW/m^2 tests even though exposure at both heat fluxes resulted in smoldering. The largest peak-burning rate achieved in the smoldering ignition tests was 4.5 g/m^2s for specimen#14 exposed to a heat flux of 15 kW/m^2. By comparison, flaming burning rates of 13 g/m^2s for wood was found in the literature [5]. Due to the large differences with respect to heat flux and the lagging nature of the quantity, mass loss rate does not provide a useful tool for determining smolder initiation.

The char depth tests showed that the rate of change of the temperatures recorded at depth increased around the time the derived char front passed. Thus the increased thermal behavior at depth at these times was attributable to the char front. Between the three ignition tests, the derived char front temperatures compared favorably.

HEATING simulation results compared favorably to experimental data for sub-critical incident heat flux temperature profiles, excepting surface temperatures. Simulation results also compared favorably to theoretical predictions of critical incident heat fluxes. At the lower heat flux, 9 kW/m^2, the simulations qualitatively matched experimental data in showing sub-surface temperatures exceeding surface temperatures during thermal runaway, indicating smolder initiates below the surface. As expected, thermal runaway initiates at the surface at higher heat fluxes. One area the simulations did not compare favorably with experimental results was for times to elevated

temperatures as an indication of smolder initiation for super-critical incident heat fluxes. The simulation times were significantly shorter than observed in experimental data.

REFERENCES

[1] Childs, K.W., "HEATING 7: Multidimensional, Finite-Difference Heat Conduction Analysis Code System, Versions 7.2i and 7.3," RSICC Report PSR-199, Oak Ridge National Laboratory, Oak Ridge, Tennessee, 1998.

[2] Bowes, P.C., Self-heating: Evaluating and Controlling the Hazard, Her Majesty's Stationery Office, London, 1984.

[3] "ASTM E 1354-02: Standard Test Method for Heat and Visible Smoke Release rates for Materials and Products Using an Oxygen Consumption Calorimeter," ASTM International, West Conshohocken, PA, 2002.

[4] Chong, L.V., Shaw, I.R, and Chen, X.D., "Thermal Ignition Kinetics of Wood Sawdust Measured by a Newly Devised Experimental Technique," Process Safety Progress, Vol. 14, No. 4, 1995.

[5] Cuzzillo, B.R., "Pyrophoria," (PhD Dissertation), University of California at Berkeley, Berkeley, CA, 1997.

APPENDIX A – RADIANT SMOLDERING IGNITION OF PLYWOOD

Introduction

Wood and wood products are subject to self-heating that may lead to smoldering combustion. Self-heating theory has been applied to a wide range of smoldering ignition scenarios [1] including elevated ambient temperature piles, hot surface conduction, radiant exposure and hot spot ignition within a pile. While there has been extensive experimental study of self-heating for piles exposed to an elevated temperature, there are very few experimental studies of other applications of self-heating theory.

This work aims to improve the practical and scientific understanding of self-heating leading to smoldering ignition of plywood, a common building material. To achieve this goal, cone calorimeter testing of thermally intermediate three-quarter inch (18 mm) maple plywood was performed. In the context of existing self-heating theory, an experimentally determined minimum incident heat flux was compared to the predicted minimum heat flux as applied to non-symmetrical radiant self-heating of wood. Thermal profiles across the depth of the wood samples were analyzed for estimation of the location of smoldering ignition below the sample surface.

Background

Reports of scientific investigation of conditions leading to ignition did not appear until the late 19th century [2]. Most of these early studies concentrated on ignition in an elevated temperature environment while a few investigated ignition with an ignition pilot present [2]. In 1960, Moran published a study of ignition of wood from a radiant heat source [2]. Since then, a small number of additional reports on ignition of wood from radiant sources have been published investigating a wide range of external influences and

wood conditions. Based on the early radiant ignition tests, in 1965 McGuire suggested 12.5 kW/m^2 as a minimum heat flux for ignition of wood [2]. This value was subsequently adopted for design purposed in many countries [2]. This value is consistent with data from experiments utilizing an ignition pilot and times of exposure from 10 to 20 minutes. Limiting of exposure time artificially inflates the minimum heat flux for ignition.

In order to determine the minimum heat flux for ignition, the ignition event needs to be defined. Babrasukas [2]. suggests ignition occurs in one of three ways: glowing, glowing to flaming or direct flaming. With respect to radiant heating, the conditions that lead to the three modes may primarily be identified as the level of the applied heat flux and the presence of an ignition pilot. In their summary, Smith and King [3] gave a good overview of the different ways wood may ignite when subjected to a radiant heat flux. The use of "very high" to "very low" to describe heat fluxes are used as aids to describe relative levels of heating and do not imply any specific ranges.

At very high heat fluxes, the wood surface pyrolyzes near instantly with the vapors igniting in flame. No pilot is necessary as the evolved gasses are sufficiently hot to support auto-ignition. At high heat fluxes, the ignition process is slower in that the surface will char before the pyrolyzates auto-ignite. At medium heat fluxes, a pilot may be required for flaming ignition. If one is not present, oxidation of the char results in glowing ignition. Glowing char may at sufficiently high temperature ignite gasses if evolved in sufficient quantities. In effect, the glowing char may act as a pilot. This is the glowing to flaming ignition identified by Babrauskas [2]. At very low heat fluxes, initial heating from a radiant source increases the surface temperature towards equilibrium

between heat gained from the radiant source and heat lost to the environment and wood interior. This is classic inert slab heating and ignition does not occur. If the equilibrium temperature is high enough, charring will occur. The charred wood may reach a new equilibrium temperature and self-heating may occur. At low heat flux, the heat flux alone is sufficient to char the surface and to heat the interior to the point that self-heating becomes significant and may lead to glowing ignition.

Martin [4] used data from a large number of experiments on spontaneous ignition of radiantly heated cellulosic solids to identify the controlling mechanisms for the paths to ignition. He developed a map, figure 1, to describe three different ignition regimes with respect to the absorbed exposure irradiance (i_o), time of exposure (t) and pertinent physical properties of the specimen; thickness (l), conductivity (K_s) , density (ρ_s) and specific heat (C_s) . The three regimes are convection, diffusion and ablation controlled ignition and may generally be considered to progress from low heat fluxes (convection controlled) to high heat fluxes (ablation controlled). Martin identified the convection control regime as being dominated by heat losses to the environment. He identified this regime as primarily relevant to cellulosic materials thin enough (or exposed to a sufficiently weak heat flux) to be considered thermally thin (i.e. to exhibit no appreciable thermal gradient through the thickness of the sample). Ignition in the diffusion-controlled regime is dependent on the diffusion of heat into the material. For the ablation-controlled regime, the surface of the material ignites prior to substantial transfer of heat to the interior. The X-axis is the intensity of the radiant flux normalized by the characteristic conduction. It is a measure of the ability of radiant heat to pass through the material. The Y-axis is the nondimensionalized radiant exposure and provides an insight

into the influence of both heat flux and time of exposure for the ignition problem. Martin identified that radiant heating of cellulosic materials in the absence of a pilot source may result in smoldering, persistent flaming or transient flaming, depending upon the incident heat flux, the sample thermal properties, and the sample thickness.

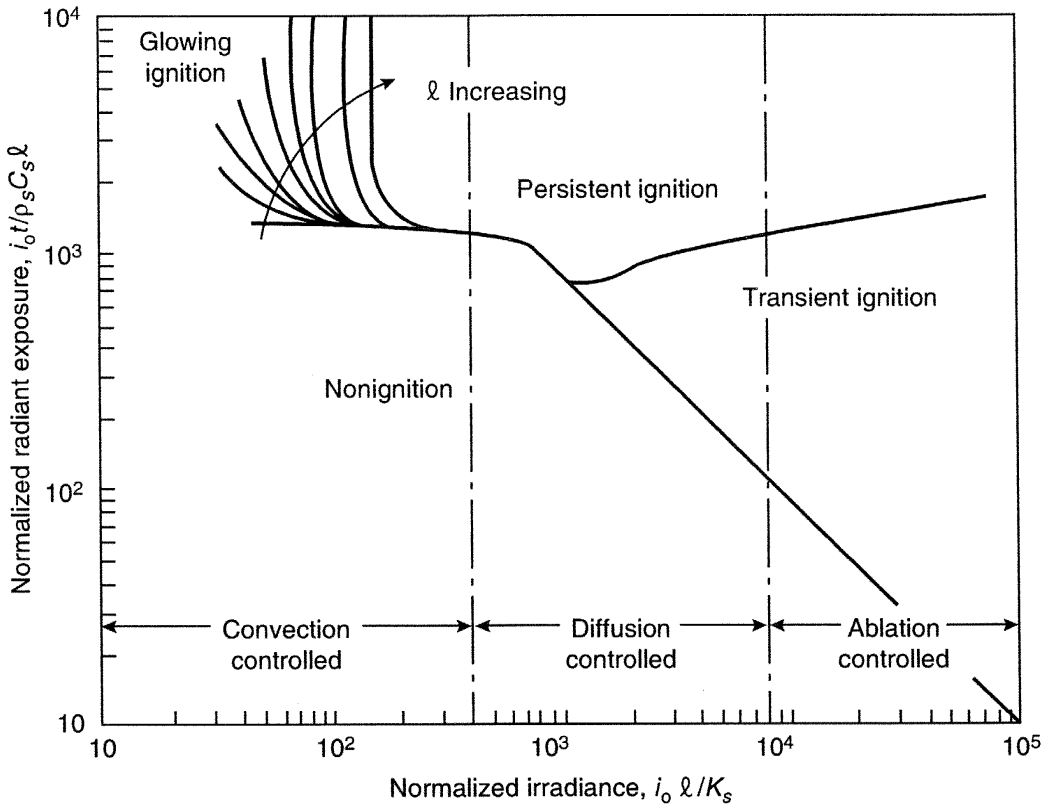

Figure 1 – Martin's map, illustrating ignition behavior regimes of cellulose, with areas controlled by convective cooling, diffusion of heat into the solid, and ablation of the exposed surface [5].

A survey of radiant heating ignition studies allowed placement of the ignition results in the context of the identified ignition regimes. Seven studies investigating radiant non-piloted ignition of wood were identified.

Moran [6] published the initial study of the ignition of wood from radiant heat in 1960. He studied 6.4 mm thick specimen of ponderosa pine in a vertical orientation. The specimens were subjected to 25-29 kW/m^2 heat fluxes from an electric radiant heater.

Surface temperatures at ignition ranged from 255-301 °C. With a maximum test length of 9 minutes, he reported 25 kW/m^2 as the minimum heat flux for ignition. Ignition started in a glowing mode.

In 1964, Shoub and Bender [7] tested 13 mm thick specimen of plywood subjected to an electric radiant panel providing a 4.3 kW/m^2 heat flux to the center of the specimen. They reported ignition of the vertically oriented plywood after 5.2 hours at a surface temperature of 254 °C. The actual incident heat flux used in the testing is questionable. Based on the available technology of the early 1960's (i.e. the expense and limited availability of temperature controllers for heating apparatus), it is likely that the close proximity of the radiant panel to the specimen resulted in a radiation feedback mechanism leading to a higher incident heat flux than initially provided by the heater alone. As such, the reported incident heat flux is not reliable, though the measured surface temperature at ignition and the time to ignition are likely reliable.

Koohyar, 1967, [8,9,10] utilized a gas-fired curtain of flame to study auto-ignition of several species of oven-dried wood of thickness ranging 12-19 mm (0.5-0.75 in). Adjusting the distance of the burners from the vertically oriented specimen varied the incident heat flux from 32-35 kW/m^2. Two-step glowing to flaming ignition was reported over this range. An average flaming ignition temperature of 402 °C was obtained from a radiometer (optical pyrometer) with a spot size of 81 mm^2 (0.125 in^2).

Smith and King (1970) tested 19 mm (0.75 in) thick Ponderosa Pine in a vertical orientation with a quartz lamp as the radiant heat source [3]. The pine was subjected to heat fluxes between 63-94 kW/m^2. Reported flaming auto-ignition temperatures of 424-543 °C, and flaming auto-ignition times of 72-25 seconds, were reported. Surface

temperatures were measured with an optical pyrometer with a spot size about 3 mm x 3 mm (0.125 in x 0.125 in).

Bilbao, et al. [11] utilized a cone calorimeter (ASTM E1354) to investigate the effects of air velocity on ignition of wood in a horizontal orientation. In still air, they subjected 19 mm (0.75 in) *Pinus Pinaster*, more commonly known as maritime pine, to heat fluxes between 24-54 kW/m^2. They identified the time to smolder as the time to surface glowing while time to ignition was defined as time to flaming. At 24 and 31 kW/m^2, the time to smolder was 110 and 13 seconds. Transition to flaming was observed at 737 and 30 seconds, respectively. Smoldering was not observed for higher fluxes. Instead, direct flaming ignition was noted in 15 seconds at 41 kW/m^2, 11 seconds at 44 kW/m^2 and 16 seconds at 54 kW/m^2.

Spearpoint [12,13] examined the minimum heat flux for piloted ignition of several wood species in the cone calorimeter. Specimens were 50 mm thick and placed in a horizontal orientation. He observed glowing ignition prior to flaming ignition for specimen subjected to heat fluxes less than 10 kW/m^2. Only limited data was reported. For maple exposed to 12 kW/m^2, the time for glowing ignition was about an hour and piloted flaming ignition occurred 10 minutes later. Surface temperatures at the time of glowing ignition were not reported.

Boonmee and Quintiere [14] studied glowing and flaming ignition of wood in a vertical orientation when exposed to a radiant flux either along the grain or perpendicular to the grain using a cone calorimeter. Above 40 kW/m^2, flaming auto-ignition was observed, while below 40 kW/m^2, glowing was observed first. From the data, they derived a critical heat flux for glowing ignition of 11 kW/m^2.

From the above seven studies, the heat fluxes as they pertain to the ignition regimes may be characterized. Wood samples exposed to heat fluxes below 40 kW/m^2 exhibited the two-step glowing-flaming ignition indicative of the diffusion-controlled regime. At higher heat fluxes above 40 kW/m^2, diffusion-controlled flaming ignition transitioned to ablation-controlled ignition. With the exception of the limited low heat flux data from Spearpoint and Shoub and Bender, none of the studies provide insight into the smoldering ignition potential of wood. By subjecting maple plywood samples to low intensity heat fluxes, this work provides insight into the smoldering ignition potential of wood.

Cone Calorimeter Testing

The cone calorimeter (ASTM E1354) is a widely used and accepted apparatus that provides an adjustable heat flux to 10 by 10 cm material samples in a horizontal orientation. While the conical heat source does not provide an ideal uniform heat source, Babrauskas [15] has shown that it does provide an average of +/-2% across the entire specimen. ASTM E 1354 [16], specifies a uniform irradiance of +/-2% within the central 5 by 5 cm area of the specimen.

Three-quarter inch maple plywood (1.8 cm, actual) was cut into ASTM E 1354 [16] standard 10 cm square samples. The plywood consists of five ply, 0.34 cm each, with top and bottom veneer with a thickness of 0.05 cm. Due to storage in the climate-controlled environment of the cone testing room (~50% RH and 20C), the moisture content of the samples fell below 4.8%, the lower limit of the available moisture-measuring device.

Type-K, Teflon/Neoflon PFA coated thermocouple wires, 30-AWG, were attached both to the surface and embedded within the sample at various depths. The clear outer sheathing insulation was removed from the thermocouples prior to installation. The

prepared samples were wrapped with aluminum foil to slightly over the top surface and placed upon a ceramic fiber blanket within a horizontal stainless steel holder as specified in ASTM E 1354. Figure 2 is a representative installation used for early heating uniformity scoping tests. A double application of wood glue was used to attach the surface thermocouples. The beads were tapped into the surface of the sample till flush after the glue set.

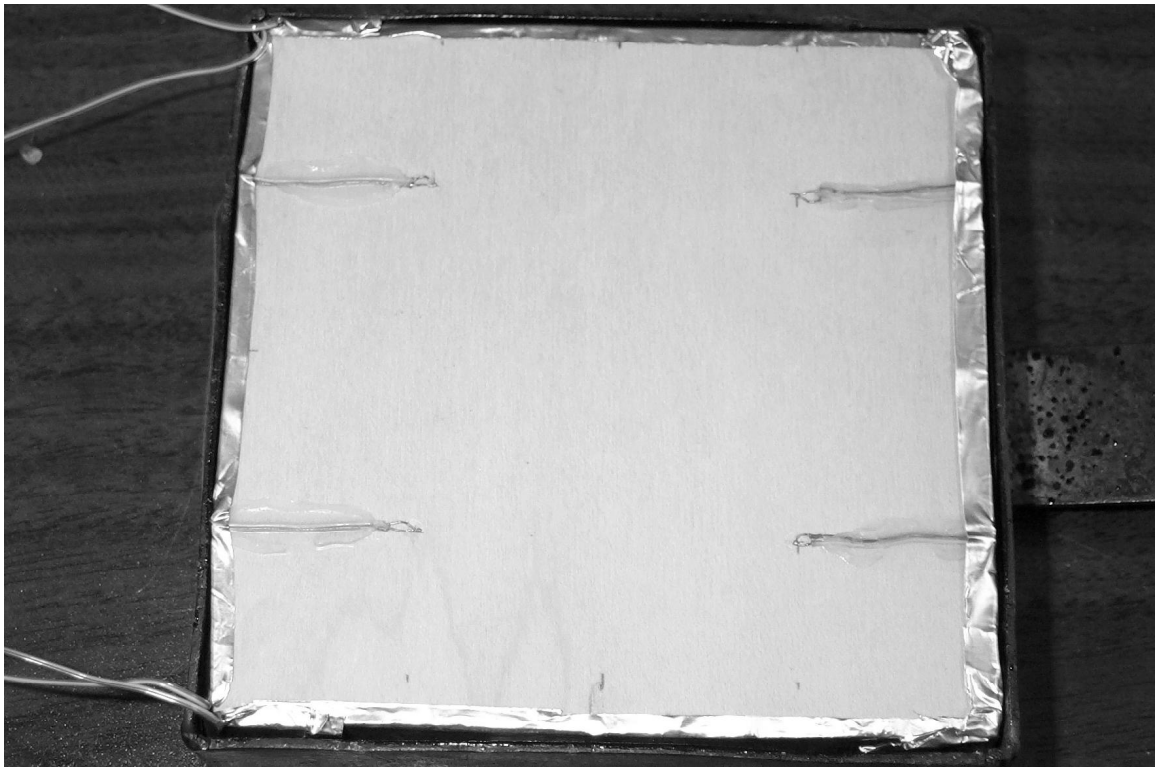

Figure 2 –Maple plywood sample (10 cm x 10 cm x 1.8 cm thick) from early heating uniformity scoping tests, wrapped with aluminum foil and placed in stainless steel holder per ASTM E1354. Thermocouples are glued down and the bead tapped into the surface.

Thermocouple leads were run along the sides of the sample to help alleviate heat losses from the sample to the holder sides by limiting conduction due to direct contact of the wood sample to the steel holder. The ceramic fiber blanket placed between the

bottom of the wood sample and the holder both limits heat transfer out the bottom of the sample and raises the sample top surface to the height of the lip of the holder.

Wood is an anisotropic material and plywood is a composite fabrication with grain direction changing 90 degrees with each layer. The rate of heating of any body is in part a function of its density. Measured density between samples ranged from 510 to 550 kg/m^3 with 520 kg/m^3 being typical. All samples were cut from the same sheet of maple plywood.

Due to wood sample variations and the limits of heat flux uniformity expected from the cone calorimeter, it is important to provide adequate opportunity to record the temperature across as much of the central area of the sample as possible. For smoldering ignition testing, all thermocouples were installed 3.5 cm in from the sample edge and 1 cm off the centerline. Figures 3 and 4 are an isometric view and top view of typical thermocouple locations. Two thermocouples are located diagonally across from each other at the surface and at each depth below the surface. These locations are distributed within the 5 by 5 cm central area and do not overlap one another. This ensures that thermocouples embedded at shallower depths do not interfere with the heat flow and thus temperature measurements of lower thermocouples. Locations 9 and 10 were only used for a few tests near the end of the test suite and were installed 3.5 cm in from the edge along the sample centerline.

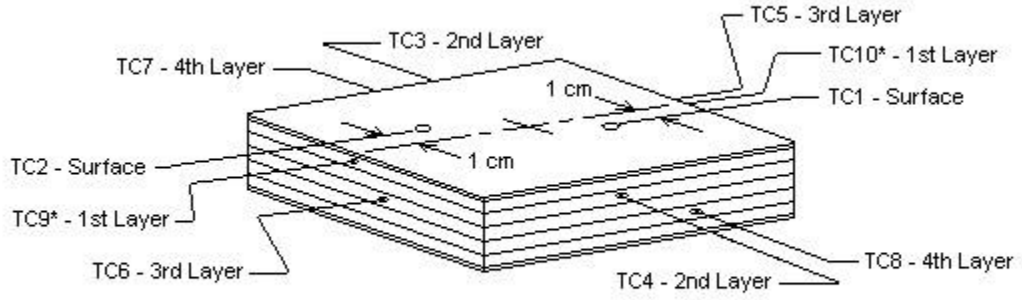

Figure 3 – Typical thermocouple locations for smoldering of 10 x 10 x 1.8 cm maple plywood samples. * - TCs 9 and 10 were only used in a single test at the end of the series.

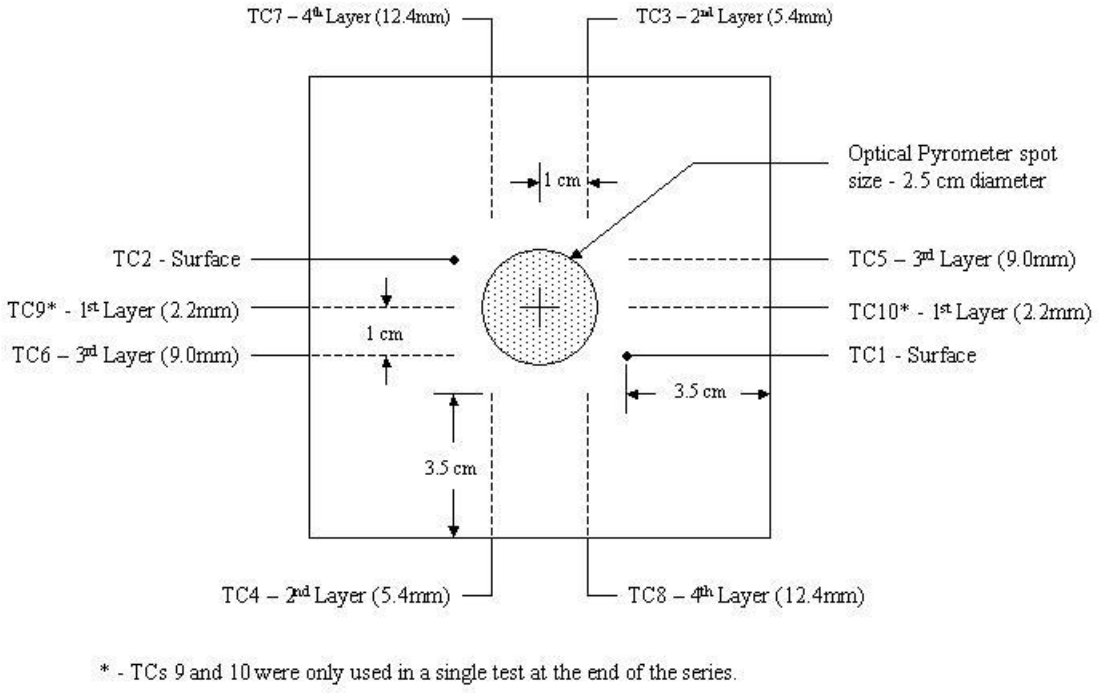

Figure 4 – Top view of typical thermocouple locations for smoldering ignition tests of 10 cm x 10 cm x 1.8 cm thick maple plywood samples. Values in parentheses indicate nominal depth of thermocouple below sample surface.

A 0.117 cm (0.046 inch) diameter drill bit in a drill press was used to drill the mounting holes for the embedded thermocouples. The length of the bit exposed from the chuck was carefully measured to ensure holes were drilled to the correct length. To test the uncertainty in depth from the sample surface, holes were drilled 3.5 cm into wood samples. Dissection and measurement of these samples showed that the drill bit tip deviated less than 5% from the intended depth from the surface. To reduce the effects of the drilled out cavity with respect to gas flow, the holes were drilled parallel to the wood grain and a dab of wood glue was applied at the top of the hole to seal the thermocouple. Prior to application of glue, the thermocouples were pushed into the holes till the bead was firmly pressed against the wood at the bottom of the hole. This ensured good thermal contact with the wood for accurate temperature measurements. Lining up a mark 3.5 cm from the end of the thermocouple with the entrance of the hole provided another indication of proper installation. This ensured that the resistance to further insertion of the thermocouple within the hole was due to the thermocouple reaching the bottom and not being hung up at a tight spot before the bottom. Thermocouples were also installed between the back face of the sample and the ceramic fiber blanket for some tests.

Other measurement equipment included a load cell to measure mass loss rate data and an optical pyrometer, used in conjunction with surface mounted thermocouples, to provide an additional measurement of the surface temperature. The optical pyrometer was a Wahl Model HSM-401H infrared heat detector (optical pyrometer) mounted coaxially with and looking down through the center of the cone heating element. It was set to an emissivity of 0.96, corresponding to the literature value for charred wood [2]. The target spot diameter was 2.5 cm.

Cone Calorimeter Test Procedures

The following procedures were used for each of the tests in the cone calorimeter. Prepared samples were weighed before being placed in the steel sample holder. Thermocouple leads were attached to the data acquisition system and the optical pyrometer and load cell were turned on.

The cone heating coil was set to the temperature corresponding to the desired heat flux and allowed to reach a steady output. The desired heat flux was verified by a heat flux gauge positioned at the center of the test area at a distance of 2.54 cm (1 inch) below the base of the conical heating coil. This is the location of the sample surface when placed in the apparatus. The cone controller maintained the set temperature within +/-2 °C resulting in an uncertainty of the heat flux of less than 2 percent.

Data acquisition was started and allowed to gather data for 30 seconds in order to verify the equipment and thermocouples were working. At 30 seconds, the sample was placed in the apparatus in the horizontal orientation. Due to the prolonged exposure times at low heat fluxes, tens of minutes to hours, shielding the sample surface from the heat flux for the second or two required to place it in the apparatus was deemed unnecessary.

Tests proceeded till either smoldering followed by signs of burnout occurred or eight hours passed. Three main physical observations were recorded during tests: char formation, surface cracking and glowing.

Blackening of the surface is the physical manifestation of the change from virgin wood to char. This corresponds to an increase in the surface emissivity to near unity [2]. The lower the incident heat flux, the more gradual the change in surface appearance. The

determination of time of char formation was a judgment of the observer. Due to the anisotropic nature of wood and the imperfect uniformity of the heat flux from the cone, samples did not blacken evenly over the surface over time. Therefore, to reduce the uncertainty in quantifying the observation, a 90% blackening of the surface was used to determine the time when char had formed. The 10% of non-charred surface was always around the edges of the sample.

Cracking of the surface occurs as the wood/char structure breaks down and shrinks due to pyrolysis. This allows air to penetrate to the interior and leads to conditions conducive to smoldering combustion. The time and location of initial cracks and further propagation were recorded.

Glowing is a visible indication of smolder. After cracks were observed, the room lights were turned off to provide a suitably dark environment for the observation of glowing. Glowing appeared in several different locations, along the edges of cracks, on the flat surfaces between cracks or deep within the crevices of a crack. Glowing along the edges of a crack was usually a point source and often transitory while glowing on the flat surfaces or within cracks was more likely to be area affects and persistent. The time, location and type of glowing were recorded as well as any growth in the areas affected over time.

Prior to smolder testing, a series of scoping tests were run utilizing both the optical pyrometer and thermocouples mounted to the sample surface. First, results of these tests showed the optical pyrometer temperature data was comparable to the thermocouple data. Second, they showed the variability of the heating of the wood surface with position and between samples. While individual thermocouples did not necessarily match each other,

across the surface the average temperatures matched those of the optical pyrometer. This is reasonable as thermocouples provide point source measurements while the optical pyrometer is an area-based measurement device. This also shows that the heat flux from the cone calorimeter to the sample is of sufficient uniformity for a one-dimensional conduction approximation through the plywood.

Minimum Heat Flux for Smoldering Ignition

To determine the minimum heat flux necessary for smoldering ignition, the plywood samples were subjected to heat fluxes between 6 and 15 kW/m^2 in the cone calorimeter for up to 8 hours. Samples were prepared according to the procedures in section 2.1 and tests were conducted per the procedures in section 2.2. No less than two samples were tested at each heat flux. To assess whether a sample smoldered, four different criteria were examined; 1) observed glowing from the sample, 2) presence of elevated temperatures over 400 °C either at the surface or at depth, 3) evidence of a smolder propagation wave and 4) post-test observation of decomposition of the sample and residual white ash.

Traditionally, glowing has been the outward sign of a smoldering fire [17]. Babrauskas [2] indicates that when a smoldering material attains sufficiently high temperatures glowing occurs. Because it is a readily observable phenomenon, glowing has been a widely reported criterion for ignition [2,6,8,9,10,11,12,13,14]. Samples tested at 9 to 15 kW/m^2 achieved glowing combustion. Glowing was also observed for one of the two tests at 8 kW/m^2, Test #19. Glowing was not observed for any samples exposed to 6 or 7 kW/m^2 for the testing limit of eight hours.

The average reported ignition temperature for both piloted and auto ignition of wood by radiant heating is 400 °C [18]. Therefore, recorded thermocouple or optical pyrometer temperatures in excess of 400 °C were considered indications of smolder. This condition was met for samples exposed to 8 kW/m^2 and above. Peak temperatures at 6 and 7 kW/m^2 were 240 and 285 °C, respectively. Figures 5 and 6 illustrate the difference in thermal response between smoldering ignition and no ignition. Specimen#19, exposed to an 8 kW/m^2 heat flux achieved quasi-steady state thermal conditions around an hour into the test. About two hours into the test, temperatures throughout the sample began to increase again past the 400 °C temperature criterion. Similarly, Specimen#23, exposed to a 7 kW/m^2 heat flux achieved steady state thermal condition around an hour into the test. However temperatures only rose an additional 30 °C at around 5.5 hours with subsequent subsiding before the end of the test. This indicated that self-heating occurred but not to the extent required for a thermal runaway condition and smoldering ignition. A specimen exposed to a 6 kW/m^2 heat flux heated as an inert slab with an initial increase in temperature to steady-state thermal conditions. No further temperature increases during the 8 hour test indicated self-heating did not occur at any appreciable level. Appendix B presents the time-temperature curves for all the tests with temperatures presented as moving average temperatures over the indicated time spans. A complete description of the legends is presented at the beginning of the appendix.

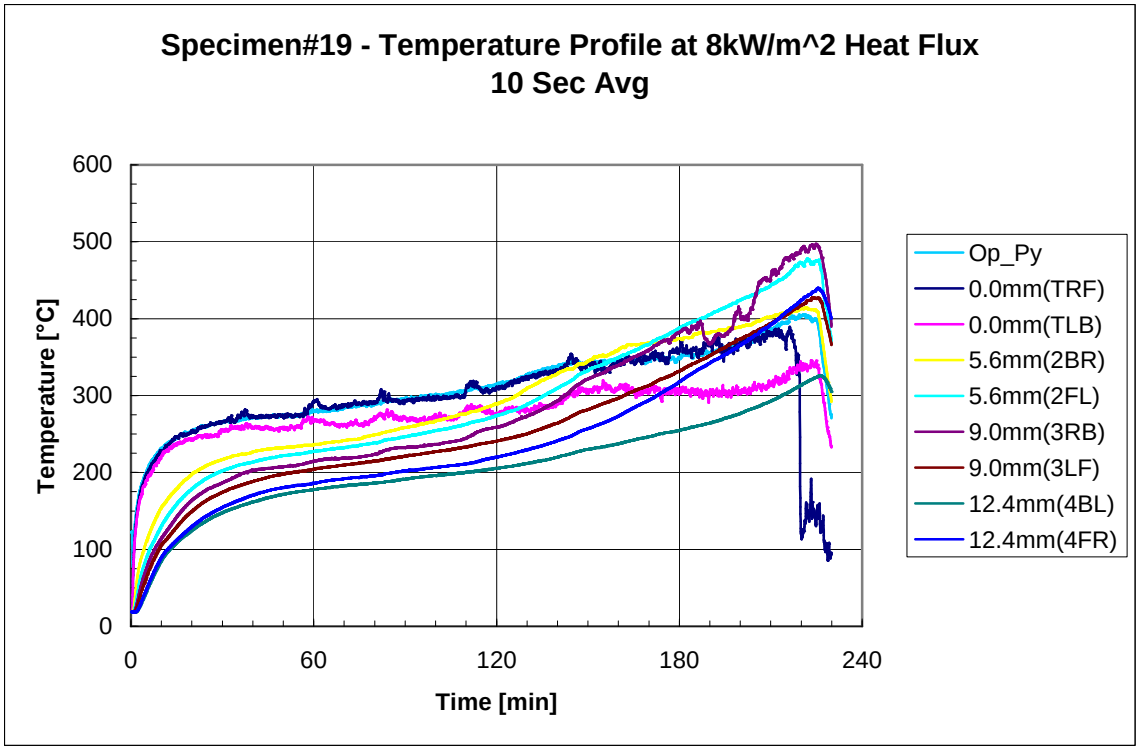

Figure 5 – Specimen#19 time-temperature curve for optical pyrometer and thermocouples installed at the indicated depths below the surface. Ignition during exposure to 8 kW/m^2 heat flux in the cone calorimeter.

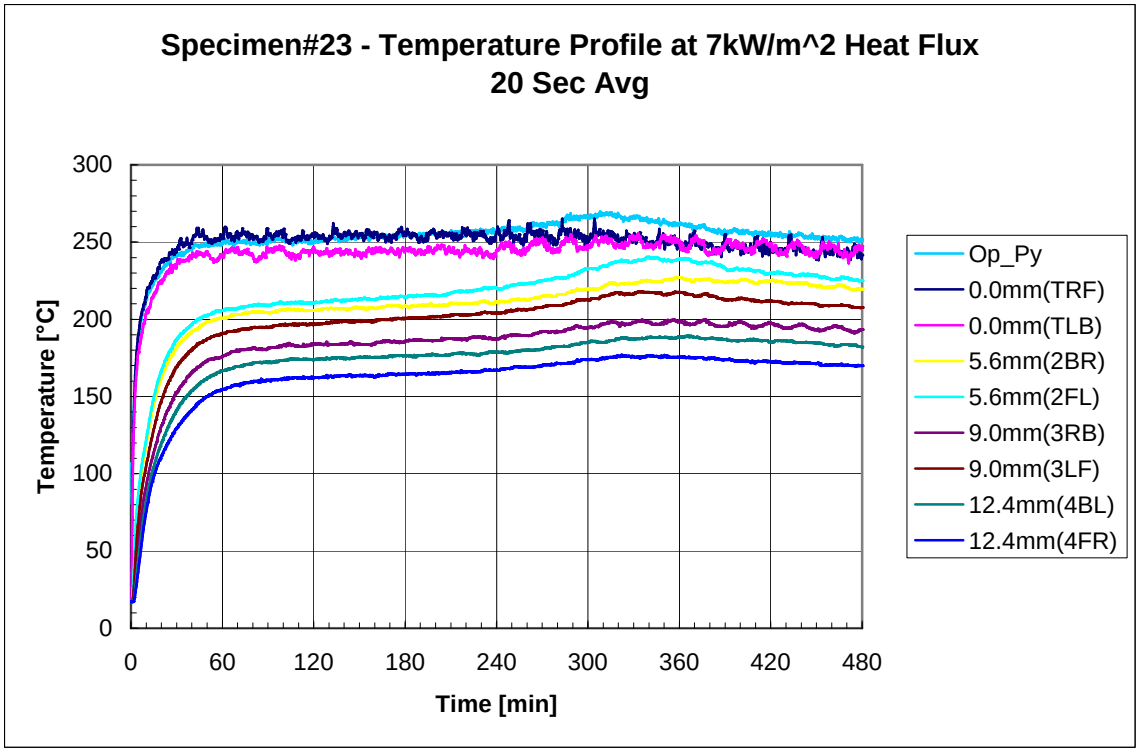

Figure 6 – Specimen#23 time-temperature curve for optical pyrometer and thermocouples installed at the indicated depths below the surface. No ignition after exposure to 7 kW/m^2 heat flux for 8 hours in the cone calorimeter.

The third criterion was smolder propagation. In general, ignition occurs at a single location at depth resulting in locally elevated temperatures. From this initial point, smolder propagates as a wave through the material. For the wood samples in the cone calorimeter, the propagation wave traveled across the depth, either up towards the surface, down towards the back face or in both directions, depending on the depth at which ignition occurs. This behavior was noted when thermocouple temperatures at succeeding depths increased to the point of exceeding those of the previous depth. Figure 7 is time temperature profile for specimen#22, exposed to 9 kW/m^2 heat flux and is a representative example of this behavior. The thermocouples mounted at a depth of 5.6 mm below the surface exceeded the surface temperatures approximately 80 minutes into the test. Approximately 30 minutes later, the first of the 9.0 mm depth thermocouples

exceeded the surface temperature. At around 150 minutes, these same thermocouples surpassed the 5.6 mm thermocouple temperatures. By the end of the test, 3 hours, the temperatures of the 12.4 mm depth thermocouples exceeded those of all thermocouples above them. This behavior was indicative of a smolder propagation wave moving down through the specimen. Similar behavior was captured in the thermocouple data for all specimen exposed to heat fluxes of 8 kW/m^2 and above.

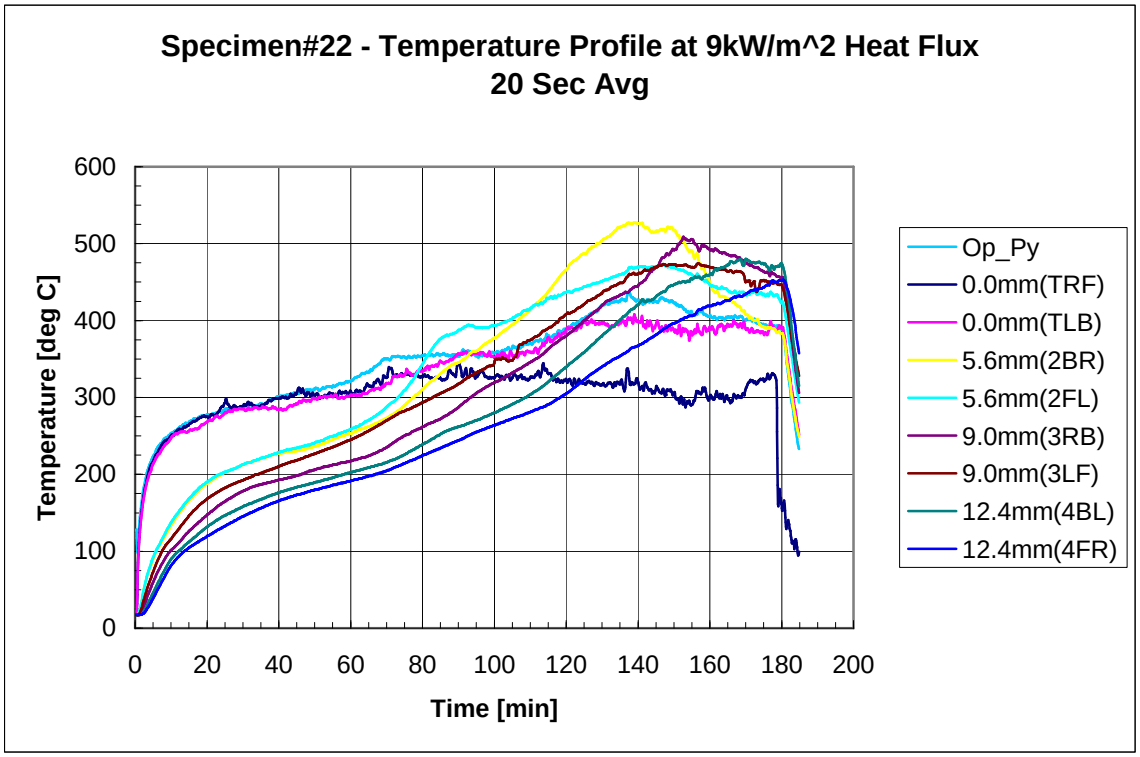

Figure 7 – Representative smolder propagation across layers, both downwards and upwards to the surface. Specimen#22 time-temperature curve for optical pyrometer and thermocouples installed at the indicated depths below the surface.

The final criterion for smoldering was significant decomposition of the sample and residual white ash at the end of the test. Significant decomposition took place if char formed through the full depth of the specimen. This was readily apparent if aluminum foil could be seen through the remains at the end of the test. Samples exposed to heat fluxes between 8 and 12 kW/m^2 exhibited this criterion. For the 15 kW/m^2 heat flux

tests, the tests were terminated after significant glowing but before decomposition progressed to the level of this criterion. It is quite reasonable to expect this level of decomposition if the tests had continued. Similarly, white ash was noted for all tests at 8 kW/m^2 and above, indicating oxidation of the char. Figure 8 shows the significant decomposition and presence of white ash for specimen#30, exposed to 9 kW/m^2 for three hours. Figure 9 shows that specimen#24, exposed to 7 kW/m^2 for eight hours, did not experience significant decomposition or leave white ash. Cracking and char formation occurred near the surface, but failed to penetrate more than two of the five ply layers, about 7.3 mm.

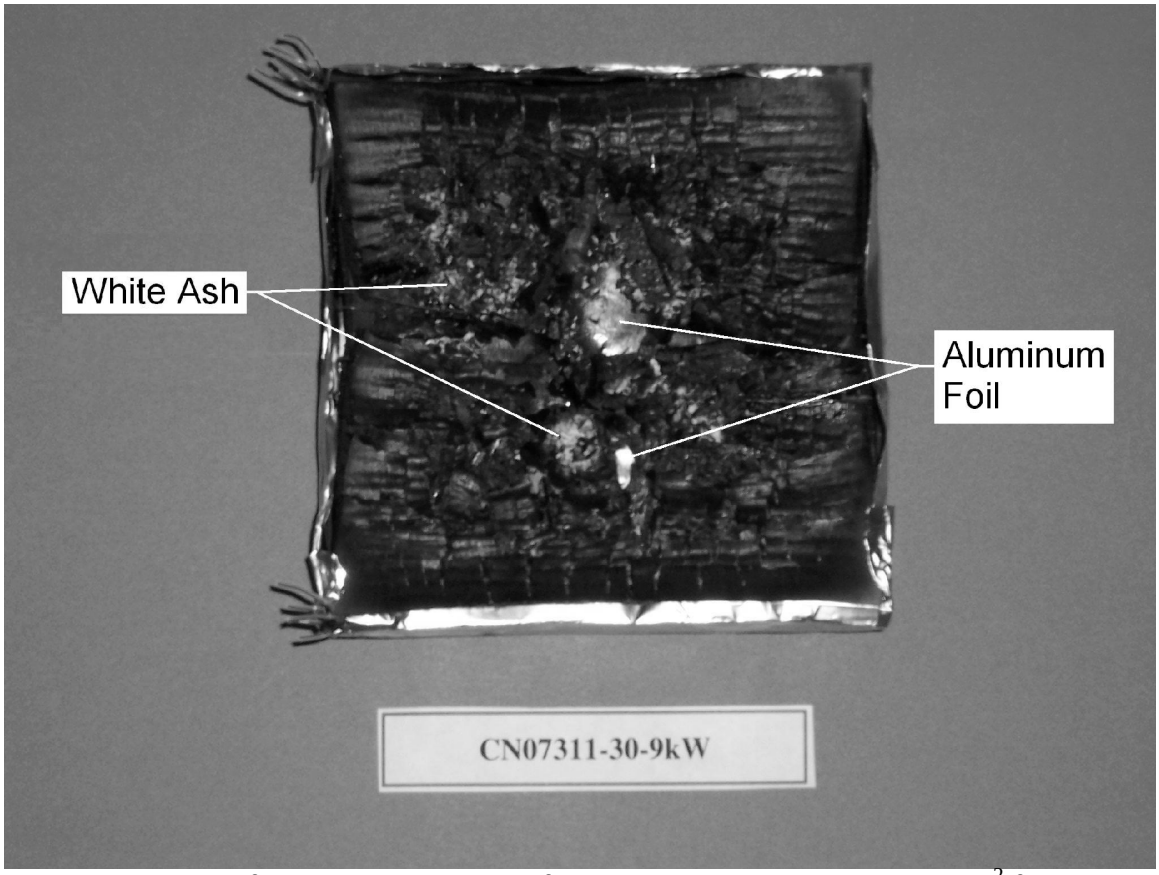

Figure 8 – Significant decomposition of specimen#30, exposed to 9 kW/m^2 for three hours. The underlying aluminum foil is visible as well as telltale white ash indicating char oxidation and thus smoldering.

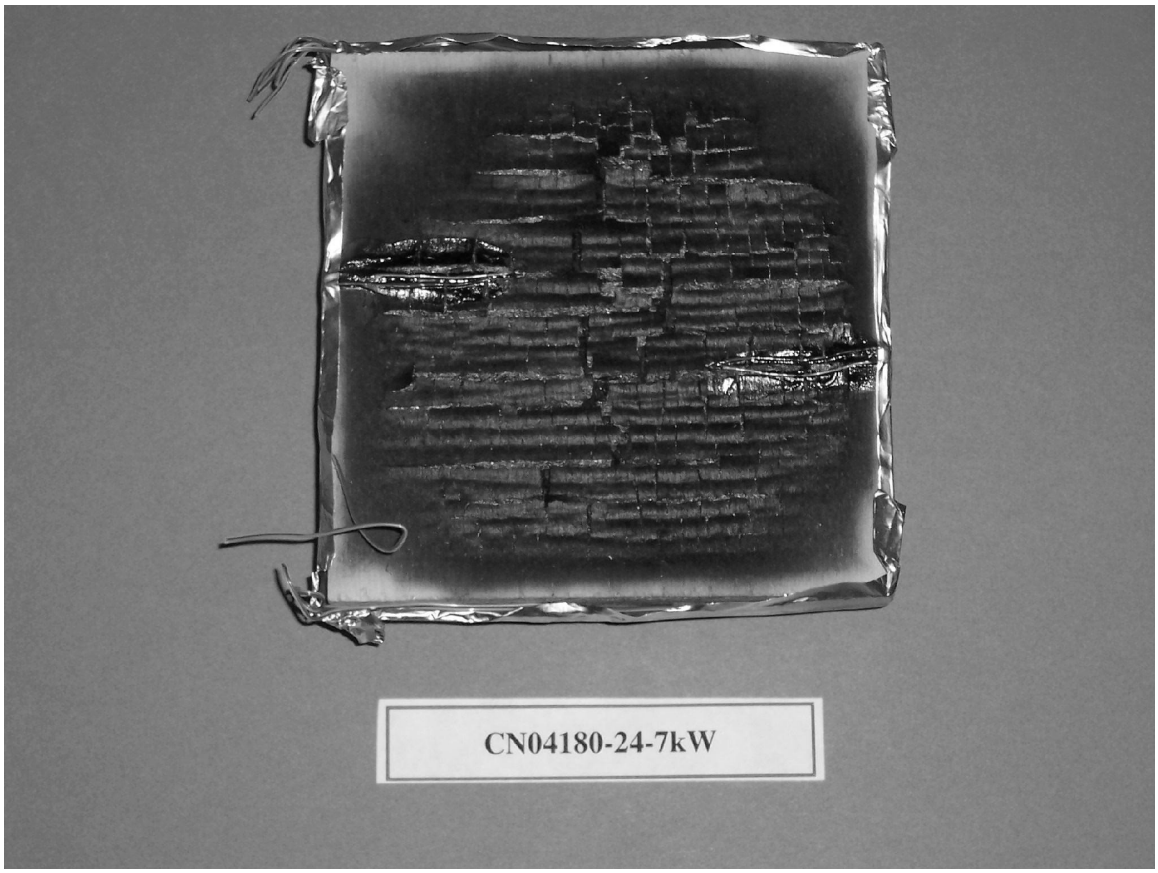

Figure 9 – Cracking and char formation near the surface of specimen#24, exposed to 7 kW/m^2 for eight hours. No significant decomposition or white ash present, indicating smolder did not occur.

Based on the failure of samples exposed to 7 kW/m^2 to exhibit any of the criteria of smoldering ignition and that samples exposed to 8 kW/m^2 or higher did exhibit signs of smolder, the minimum heat flux for smoldering ignition was taken to be 7.5 kW/m^2.

Existing Self-Heating Ignition Theory

Of the forces driving the radiant smoldering ignition of wood, for the low heat flux diffusion controlled regime, self-heating provides the energy to the system that results in ignition. The propensity of a material to self-heat to the point of ignition depends on the balance between heat gained through heat generation and net heat lost to the environment. Martin [4] provides the basic parameters that determine if conditions will

lead to self-heating and possible ignition of the material. The absorbed heat flux is a measure of the transfer of heat from the environment to the material. The conductivity, density and specific heat are all familiar quantities that govern the flow of heat within the material. Finally, thickness and time of exposure give an indication whether a particular material may behave thermally thin, thermally thick or exhibit some intermediate behavior. Due to exposure of the three-quarter inch plywood to low heat fluxes over periods of up to eight hours, the behavior cannot be considered either thermally thin or thermally thick as a temperature gradient will exist within the specimen with elevated temperatures at the back face.

Due to the uniformity of the output of the conical heating element, modeling of heat flow within the wood samples in the cone calorimeter may be approximated as a one-dimensional heat flow problem. The development of the solution and its application to the determination of the minimum heat flux for smoldering ignition of plywood is presented below.

Within the material volume, one-dimensional heat flow may be expressed as,

$$-k\frac{\partial^2 T}{\partial x^2}+\dot{q}'''(T)=\rho c\frac{\partial T}{\partial t}. \qquad (1)$$

The first term on the left is the heat transfer due to conduction. The second term is the heat generation rate from the oxidation of the char; assumed an Arrhenius-type reaction dependent on temperature, as shown in equation 2.

$$q'''(T)=\rho QAe^{-E/RT} \qquad (2)$$

The term on the right is the heat storage within the volume. No temperature dependence is assumed for the thermal conductivity, density or specific heat. Note that

during initial heating, the conduction term is a net positive as heat is being conducted into the volume due to radiant heating from the surface.

A theoretical model, developed by Frank-Kamenetskii, introduced an important dimensionless term known as the Frank-Kamenetskii parameter, δ. This parameter gives an indication of whether the heat generation within the material will be greater than the heat loss to the environment and thus result in thermal runaway and ignition. Equation 3 is the definition of the Frank Kamenetskii parameter from Beever [19],

$$\delta = \frac{E}{R}\frac{\rho Q}{k}\frac{r^2}{T_R^2} A \exp\left(\frac{-E}{RT_R}\right). \tag{3}$$

It can be seen that δ is not a simple function. It includes the Arrhenius-type reaction dependent on temperature as well as on material and thermal properties, geometry and environmental conditions. In developing the theoretical model, Frank-Kamenetskii made five basic assumptions [19] that provide a basis for application to actual scenarios.

1) The heat generation rate is primarily an Arrhenius function of temperature and independent of time as shown in equation 2. The material density and pre-exponential heat of reaction, *QA*, determine the extent of self-heating while the activation energy, *E*, determines at what temperature the exponential term begins to grow from near zero to one and thus acts as the switch for significant heat generation.
2) The activation energy is sufficiently high that $\varepsilon = \frac{RT_R}{E} \langle\langle 1$, where T_R is a reference temperature, nominally taken as the ambient temperature.
3) The heat transferred through the body is by conduction.

4) The heat transferred from the surface to the environment is via convection and radiation. The rate of heat transfer is high, such that the surface temperature remains at ambient.
5) The material is isotropic and homogenous with physical properties that do not depend on temperature.

Beever [19] noted that while these assumptions appear rather restrictive, the assumptions hold for many cases and reasonable estimates may still be obtained. For the plywood samples in the cone calorimeter, the first three assumptions were quite reasonable. Literature values from Bowes and Chong [1,20] for activation energy for sawdust was found to be on the order of 10^8. Thus ε is of order 10^{-2}. While sawdust is not in the same form as plywood, composition and kinetics properties are reasonably similar [1] and data for sawdust is readily available. For the fourth assumption, the surface heat transfer is indeed convection and radiation to the environment. However, the application of a heat flux precludes the surface temperature from remaining at ambient. This may be accounted for by taking the reference temperature as the steady state surface temperature in the absence of self-heating instead of at ambient. Finally, plywood is highly anisotropic with the wood grain direction altering by ninety degrees in each layer and reduced thermal and diffusion properties across the grain [2]. Additionally, while the thermal properties of wood are only mildly temperature dependent [Atreya, 21], it thermally decomposes to char, which has significantly different thermal properties. To account for this, the thermal properties of char may appropriately be used at the temperatures where smolder may initiate.

Since the Frank-Kamenetskii parameter is a measure of the thermal stability of the system, there is some critical condition at which the heat generation matches the heat losses. For a given material and geometry, the independent and thus critical parameter is temperature. Thus, for surface temperatures up to some critical limit, the initially transient system will reach a steady state. Above this temperature, the system is unstable and no steady-state solution exists, signifying thermal runaway. The definition of the Frank-Kamenetskii parameter may be rearranged to give an expression, from which the critical surface temperature may be determined for a given sample [19],

$$\ln\left(\frac{\delta_c T_c^{\,2}}{r^2}\right) = P - \frac{E/R}{T_c} \tag{4}$$

where r is the half-thickness and,

$$P = \ln\left(\frac{E}{R}\rho\frac{QA}{k}\right). \tag{5}$$

Note that equation 4 is in the form of the equation of a line with P representing the intercept and E/R the slope. Bowes experimented with the self-heating of sawdust [1] and applied the above theory to the experimental data to determine suitable values for the intercept and slope at the critical condition, equation 6, where r is in millimeters, and temperature is in Kelvin.

$$\ln\left(\frac{\delta_c T_c^{\,2}}{r^2}\right) = 34.9456 - \frac{13030}{T_c} \tag{6}$$

Application to the Cone Calorimeter

A plywood sample in the cone calorimeter is subjected to a constant heat flux with (Newtonian) cooling on the hot face and insulated backing with Newtonian cooling on the back face of the holder. The efficiency of the transfer of heat to the material is

expressed in the form of the Biot number, α , the ratio of the combined convection and radiation heat transfer at the surface to the thermal conduction into the material, equation 7.

$$\alpha = \frac{h_t r}{k_c} \tag{7}$$

Bowes [1] developed an approximation suitable to describe a plywood specimen subject to radiant heat in the cone calorimeter. His approximation, described below, allows for the ignition problem, a transient phenomenon, to be analyzed as two separate steady-state problems, a self-heating problem and a radiant exposure problem, linked by the surface temperature. For sub-critical radiant heating of plywood, the surface will eventually reach a steady-state temperature. This will be the case up to some critical heat flux. Therefore, by finding the critical surface temperature for self-heating, a critical radiant heat flux may be determined from a heat balance analysis at the surface.

Bowes determined that the self-heating problem for asymmetric radiant heating of a slab may be simplified by assuming a constant hot temperature at the surface with Newtonian cooling at the back face. Furthermore, Bowes noted that provided δ_c is large enough (>5), the problem might be further simplified by approximating the surface boundary condition as a perfect insulator with zero temperature gradient. This allows the critical condition, δ_c , to be related to the Biot number and a non-dimensional temperature rise, θ_a . This relationship is shown in equation 8, Bowes equation for criticality.

$$\sqrt{2\delta_c}\tanh\sqrt{2\delta_c} + 2\alpha\ln\left(\cosh\sqrt{2\delta_c}\right) = -\alpha\theta_a \tag{8}$$

Equation 9 defines the non-dimensional temperature rise with the surface temperature as the reference temperature.

$$\theta_a = \frac{E/R}{T_R^2}(T_a - T_R) \tag{9}$$

The approximate solution to equation 8 is given by equation 10 and assumes δ_c is large enough (>5) that $\tanh\sqrt{2\delta_c}$ is close to unity [1]. An examination of the δ_c approximation shows that it maintains dependencies on the geometry and thermal properties of the material as represented in the Biot number and the self-heating kinetics as represented by θ_a.

$$\delta_c \approx \frac{1}{2}\left(\frac{\alpha}{1+2\alpha}\right)^2 (1.4 - \theta_a)^2 \tag{10}$$

With equations 6, 9 and 10, the Biot number, α, is the only variable unaccounted for to determine the critical surface temperature for the plywood samples in the cone calorimeter as the half-thickness of the sample is a known quantity. To evaluate the Biot number, suitable estimates of the thermal conductivity and the combined convection and radiation heat transfer coefficient are needed.

Noting that the plywood chars prior to smolder, the thermal conductivity of char is appropriate for evaluating the Biot number. Atreya [21] shows the conductivity of char to be a mild function of temperature, equation 11.

$$k_c = 1.7x10^{-4} + 0.29x10^{-6}(T - T_o) \text{ cal/cm sec K} \tag{11}$$

$$7.1x10^{-2} + 1.2x10^{-4}(T - T_o) \text{ W/m K}$$

The combined convection and radiation heat transfer coefficient, h_t, is the sum of the convective heat transfer coefficient, h_c, and a linearization of the radiation losses from the hot surface to the environment, h_r.

The convective heat transfer coefficient is estimated using the correlations for cooling of a horizontal plate with the hot face up, Atreya [22]. This is shown in equations 12 through 15.

$$h_c = \frac{\overline{N}u_L k}{L} \tag{12}$$

where,

$$\overline{N}u_L = 0.54 Ra_L^{1/4} \qquad 10^5 \approx\leq Ra_L \approx\leq 10^7 \tag{13}$$

and,

$$Ra_L = \frac{g\beta(T_s - T_a)L^3}{\nu\alpha}. \tag{14}$$

T_s is the surface temperature. All properties are evaluated at the film temperature, equation 15.

$$T_f = (T_s + T_a)/2 \tag{15}$$

Equating the equation for radiation heat transfer to a linear representation of a radiation heat transfer coefficient in the convective form [23] allows the two to be summed into a combined heat transfer coefficient.

$$\dot{q}'' = \varepsilon\sigma(T_s^4 - T_a^4) = h_r(T_s - T_a) \tag{16}$$

Solving for h_r yields,

$$h_r = \varepsilon\sigma(T_s^2 + T_a^2)(T_s + T_a) \tag{17}$$

As wood heats, thermal decomposition darkens the wood till a char forms. As such, properties of char are appropriate for these calculations. Since char emissivity approaches one, a value of 0.96 is reasonable [2].

Critical Surface Temperature and Experimental Results Comparison

With the means to estimate the Biot number, the critical value for the Frank-Kamenetskii parameter, δ_c, can be calculated and thus the critical surface temperature may be found through an iterative solution of equation 6. δ_c was calculated to be 13.6 and the critical surface temperature was determined to be 267 °C. Therefore, for surface temperatures below 267 °C, the plywood sample can be expected to reach equilibrium and smolder will not occur. However, if the surface temperature exceeds 267 °C, thermal runaway is predicted, resulting in smolder.

Recall that the criterion for smoldering was temperatures greater than 400 °C. Only three specimens failed this criterion. One was subjected to a heat flux of 6 kW/m^2 and achieved a maximum temperature of 240 °C. The other two, specimen #23 and #24, were subjected to a heat flux of 7 kW/m^2. Discounting spikes up to 286 °C in the temperature profile of specimen #24, the maximum sustained temperature for each was 270 °C. Even though smoldering was determined not to have occurred, the fact that self-heating was evident in both samples shows that the theoretical calculations are quite reasonable. The difference may be attributable to uncertainties in the composition of the actual samples and experimental errors.

Critical Heat Flux and Experimental Results Comparison

The next step is to tie the critical temperature to a radiant energy level to determine the critical heat flux above which smoldering ignition is predicted. Equation 18 is the steady-state heat balance at the sample surface while ignoring in depth heat losses.

$$\dot{q}_i'' = \varepsilon\sigma(T_s^4 - T_a^4) + h_t(T_s - T_a) \qquad (18)$$

Where,

$\dot{q}_i''$ = Incident heat flux per unit area, W/m^2,

T_s = Sample surface temperature, K,

T_a = Ambient temperature, 294 K,

h_t = Combined convection and radiation heat transfer coefficient, W/m^{2}K,

ε = Emissivity of sample, 0.96,

σ = Stefan-Boltzmann constant, 5.67x10^{-8} W/m^{2}K^4.

For the cone calorimeter, the incident heat flux is a known quantity and shall be the independent variable. With the combined heat transfer coefficient calculated using equations 12 through 17, equation 18 may be solved for the steady-state surface temperature as a function of incident heat flux.

The critical incident heat flux is determined by comparing the calculated critical surface temperature to the predicted steady-state surface temperature for a given heat flux. From this comparison, a critical incident heat flux of 7.2 kW/m^2 is predicted for the plywood samples. Thus, samples exposed to 7 kW/m^2 heat flux were not predicted to smolder, as seen for specimen #23 and #24. By treating the transient ignition problem as two separate steady-state problems linked by the conditions at the surface, a critical incident heat flux was determined.

Sensitivity Analysis

The maple plywood tested in this effort had very minor variations in thickness, between 1.80 and 1.84 cm. A small increase in thickness such as this results in a predicted decrease in the critical surface temperature of only a few tenths of a degree and thus a marginal increase in the critical heat flux. For comparison, the theory predicts for samples twice as thick, a critical surface temperature decrease of less than 30 °C over the range of incident heat fluxes of interest. Conversely, halving the thickness results in an increase of less than 30 °C for the predicted critical surface temperature over the same range. The corresponding calculated critical heat fluxes are 6.0 and 8.8 kW/m^2 for the double and half-thickness plywood, respectively.

As mentioned earlier, the kinetics of plywood is similar to those of sawdust [1]. An examination of other reported sets of kinetics data provides further insight into the appropriateness of the data. Cuzzillo [24] reported two different values of QA, the theoretical maximum heat release rate per unit mass, for sawdust. The first, by Chong, was 3.19×10^{11} J/kg-s. The second, Bowes data, calculated by Chong and corrected for unit conversion errors by Cuzzillo, was 1.54×10^{13} J/kg-s. Cuzzillo then showed that Bowes' intercept fell within the 90% confidence bounds on the linear regression fit of Chong's experimental data. While this is true, the differences in QA have a significant effect on the theoretical critical surface temperature. Chong's data suggests an intercept P of 31.0687 as compared to Bowes value of 34.9456, a difference of 11.1%. Likewise, Chong calculated the activation energy for untreated sawdust as 0.90×10^8 J/kg-mol. When used to calculate critical surface temperatures of the maple plywood, Chong's data yields a critical temperature of 251 °C as compared to the Bowes calculated temperature

of 267 °C. The theory also predicts a critical incident heat flux of 6.5 kW/m^2 using Chong's kinetic constants.

The activation energy has a significant impact on the likelihood of smolder. Cuzzillo's corrected value for E from Bowes sawdust data is 1.08x10^8 J/kg-mol. Bowes [1] also suggests that 1.00x10^8 J/kg-mol is a reasonable value for oxidative self-heating of carbonaceous materials. Given Bowes value of 13030 K for E/R for sawdust, an E/R of 12027 K is calculated for the general value of E. Maintaining the Bowes value for the P intercept, 34.9456, this yields a calculated critical surface temperature of 217 °C. Experimental data clearly shows this is incorrect.

Due to the large difference in values for QA between Bowes and Chong, an average value, 7.86x10^{12} J/kg-s, along with an average of the two Bowes suggested values for activation energy, 1.04x10^8 J/kg-mol, might be an appropriate set for calculations. Applying this kinetics data set to Bowes theory yields a critical surface temperature of 257 °C and a critical incident heat flux of 6.8 kW/m^2, comparing favorably with the results using Bowes kinetic data.

Table 1summarizes the kinetics data along with the predicted and experimental critical incident heat flux and surface temperature. Note that despite the wide spread of the kinetics data, the differences in the critical values are quite small.

Table 1 – Kinetics data and predicted critical values

Kinetic Data Source	E [J/kg-mol]	QA [J/kg-s]	$q''_{i,crit}$ [kW/m^2]	T_{crit} [°C]
Bowes sawdust	1.08x10^8	1.54x10^{13}	7.2	267
Modified Bowes	1.04x10^8	7.86x10^{12}	6.8	257
Chong untreated sawdust	0.90x10^8	3.19x10^{11}	6.5	251
Experimental Results	N/A	N/A	7.5	270

Thermal Profiles

Evaluating the thermal conditions leading up to ignition provides insight into the behavior of plywood subject to radiant heat. The changes in the thermal profiles over time show the dynamic nature of the ignition process. Dimensional and non-dimensional analyses of the profiles illustrate the heating progression from just after inert heating at the establishment of self-heating through ignition. The profiles show how the depth of the ignition event changes with the heat flux. To evaluate the thermal profiles, several data reduction techniques were required and thus are addressed first.

Data reduction consisted of two steps. First, to reduce noise associated with thermocouple measurements, reported temperatures were averaged over a moving block of time, between 30 and 120 seconds. The moving average time scale for each data set was balanced between smoothing the data and maintaining the profile of changes in conditions. Heating occurred much slower at the lower heat fluxes, permitting averages over 120 seconds for 7 and 8 kW/m^2 while heating was much faster at higher heat fluxes necessitating a 30 second average for 12 and 15 kW/m^2. A moving average of 60 seconds was used for 9 and 10 kW/m^2 heat fluxes.

The second step draws from a conclusion of the baseline temperature measurements. The averaging of the thermocouple temperatures at the surface compared favorably with the area temperature measurements of the optical pyrometer and thus provided an overall temperature at the surface. Unless otherwise specified in the text, the measurements from the thermocouple pair at each depth were smoothed and averaged to obtain the overall temperature at that depth.

The Fourier number, *Fo*, is a common measure of the thermal wave penetration depth. As such, estimates of the Fourier number were made for the three thermal conditions evaluated. Equation 19 shows the definition of the Fourier number,

$$Fo = \frac{k\tau}{\rho C s^2} \tag{19}$$

where time, τ , is in seconds and the half-thickness of the material, *s*, is in meters. To evaluate *Fo*, the thermal characteristics of the plywood were assumed to not change over time. Because the specimen is char over the times and depths of interest, the properties of char were used.

Thermal Profiles Discussion

Three significant events were identified that highlight the response of the plywood to the radiant heat flux and the self-heating that leads to ignition. The first was the establishment of self-heating as the predominant heating mechanism. The second was the time at which sub-surface temperatures exceed surface temperatures. The third was the time of glowing, the outward sign of ignition. The order of these events provides insight into the depth of the ignition event.

Transition to Self-Heating

It is clear from the reviewed literature, theory and analysis to this point that self-heating is the critical component that determines if plywood, subject to a sufficiently low heat flux, will achieve smoldering ignition. Therefore, evidence of self-heating was desired from the recorded temperature data. Analysis of temperature measurements at depth resulted in identification of the time at which self-heating within the specimen overtook radiant heating as the predominant heating mechanism. This time, $t_{self\text{-}heat}$, occurred at the quasi-steady state condition of a minimum in the rate of temperature

change. Figure 10 is representative of the rate of temperature change profiles around this minimum and is from specimen#18, exposed to a heat flux of 10 kW/m^2. Plots of the rate of temperature changes for each of the ignition tests are presented in Appendix C.

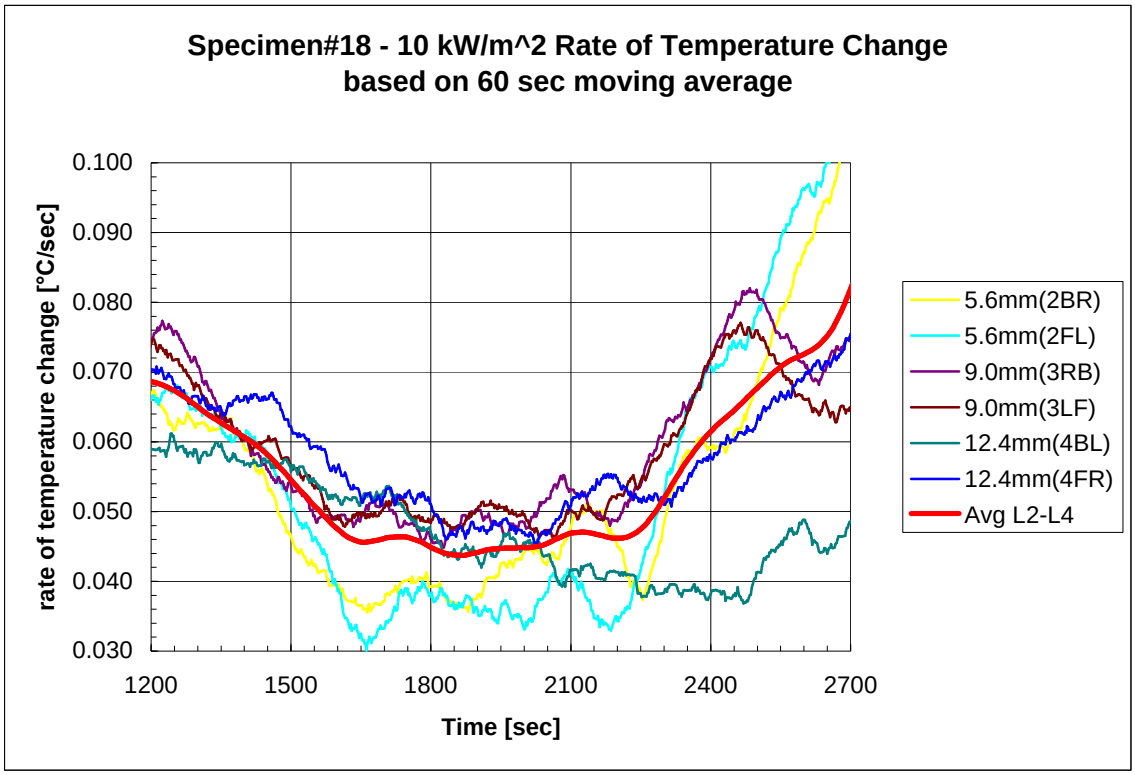

Figure 10 – Rate of temperature change over time neat the minimum rate for specimen#18, exposed to a heat flux of 10 kW/m^2.

The initial high rates of temperature change both at the surface and at depth decreased rapidly as the specimen appropriately behaved as an inert slab undergoing initial radiant heating and approached thermal equilibrium. Over time, the rate of temperature change for all the sub-surface thermocouples decreased towards the steady-state condition. The high levels of noise associated with surface temperature measurements prevented useful analysis of these data points and were subsequently dropped from consideration. For specimen#18, the rate of temperature change reached an average minimum of 0.044 °C/sec across the sub-surface thermocouples at around 1870 seconds after initial

exposure to the heat flux. After 1870 seconds, rates of temperature change increased again, starting with thermocouples mounted at a depth of 5.6 mm, followed by those at 9.0 and 12.4 mm depth. The behavior shown in figure 10 exemplifies self-heating becoming the predominant heating mechanism within the specimen. Figure 11 is a plot of the time and rate of minimum rate of temperature change as a function of the applied heat flux. The figure shows the minimum rate increases and the time to the minimum rate decreases with heat flux.

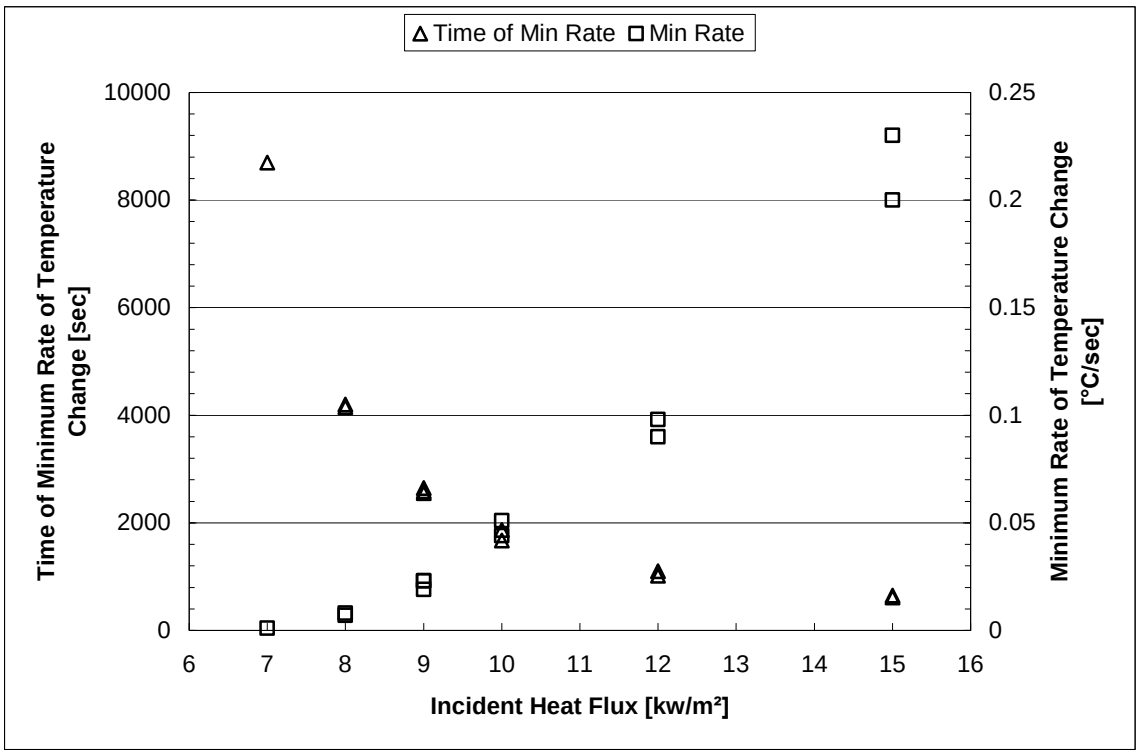

Figure 11 – Co plot of time and rate of minimum rate of temperature change for specimen exposed to heat fluxes between 7 and 15 kW/m^2.

Specimen#31, exposed to 6 kW/m^2 was not included in figure 11 as rates of temperature change decayed asymptotically to zero, indicating no appreciable levels of self-heating and thus $t_{self\text{-}heat}$ was indeterminate. Similarly, $t_{self\text{-}heat}$ for the second sample

exposed to 7 kW/m^2 could not be determined from the data even though some self-heating was evident in the time-temperature profiles.

A representative profile was developed for each heat flux by averaging the temperature data at $t_{self\text{-}heat}$ for each test at that heat flux. The individual times of $t_{self\text{-}heat}$ were then averaged to obtain the representative time of $t_{self\text{-}heat}$ at that heat flux. Figures 12 and 13 provide the dimensional and non-dimensional (θ_a) representative thermal profiles for each heat flux at $t_{self\text{-}heat}$. The dashed line for the 9 kW/m^2 profile is for the data measured at a depth of 12% in only one test. Note that the surface temperature at $t_{self\text{-}heat}$ was above the calculated critical surface temperature, 267°C, for all heat fluxes except 7 kW/m^2, which did not ignite. Because θ_a represents an interior temperature excess above the surface temperature, interior temperatures less than the surface temperature have a negative value for θ_a.

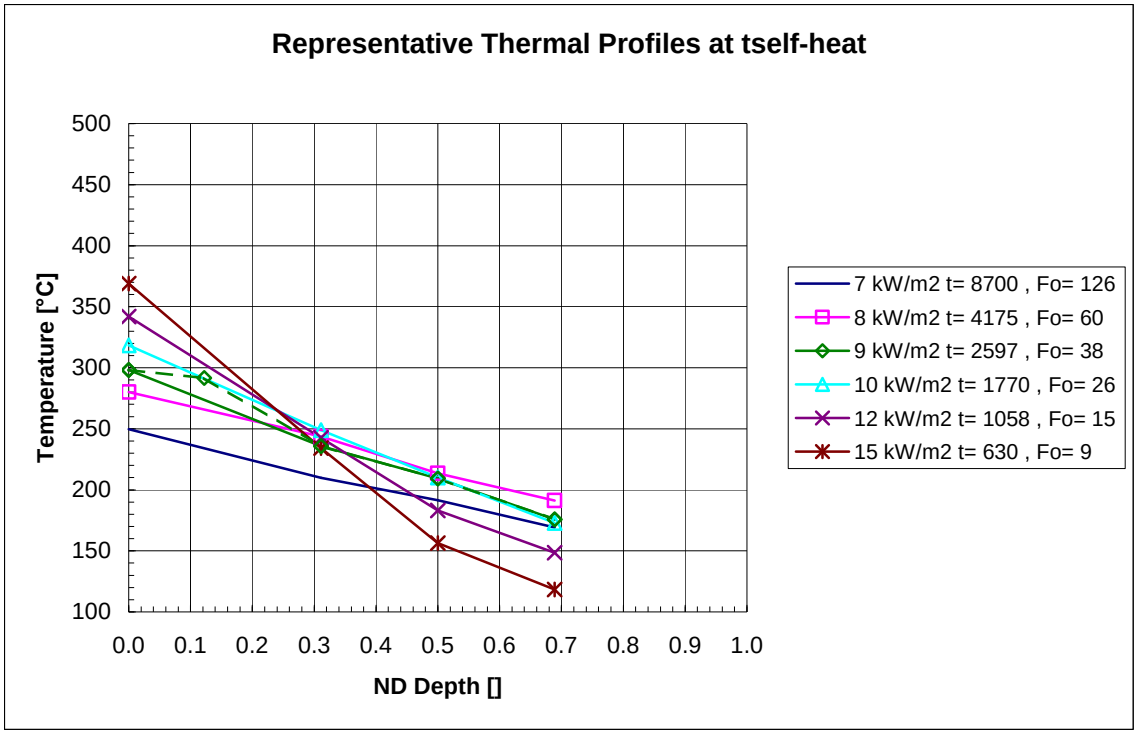

Figure 12 – Representative thermal profiles at the time of the shift of the predominant heating mechanism to self-heating, $t_{self\text{-}heat}$ for maple plywood exposed to heat fluxes from 8 to 15 kW/m^2 in the cone calorimeter. The dashed line for the 9 kW/m^2 profile is for the data measured at a depth of 12% in only one test.

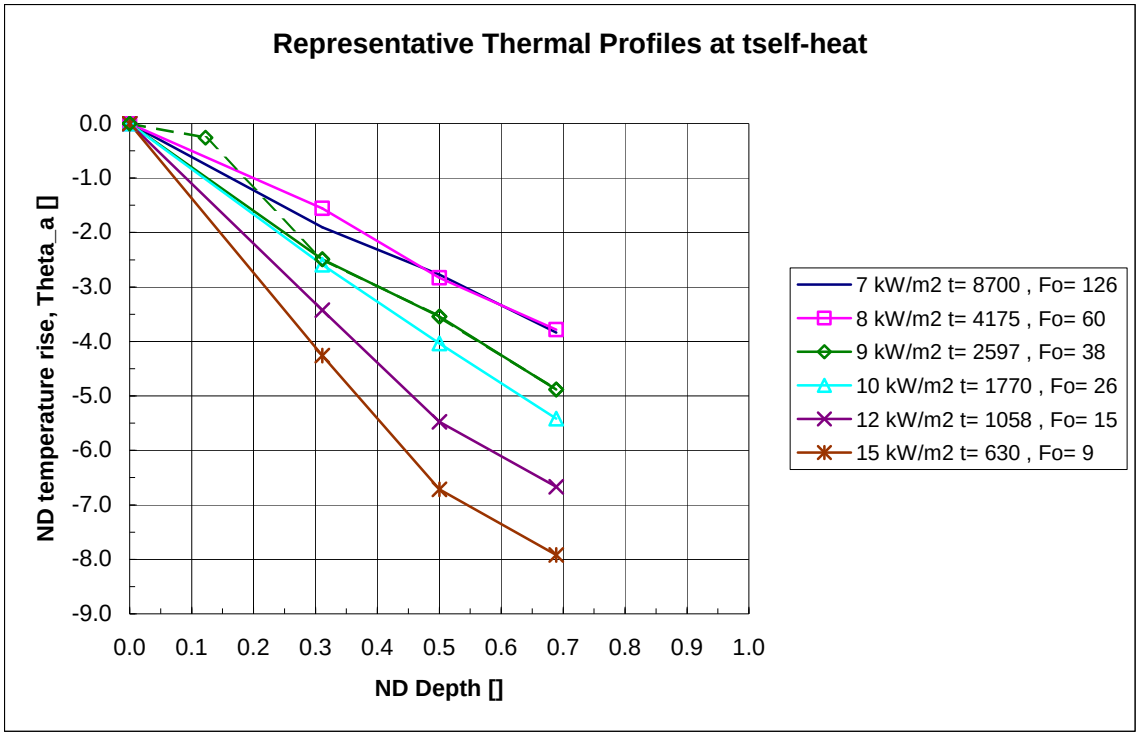

Figure 13 – Representative thermal profiles, as a function of temperature excess as compared to the reference surface temperature, at the time of the shift of the predominant heating mechanism to self-heating, $t_{self\text{-}heat}$ for maple plywood exposed to heat fluxes from 8 to 15 kW/m^2 in the cone calorimeter. Negative values represent temperatures cooler than the surface. The dashed line for the 9 kW/m^2 profile is for the data measured at a depth of 12% in only one test.

Temperature Crossover

Temperature crossover occurred when the first sub-surface temperature exceeded the surface temperature. At that point, the flow of heat is no longer from the surface to the backside. Thermal equilibrium exists, if only for an instant. Further increases in sub-surface temperatures relative to the surface results in heat flow from the interior back to the surface as well as continued losses out the backside. Figure 14 shows the times of temperature crossover for specimen exposed to heat fluxes between 8 and 15 kW/m^2. The time to temperature crossover decreased with increasing heat flux. Crossover behavior was not recorded for samples exposed below 8 kW/m^2. For most tests, the

shallowest sub-surface thermocouple was mounted at 31% depth and was the location of the temperature crossover. Specimen#30 had thermocouples mounted at a depth of 12%. The temperature crossover at this depth occurred earlier than at the 31% depth. The time of temperature crossover for specimen#30 in figure 14 reflects the temperatures at the 31% depth for consistency.

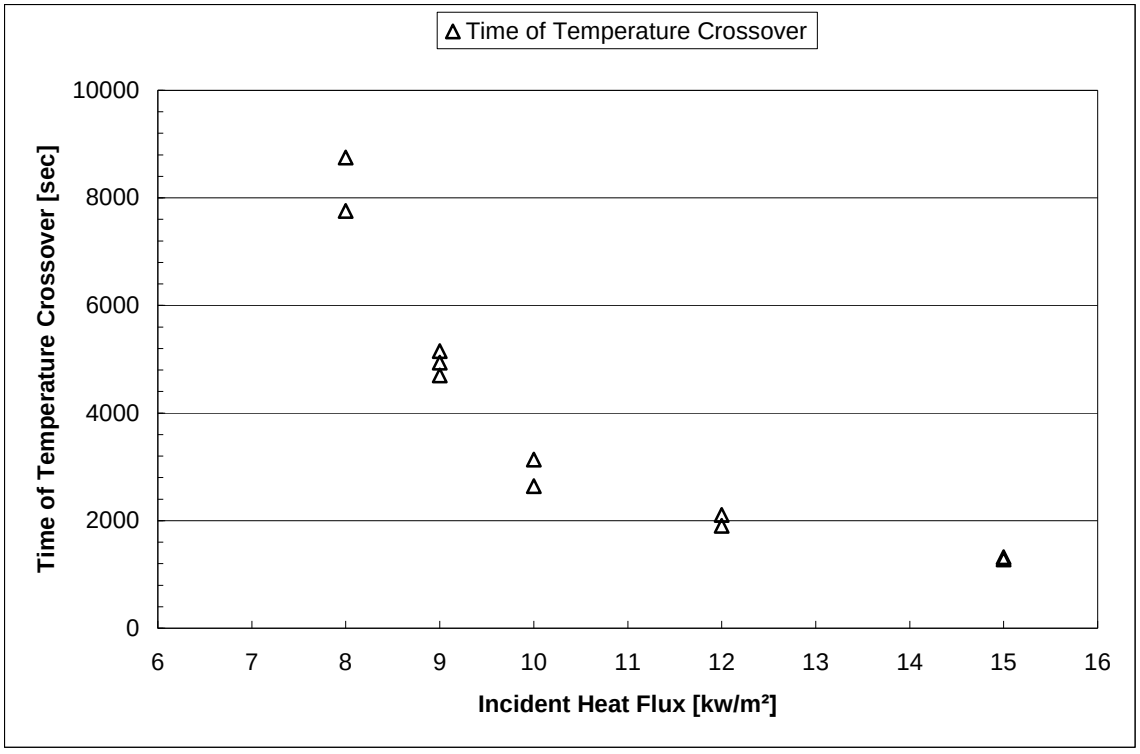

Figure 14 – Time to temperature crossover for specimen exposed to heat fluxes between 8 and 15 kW/m^2.

Figure 15 and 16 provide the dimensional and non-dimensional (θ_a) representative thermal profiles for each heat flux at the time of temperature crossover. Note that the temperature at a depth of 12% for the 9 kW/m^2 case is significantly above the surface temperature. This shows that the depth of the initial crossover does not necessarily occur first at the 31% depth.

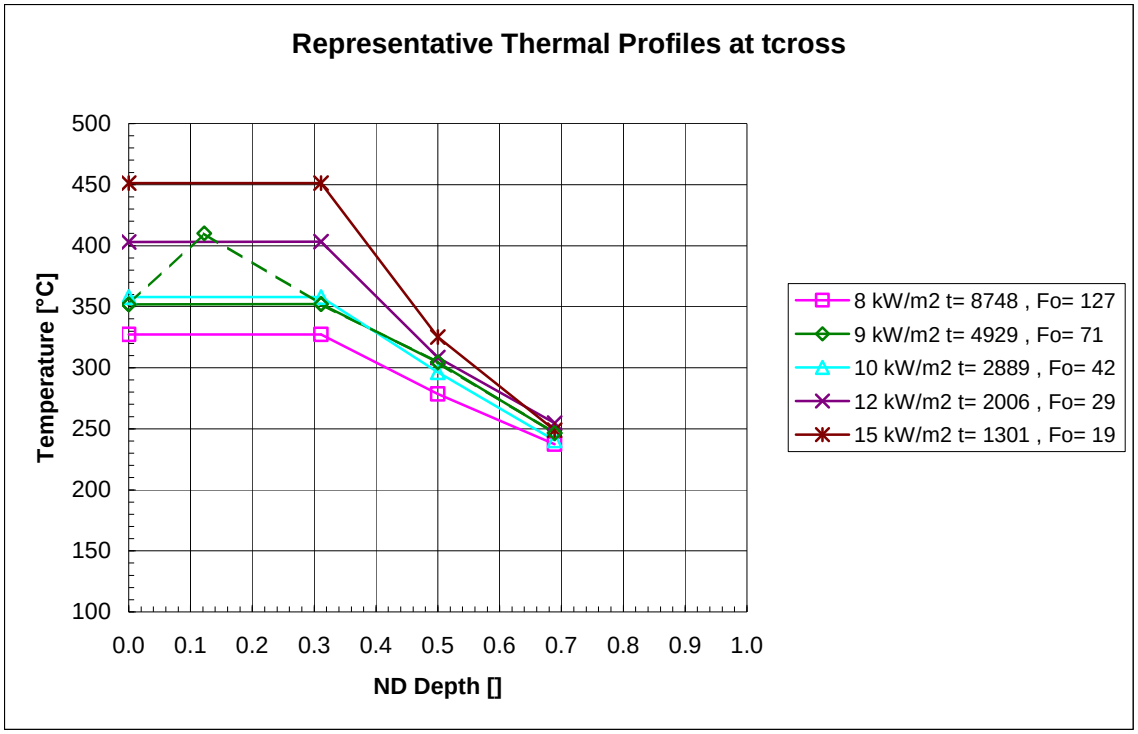

Figure 15 – Representative thermal profiles at the time of temperature crossover, t_{cross} for maple plywood exposed to heat fluxes from 8 to 15 kW/m^2 in the cone calorimeter. The dashed line for the 9 kW/m^2 profile is for the data measured at a depth of 12% in only one test.

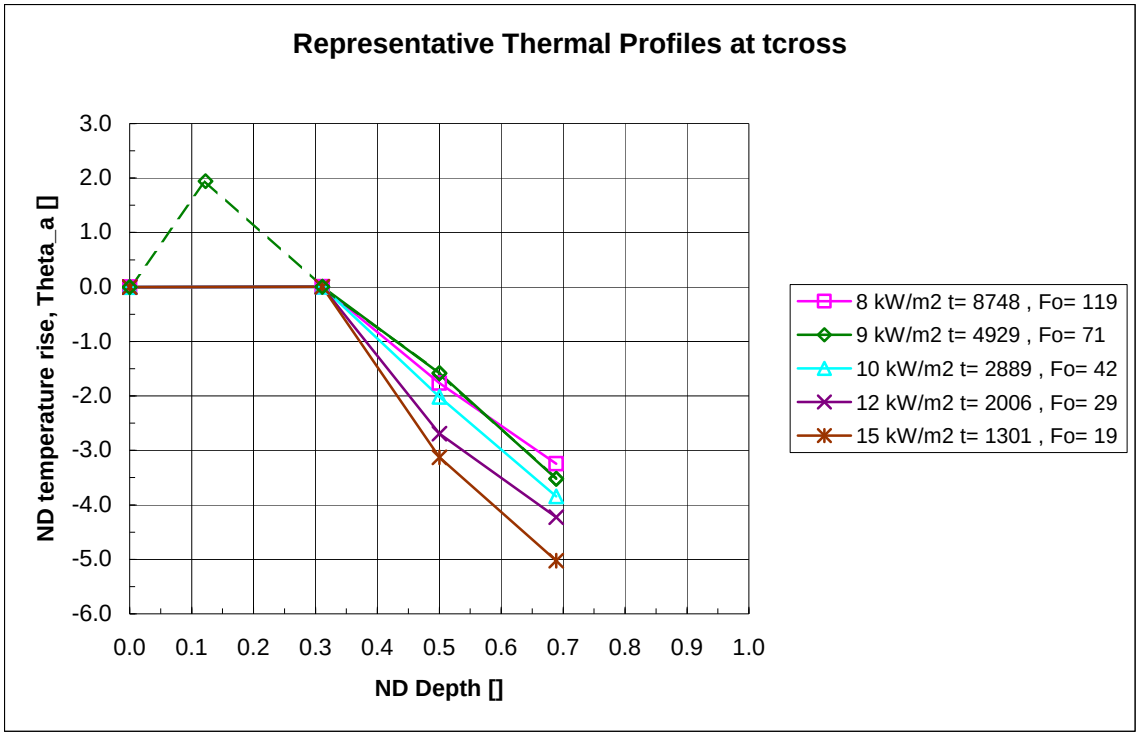

Figure 16 – Representative thermal profiles, as a function of temperature excess as compared to the reference surface temperature, at the time of temperature crossover, t_{cross} for maple plywood exposed to heat fluxes from 8 to 15 kW/m^2 in the cone calorimeter. Negative values represent temperatures cooler than the surface. The dashed line for the 9 kW/m^2 profile is for the data measured at a depth of 12% in only one test.

Observed Glowing

Glowing is an observed phenomenon and as such the time at which glowing starts is subjective. As mentioned in section 2.2.3, the procedures for each ignition test called for the room lights to be turned off and the time, type and location of the glowing to be recorded. Transitory glowing (1 or 2 seconds) at the edges of cracks was more prevalent at heat fluxes of 12 and 15 kW/m^2. Glowing on the flat surfaces or within cracks was more likely to be an area effect and persistent. The recorded time of glowing was based on persistent glowing regardless of location. Figure 17 plots the time at which glowing was observed for specimen exposed to heat fluxes between 8 and 15 kW/m^2. As expected, the time to glowing ignition decreased with increasing heat flux. Recall that

glowing was not observed for any of the samples exposed to a 7 kW/m^2 heat flux and that glowing was only observed in one of the two samples at 8 kW/m^2 heat flux and it was very faint.

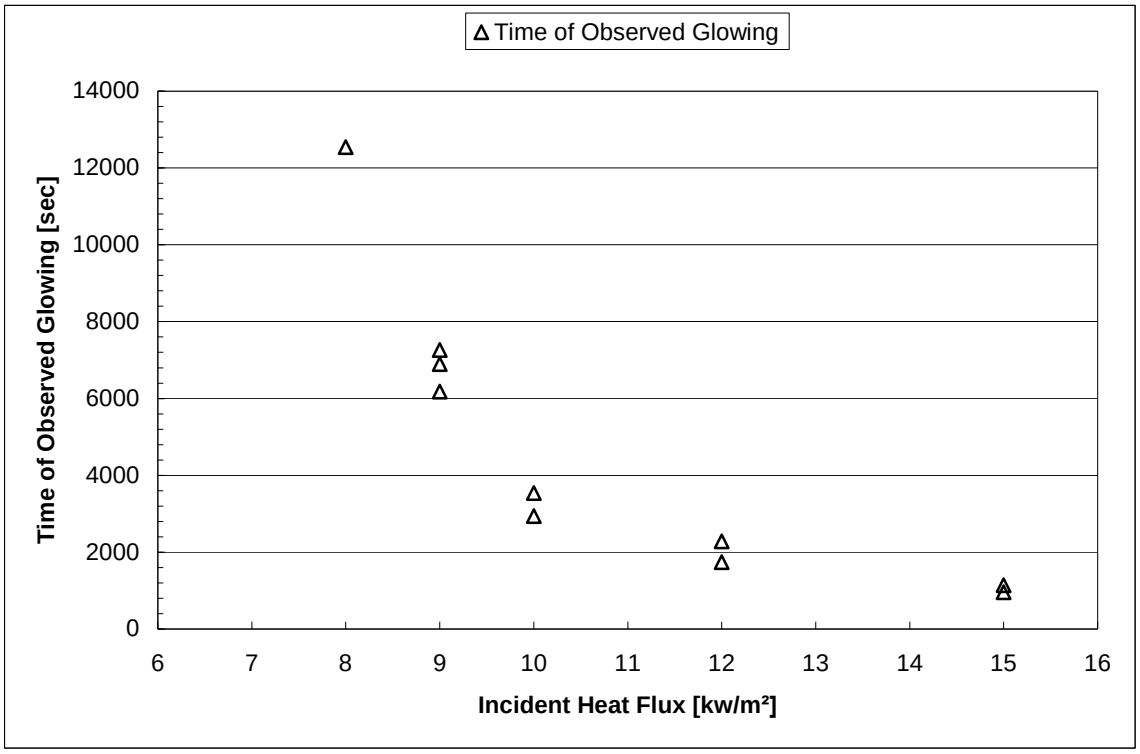

Figure 17 – Time to observed glowing for specimen exposed to heat fluxes between 8 and 15 kW/m^2.

The dimensional and non-dimensional (θ_a) representative thermal profiles for each heat flux at the time of observed glowing are shown in figures 18 and 19. The dashed line for the 9 kW/m^2 profile is for the data measured at a depth of 12% in only one test.

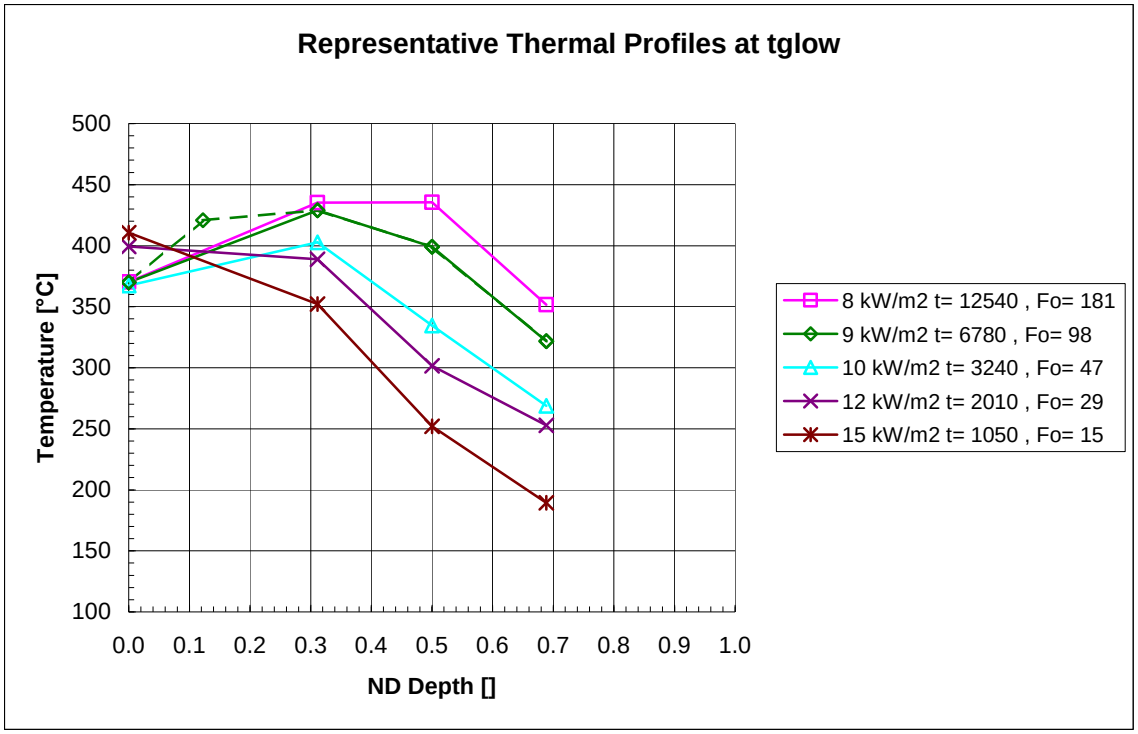

Figure 18 – Representative thermal profiles at the time of observed glowing, t_{glow} for maple plywood exposed to heat fluxes from 8 to 15 kW/m^2 in the cone calorimeter. The dashed line for the 9 kW/m^2 profile is for the data measured at a depth of 12% in only one test.

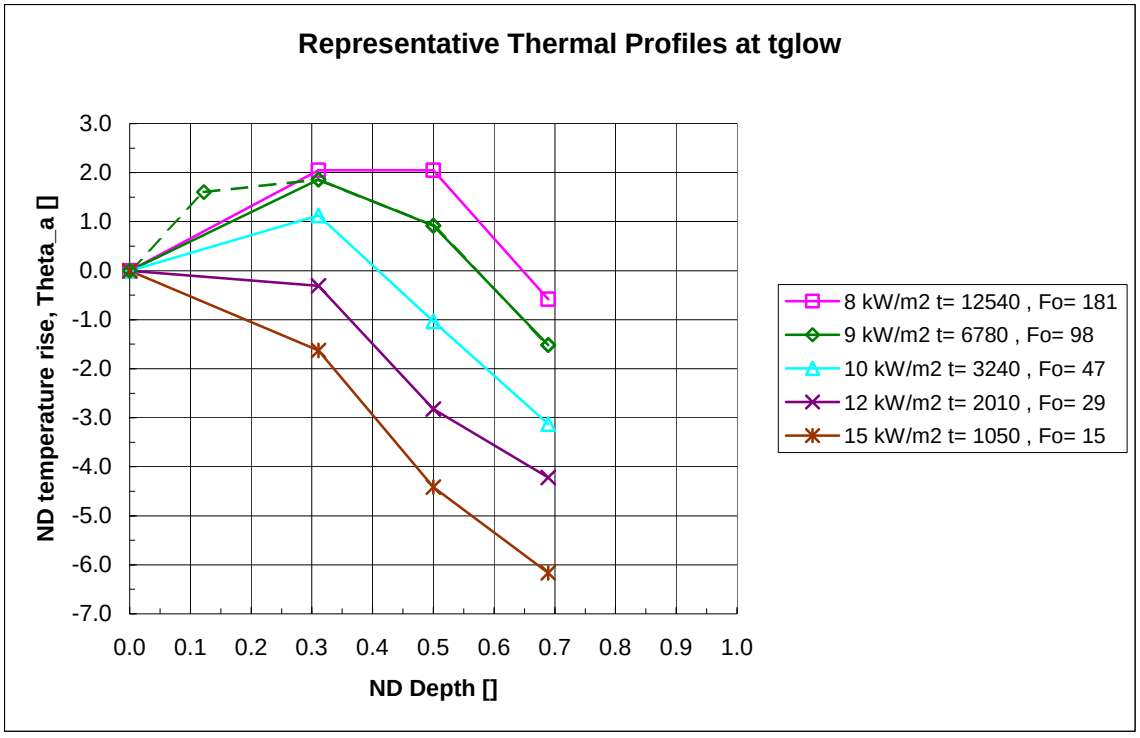

Figure 19 – Representative thermal profiles, as a function of temperature excess as compared to the reference surface temperature, at the time of observed glowing, t_{glow} for maple plywood exposed to heat fluxes from 8 to 15 kW/m^2 in the cone calorimeter. Negative values represent temperatures cooler than the surface. The dashed line for the 9 kW/m^2 profile is for the data measured at a depth of 12% in only one test.

Thermal Profile History

The thermal profile data provides a comparison of the representative thermal response of wood subject to varying heat fluxes at three discrete events. Examination of the thermal profiles of a specimen over time provides insight into the roles of the incident heat flux and self-heating leading to ignition. Figures 20 and 21 show the relevant thermal profile history for a specimen subject to a 9 kW/m^2 heat flux. The profile times begin at 1950 seconds into the exposure and continue at 600-second intervals till 1200 seconds after observed glowing when the thermal propagation wave reaches the sample midpoint. The initial time is late inert slab heating and near the beginning of self-heating. Between 3150 and 4350 seconds, the thermal activity in the 12% depth increased

significantly indicating first evidence of ignition at depth. By 6150, the thermal propagation wave reached the surface with increases in temperature coinciding with observed glowing. The thermal propagation wave also moved to the interior as seen by temperatures above that of the previous depths at times 6150 seconds for 31% depth and 7350 seconds for 50% depth. The relative changes in temperatures are more readily apparent in figure 4.10 where the temperature at the 12% depth reached its maximum as compared to the surface at 5550 seconds while the maximums were at 6750 and 7350 seconds for 31 and 50% depths, respectively.

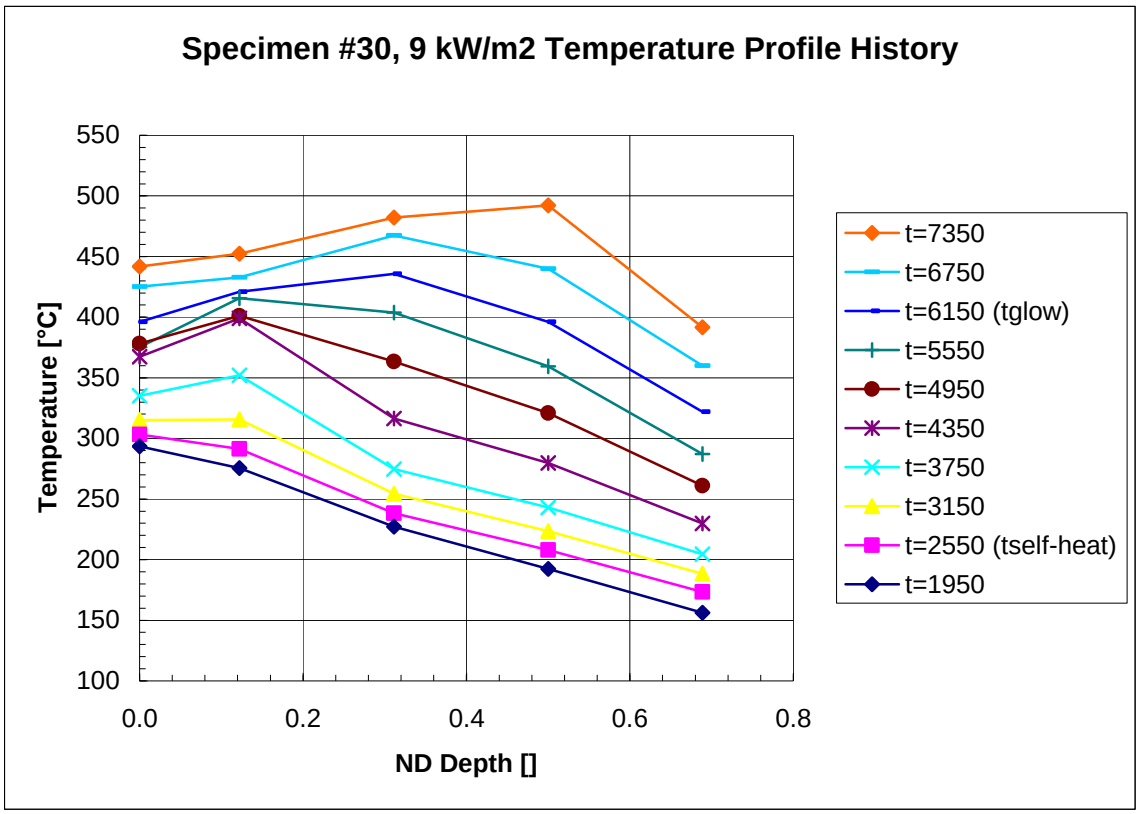

Figure 20 – Thermal profile history for maple plywood Specimen #30 exposed to a heat flux of 9 kW/m^2 in the cone calorimeter. Profile times begin 600 seconds before $t_{self\text{-}heat}$ with a 600 second interval till 1200 seconds after observed glowing.

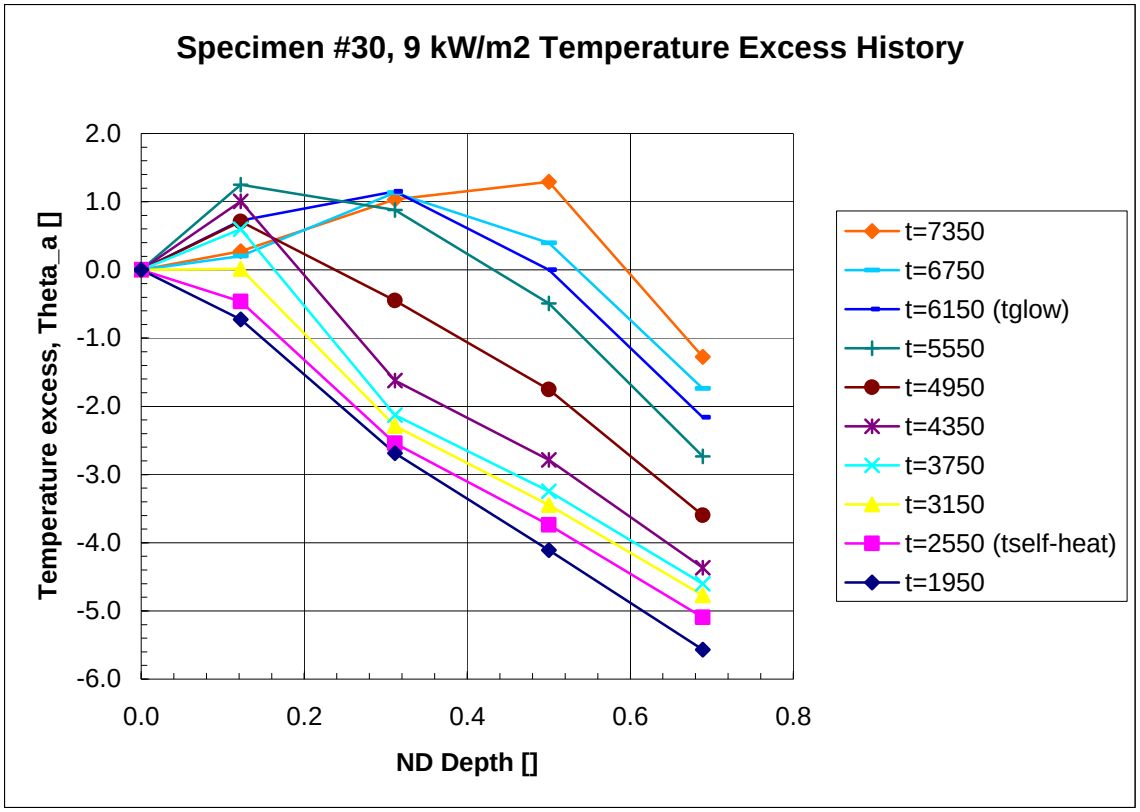

Figure 21 – Thermal profile history of temperature excess for maple plywood Specimen #30 exposed to a heat flux of 9 kW/m^2 in the cone calorimeter. Profile times begin 600 seconds before $t_{self\text{-}heat}$ with a 600 second interval till 1200 seconds after observed glowing.

Ignition Depth

Ignition predominantly occurs at a single location with further burning propagating from there. For the self-heating problem the location is a depth below the specimen surface followed by the propagation of the smolder wave towards the surface and down into the specimen. The number and placement of thermocouples at depth were insufficient to provide a precise ignition depth as a function of the applied heat flux. However, they were sufficient to show that ignition occurs closer to the surface with higher heat fluxes.

Since glowing is the first outward sign of ignition, the temperature at the surface must be sufficiently high for ignition. Therefore, temperatures at depth in excess of this temperature is an indication that ignition already occurred at that depth and that the glowing is the manifestation of the propagation of the smolder wave at the surface. As such, figure 19 shows that the temperature excess at depth decreased with an increase in heat flux at glowing ignition and that the negative temperature excess for the 12 and 15 kW/m^2 profiles show that the surface was hotter than the interior at glowing. Therefore, for these heat fluxes, ignition occurred at or near the surface. This is supported by the crossover times. The 12 kW/m^2 temperatures crossed over at about the same as glowing, while the 15 kW/m^2 temperatures crossed over 250 seconds after glowing was observed.

Examination of the 8 and 9 kW/m^2 profiles at glowing show a similar trend. For the 8 kW/m^2 profiles, the highest temperature excesses were at depths of 31 and 50%, while the highest temperature excesses for the 9 kW/m^2 profiles were at depths of 12 and 31%.

With higher heat fluxes, the role of self-heating diminishes and the applied heat flux is sufficient for ignition. The temperature data from the experiments at 15 kW/m^2 heat flux was insufficient to determine the relative contributions of incident heat flux and self-heating to the ignition process near the surface.

Conclusions

The unpiloted response of 1.8 cm maple plywood to radiant heat fluxes from 6 to 15 kW/m^2 in the cone calorimeter was investigated. The minimum heat flux for smoldering ignition was determined to be 7.5 kW/m^2 and compared favorably to a predicted minimum heat flux of 7.2 kW/m^2.

As expected, times to significant thermal events (minimum heating rate, subsurface temperature crossover and observed glowing) decreased with higher applied heat fluxes. The times ranged from several hundred seconds to many thousands of seconds. The minimum heating rate increased from zero for low heat flux inert heating to 0.23 °C/sec at 15 kW/m^2, the highest heat flux applied.

Evaluation of the thermal profiles showed that self-heating becomes an important mechanism for ignition as the incident heat flux decreases to a critical minimum. Ignition occurs below the surface and smolder propagates from the ignition depth towards the surface and into the specimen. The ignition depth was shown to vary with the applied heat flux. At high heat fluxes, ignition occurs at or near the surface. As the applied heat flux approaches the minimum for smoldering ignition, the ignition location was shown to move between 31 and 50% into the depth of the wood.

REFERENCES

[1] Bowes, P.C., Self-heating: Evaluating and Controlling the Hazard, Her Majesty's Stationery Office, London, 1984.

[2] Babrauskas, V., Ignition Handbook, Fire Science Publishers, Issaquah, WA, 2003.

[3] Smith, W.K. and King, J.B., "Surface Temperatures of Materials during Radiant Heating to Ignition," J. Fire and Flammability, Vol. 1, 1970.

[4] Martin, S.B., "Diffusion-Controlled Ignition of Cellulosic Materials by Intense Radiant Energy," *10th Symposium (International) on Combustion*, 1965, The Combustion Institute, pp. 877-896.

[5] Kanury, A.M., "Flaming Ignition of Solids," In The SFPE Handbook of Fire Protection Engineering, 3rd Ed., National Fire Protection Association, Quincy, MA, 2002.

[6] Moran, H.E. jr., "Effectiveness of Water Mists for Protection from Radiant Heat Ignition," NRL Report 5439, US Naval Research Laboratory, Washington, 1960.

[7] Shoub, H. and Bender, E.W., "Radiant Ignition of Wall Finish Materials in a Small Home," NBS 8172, National Bureau of Standards, Washington, DC, 1961.

[8] Koohyar, A.N., et al., "An Experimental Technique for the Ignition of Solids by Flame Irradiation," Fire Technology, Vol. 4, No. 3, 1968.

[9] Koohyar, A.N., et al., "The Irradiation and Ignition of Wood by Flame," Fire Technology, Vol. 4, No. 4, 1968.

[10] Koohyar, A.N., "Ignition of Wood by Flame Radiation," (PhD Dissertation), University of Oklahoma, Norman, 1967.

[11] Bilbao, R. et al., "Experimental and Theoretical Study of the Ignition and Smoldering of Wood Including Convective Effects," Combustion and Flame, Vol. 126, 2001.

[12] Spearpoint, M.J. and Quintiere, J.G., "Predicting the Piloted Ignition of Wood in the Cone Calorimeter Using an Integral Model," Fire Safety Journal, Vol. 36, No. 4, 2001.

[13] Spearpoint, M.J., "Predicting the Ignition and Burning Rate of Wood in the Cone Calorimeter Using an Integral Model," (Masters Thesis), University of Maryland, College Park, 1999.

[14] Boonmee, N. and Quintiere, J.G., "Glowing and Flaming Autoignition of Wood," *29th Symposium (International) on Combustion*, 2002, The Combustion Institute, pp. 289-296.

[15] Babrauskas, V., "Development of the Cone Calorimeter," Fire and Materials, Vol. 8, No. 2, 1984.

[16] "ASTM E 1354-02: Standard Test Method for Heat and Visible Smoke Release rates for Materials and Products Using an Oxygen Consumption Calorimeter," ASTM International, West Conshohocken, PA, 2002.

[17] DeHaan, J.D., Kirk's Fire Investigation, 4th Edition, Prentice-Hall, Inc., Upper Saddle River, New Jersey, 1997.

[18] Babrauskas, V., "Ignition of Wood, A Review of the State of the Art," Journal of Fire Protection Engineering, Vol. 12, , 2002.

[19] Beever, P.F., "Self-heating and Spontaneous Combustion," In The SFPE Handbook of Fire Protection Engineering, 3rd Ed., National Fire Protection Association, Quincy, MA, 2002.

[20] Chong, L.V., Shaw, I.R, and Chen, X.D., "Thermal Ignition Kinetics of Wood Sawdust Measured by a Newly Devised Experimental Technique," Process Safety Progress, Vol. 14, No. 4, 1995.

[21] Atreya, A., "Pyrolysis, Ignition and Fire Spread on Horizontal Surfaces of Wood," (PhD Dissertation), Harvard University, Cambridge, MA, 1983.

[22] Atreya, A, "Convection Heat Transfer," In The SFPE Handbook of Fire Protection Engineering, 3rd Ed., National Fire Protection Association, Quincy, MA, 2002.

[23] Holman, J.P., Heat Transfer, Ninth Edition, McGraw Hill, New York, 2002.

[24] Cuzzillo, B.R., “Pyrophoria,” (PhD Dissertation), University of California at Berkeley, Berkeley, CA, 1997.

APPENDIX B - TIME-TEMPERATURE PROFILES

Data from individual thermocouples and the optical pyrometer is presented as a moving average over a time period as specified on each plot. The moving average encompasses multiple raw data points. Table B-1 lists the recording frequency of the raw data as well as the moving average period.

Table B-1 – Data recording frequency and moving average period

Heat Flux (kW/m^2)	Specimen#	Raw Data Recording Frequency (sec)	Moving Average Period (sec)
6	31	5	30
7	23	5	20
7	24	5	20
8	19	2	10
8	20	5	20
9	21	5	20
9	22	5	20
9	30	2	10
10	17	2	10
10	18	2	10
12	15	1	10
12	16	1	10
15	14	1	10
15	28	1	10

Legend Description

(Orientations are given for the specimen placed in the cone and the observer standing in front looking down at the sample. Thus a location described as "right front" indicates the location is to the right of center and nearer the observer. For further specification of locations see Appendix A.)

Op_Py – Optical pyrometer

#.#mm – Thermocouple was mounted at #.# mm below sample surface

(TRF) – Surface mounted thermocouple at the right front of the sample

(TLB) – Surface mounted thermocouple at the left back of the sample

(1LM) – Thermocouple mounted in the first ply layer at the left middle of the sample

(1RM) – Thermocouple mounted in the first ply layer at the right middle of the sample

(2BR) – Thermocouple mounted in the second ply layer at the back right of the sample

(2FL) – Thermocouple mounted in the second ply layer at the front left of the sample

(3RB) – Thermocouple mounted in the third ply layer at the right back of the sample

(3LF) – Thermocouple mounted in the third ply layer at the left front of the sample

(4BL) – Thermocouple mounted in the fourth ply layer at the back left of the sample

(4FR) – Thermocouple mounted in the third ply layer at the front right of the sample

(BF) – Thermocouple mounted at the center of the sample between the back face and the insulation

(HB) – Thermocouple mounted at the center of the sample between the bottom of the steel holder and plate of the load cell

Time Temperature Profiles

6 kW/m^2 Heat Flux (1):

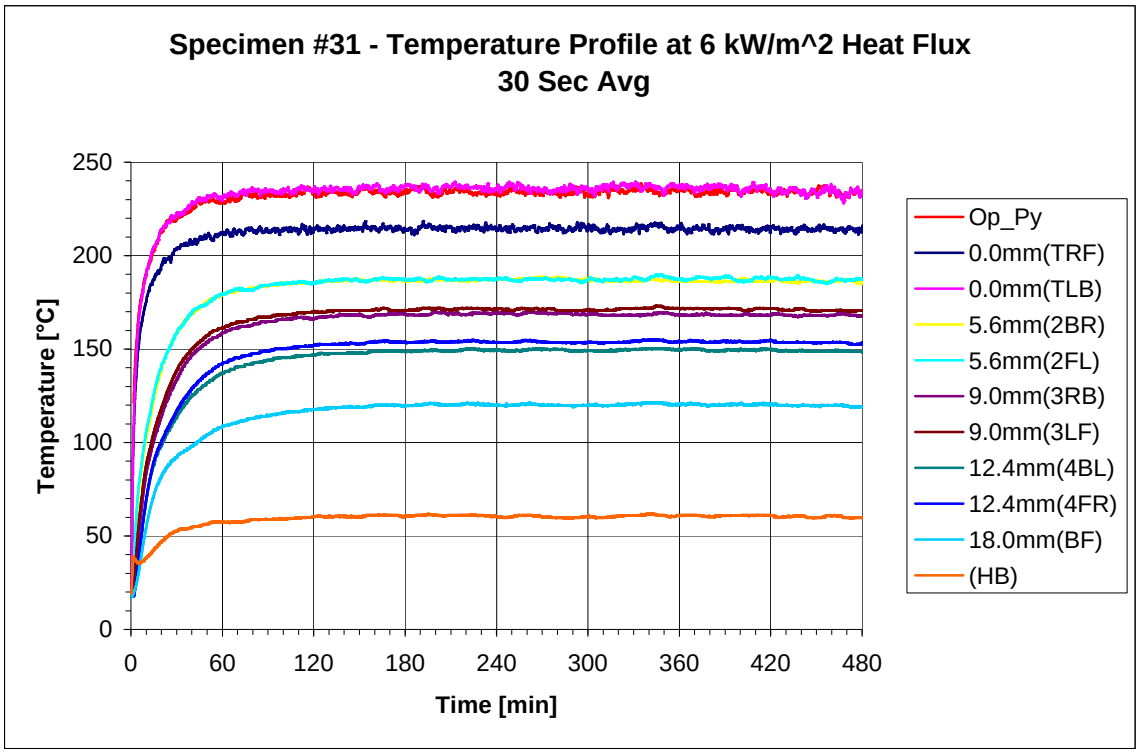

Figure B-1 – Time-temperature history of specimen #31, exposed to a 6 kW/m^2 heat flux.

7 kW/m^2 Heat Flux (2):

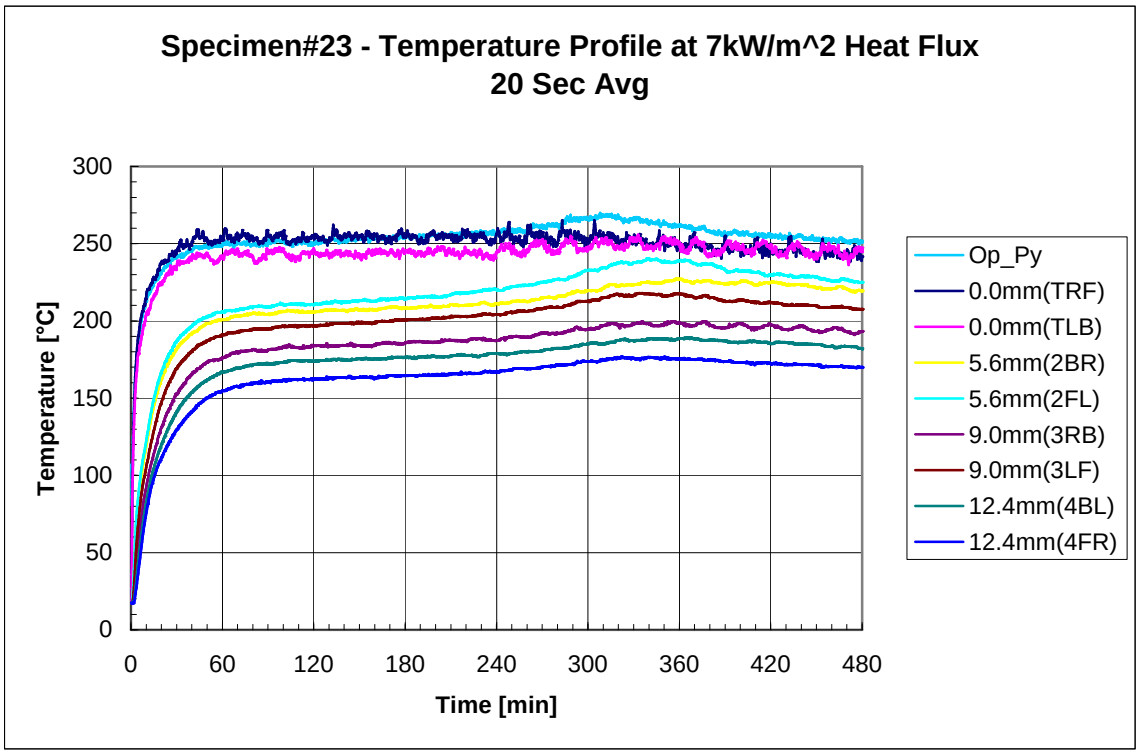

Figure B-2 – Time-temperature history of specimen #23, exposed to a 7 kW/m^2 heat flux.

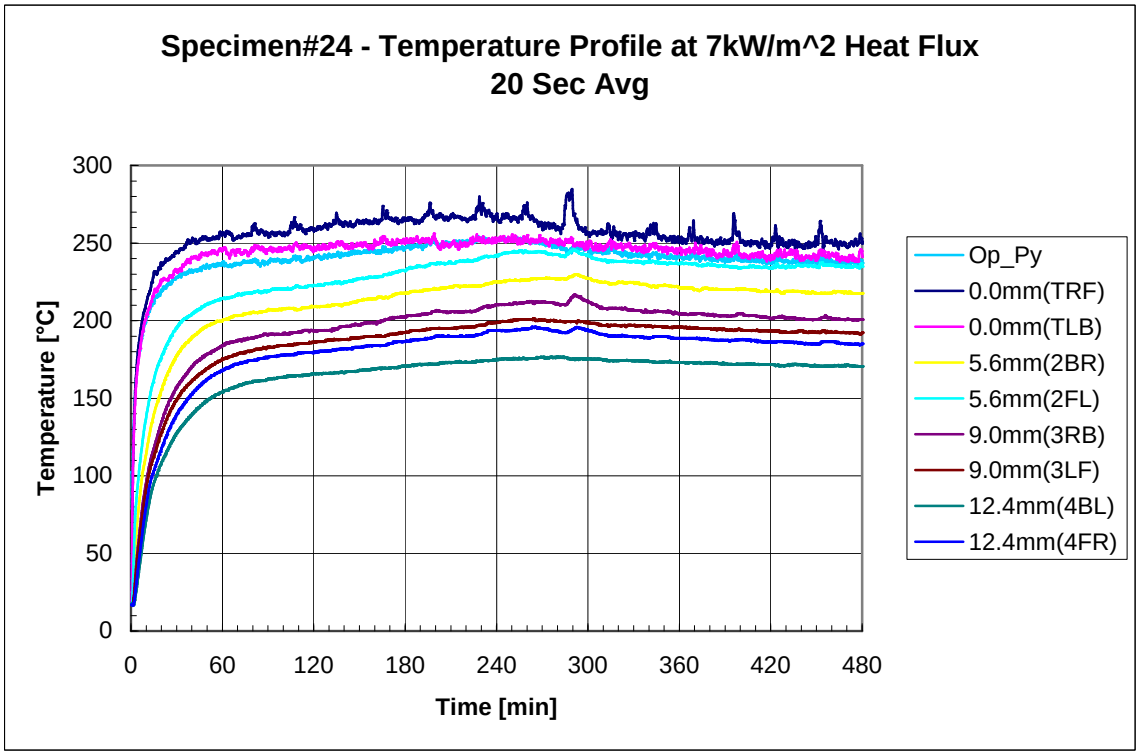

Figure B-3 – Time-temperature history of specimen #24, exposed to a 7 kW/m^2 heat flux.

8 kW/m^2 Heat Flux (2):

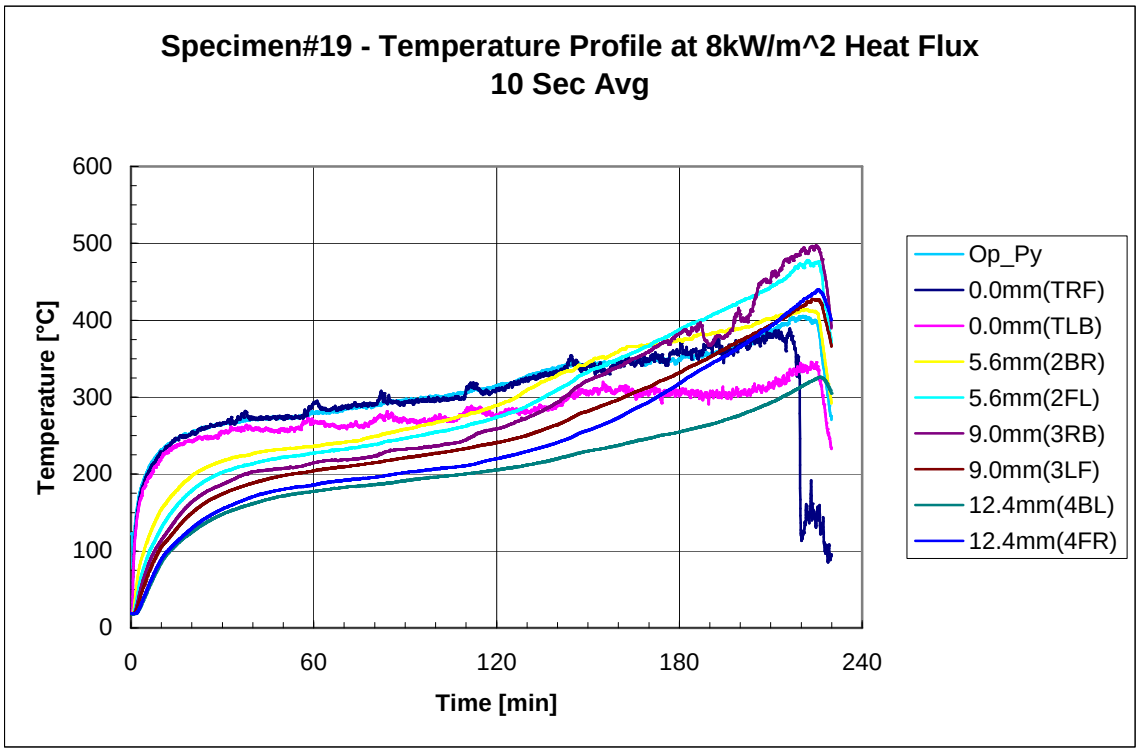

Figure B-4 – Time-temperature history of specimen #19, exposed to an 8 kW/m^2 heat flux.

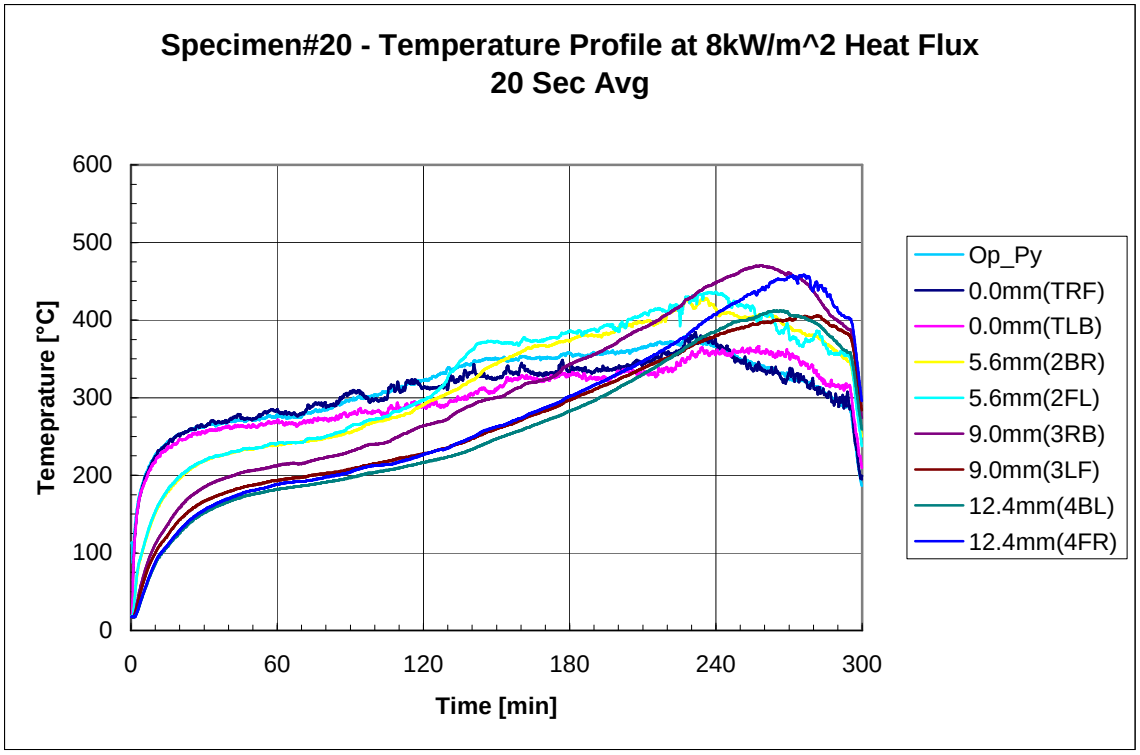

Figure B-5 – Time-temperature history of specimen #20, exposed to an 8 kW/m^2 heat flux.

9 kW/m^2 Heat Flux (3):

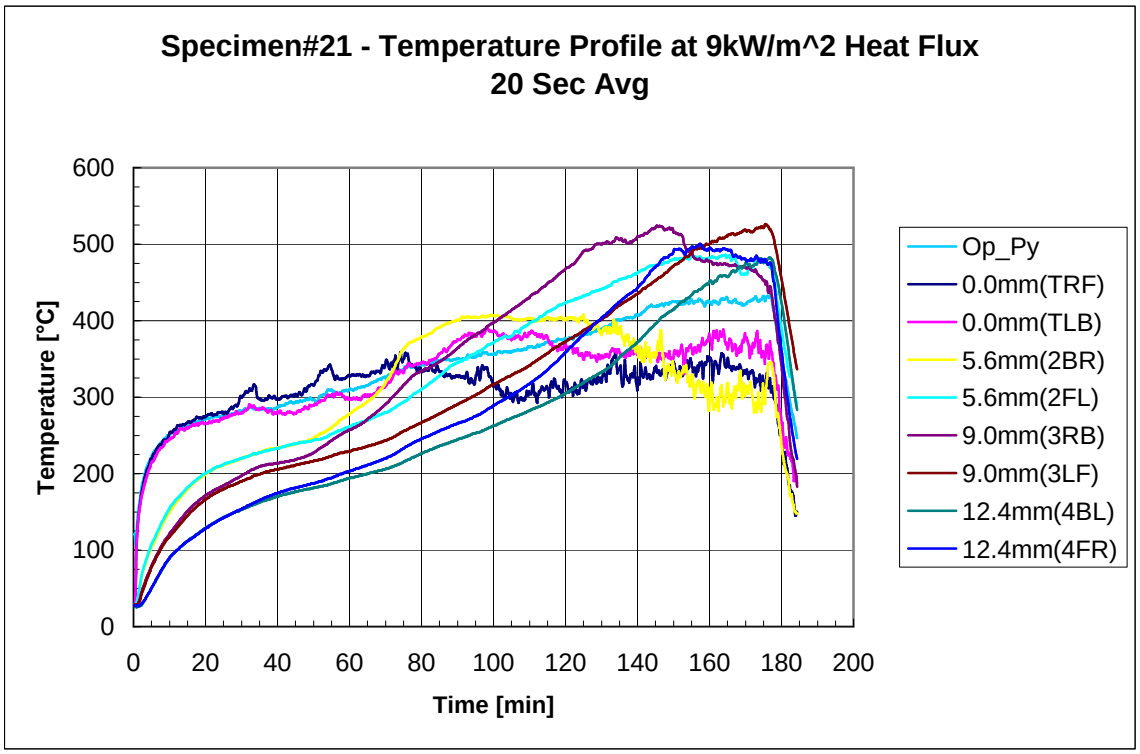

Figure B-6 – Time-temperature history of specimen #21, exposed to a 9 kW/m^2 heat flux.

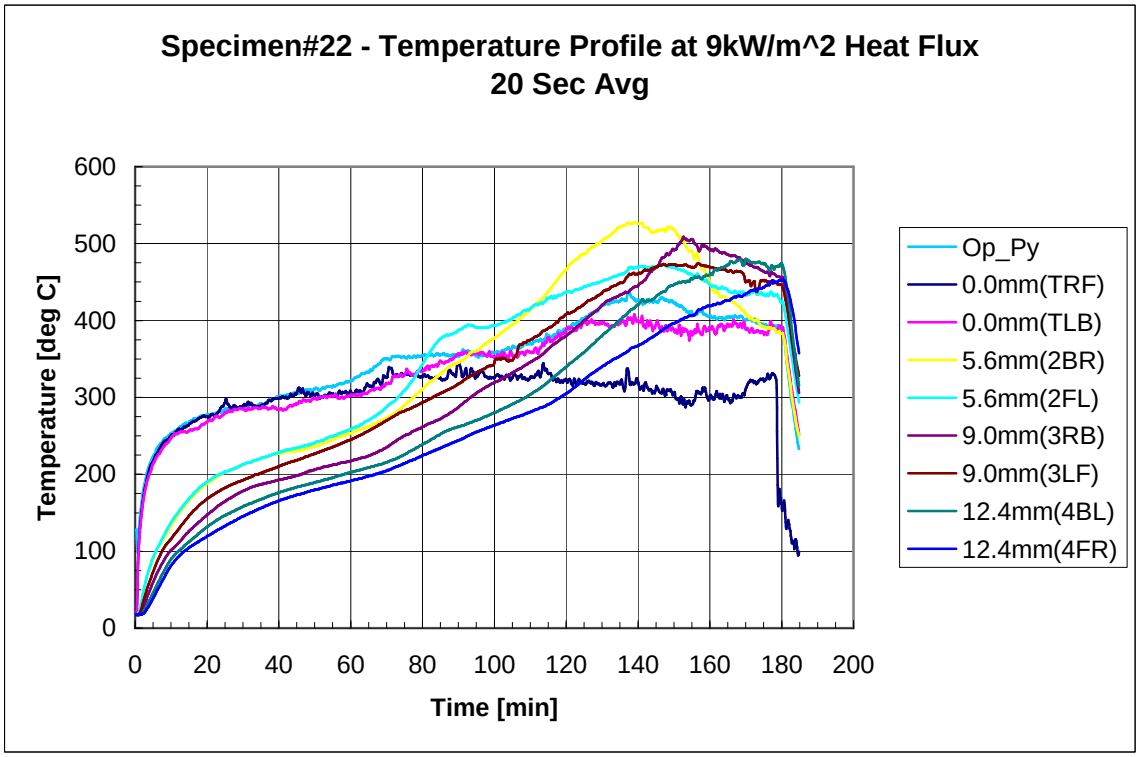

Figure B-7 – Time-temperature history of specimen #22, exposed to a 9 kW/m^2 heat flux.

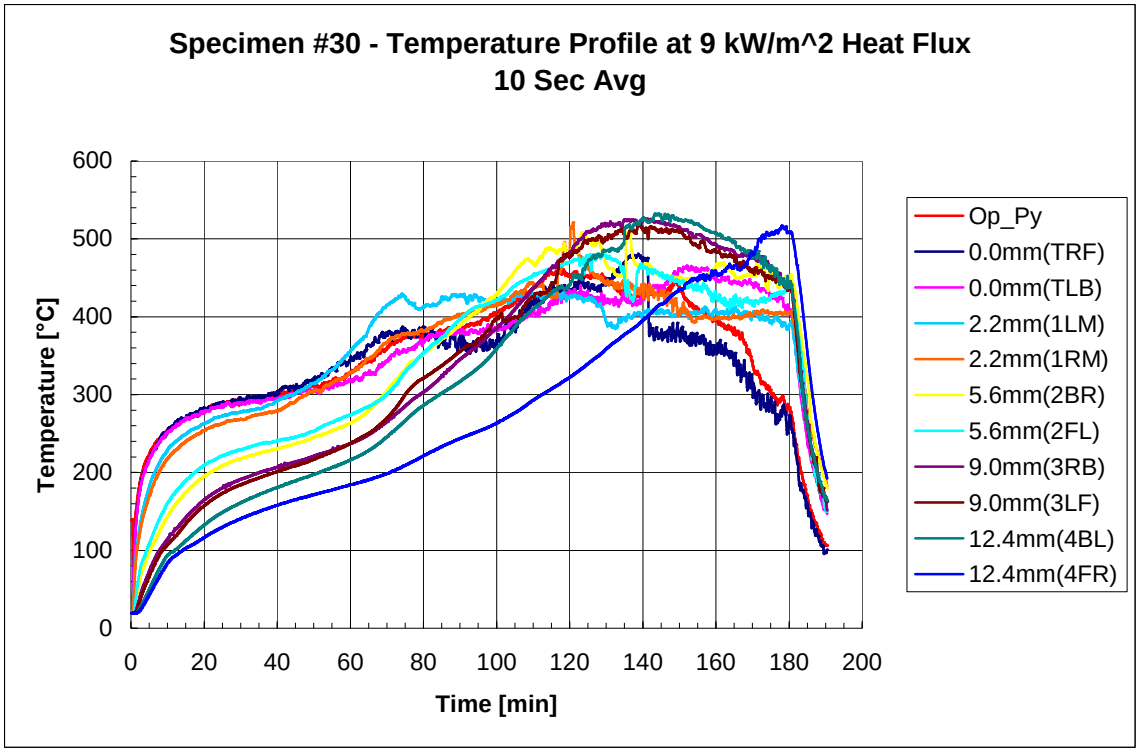

Figure B-8 – Time-temperature history of specimen #30, exposed to a 9 kW/m^2 heat flux.

10 kW/m^2 Heat Flux (2):

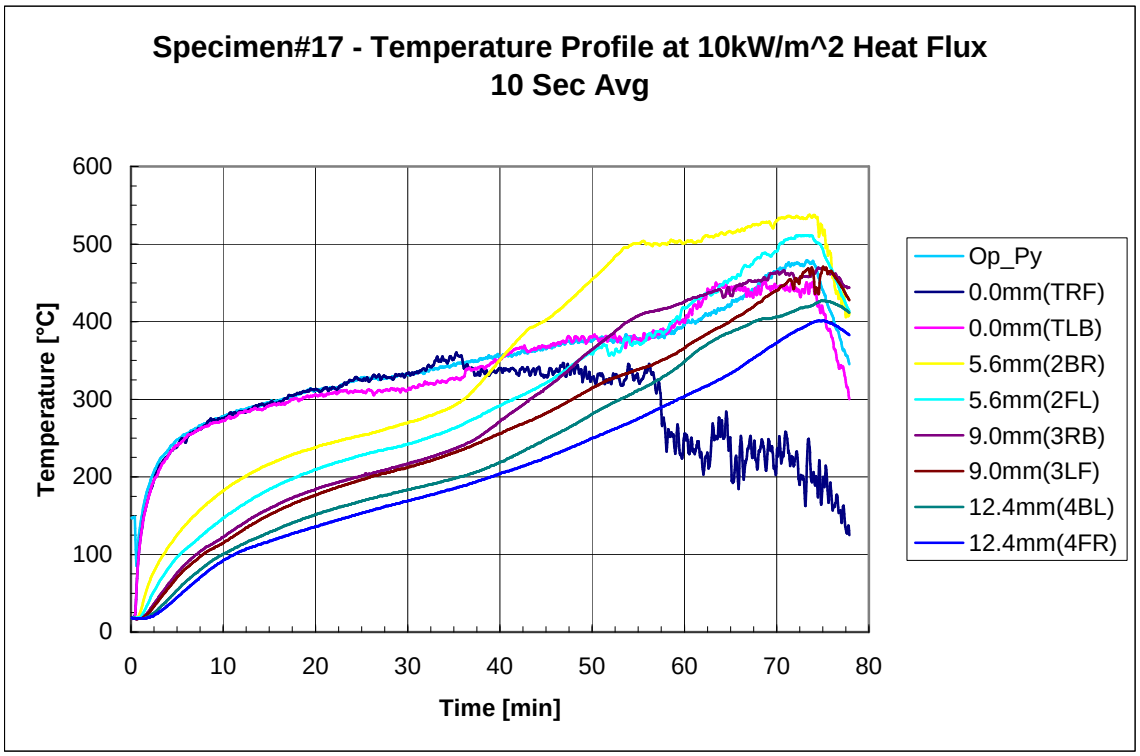

Figure B-9 – Time-temperature history of specimen #17, exposed to a 10 kW/m^2 heat flux.

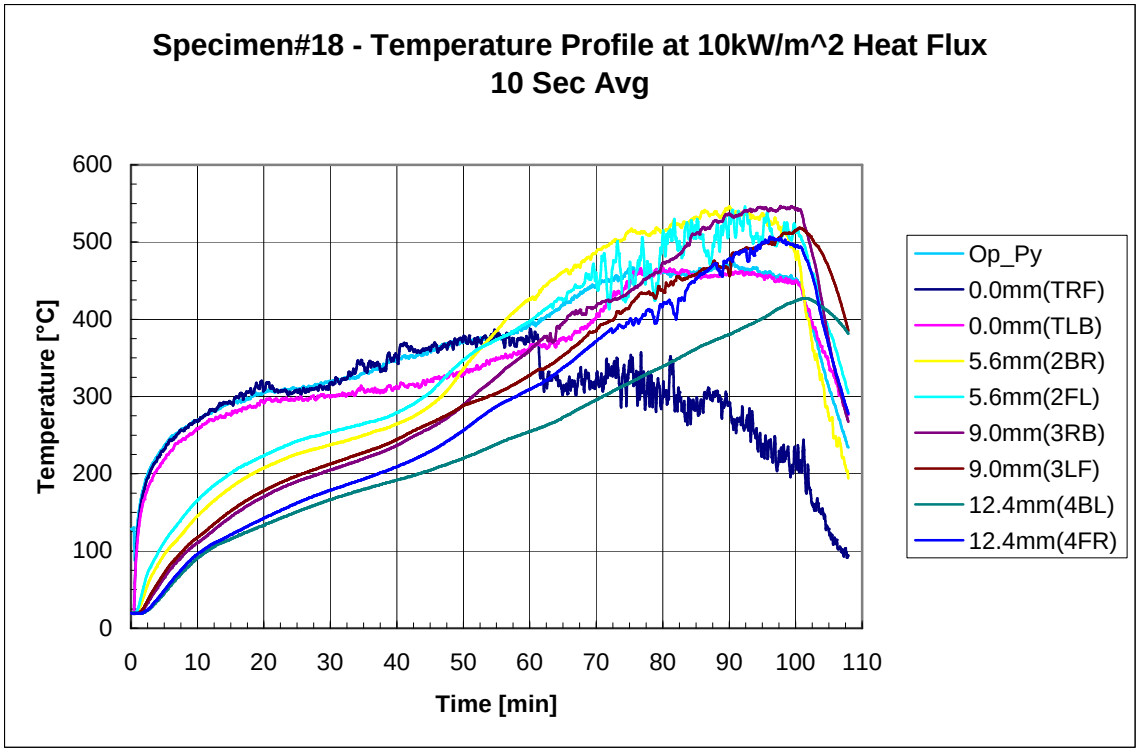

Figure B-10 – Time-temperature history of specimen #18, exposed to a 10 kW/m^2 heat flux.

12 kW/m^2 Heat Flux (2):

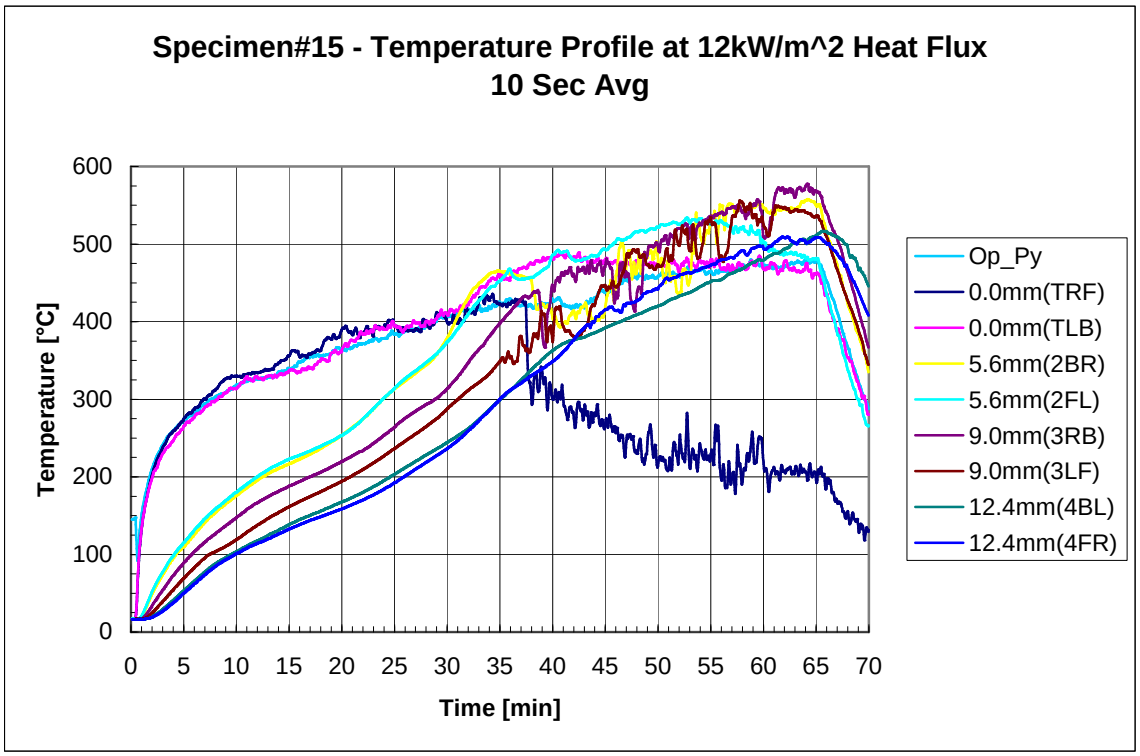

Figure B-11 – Time-temperature history of specimen #15, exposed to a 12 kW/m^2 heat flux.

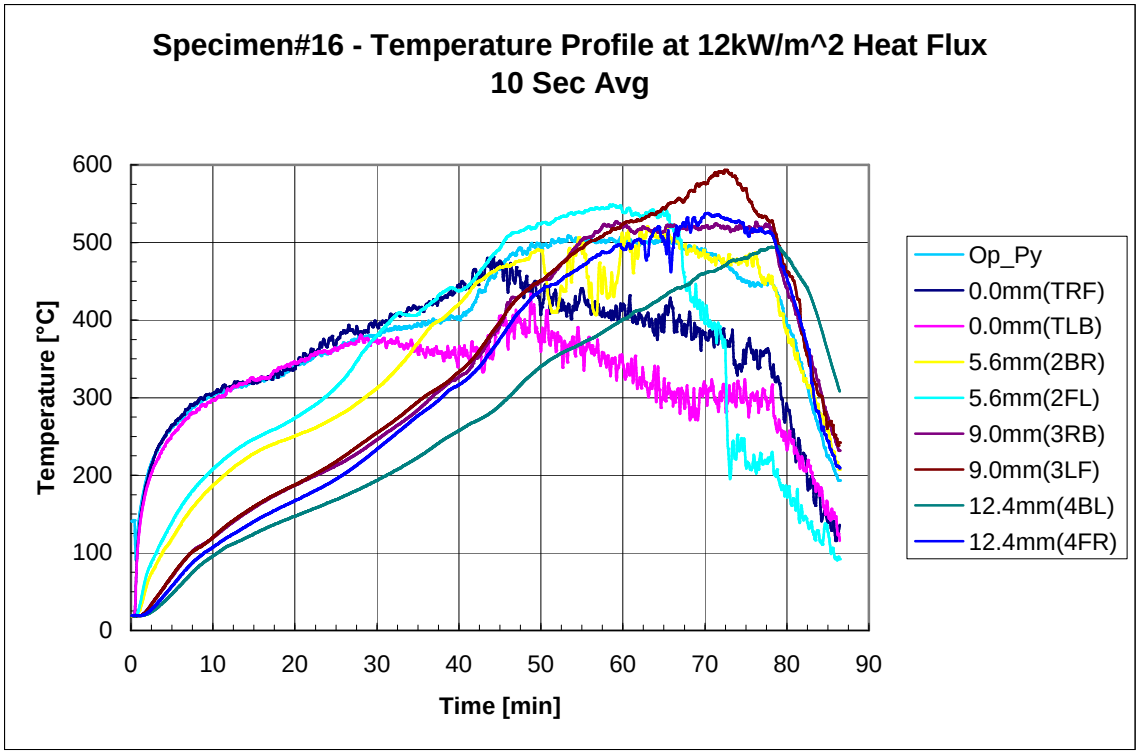

Figure B-12 – Time-temperature history of specimen #16, exposed to a 12 kW/m^2 heat flux.

15 kW/m^2 Heat Flux (2):

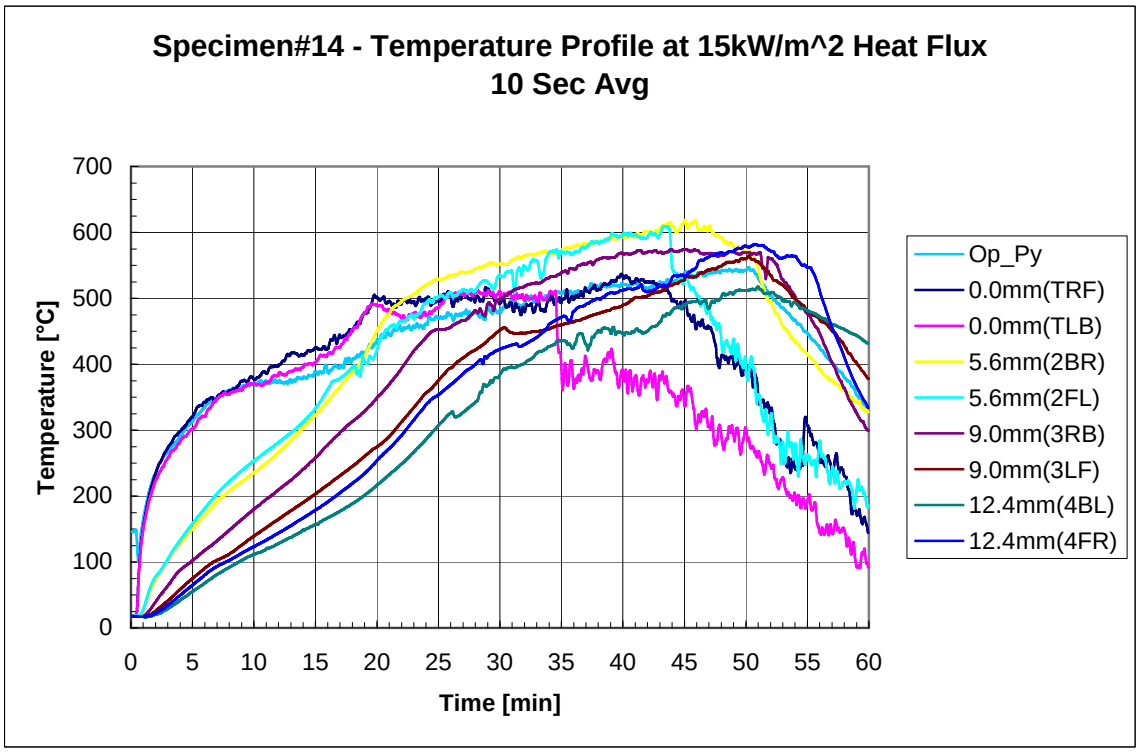

Figure B-13 – Time-temperature history of specimen #14, exposed to a 15 kW/m^2 heat flux.

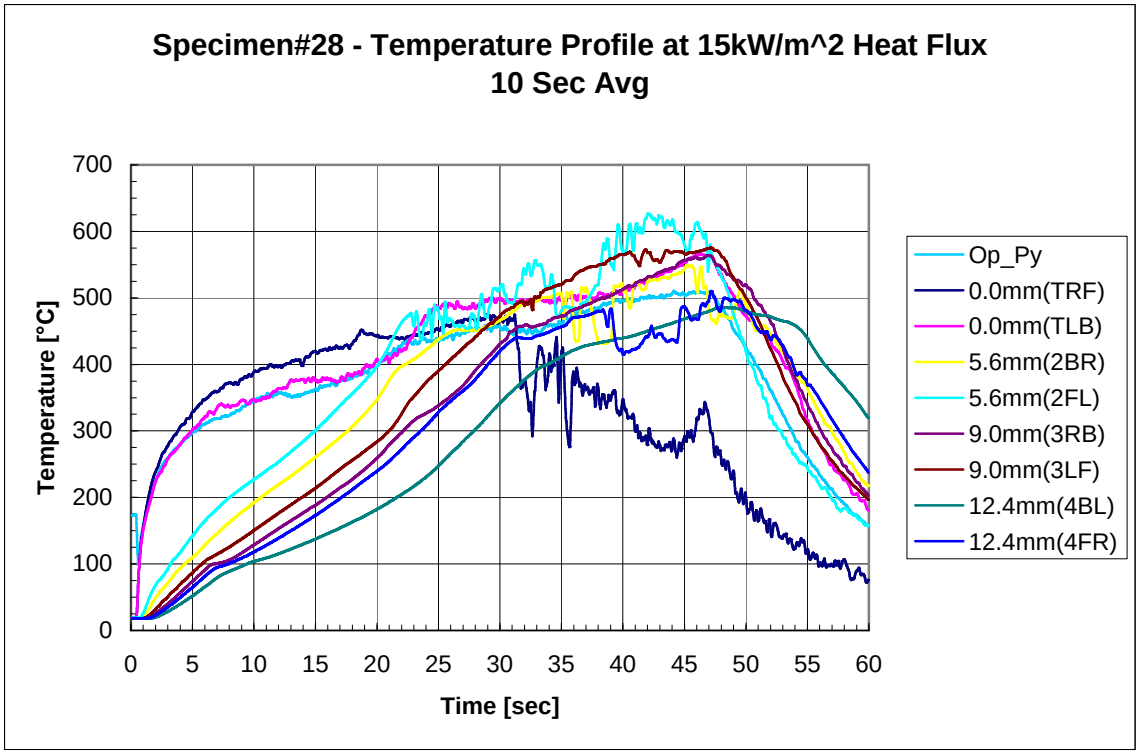

Figure B-14 – Time-temperature history of specimen #28, exposed to a 15 kW/m^2 heat flux.

APPENDIX C - TIME-RATE OF TEMPERATURE CHANGE PROFILES

The rate of temperature changes at a given time, $\dot{T}$, was calculated from the numerical differentiation of the moving average temperature of each thermocouple or optical pyrometer, $\overline{T}$, and is of the form,

$$\dot{T}_t = \left(\overline{T}_{t-2\Delta t} - 8\overline{T}_{t-\Delta t} + 8\overline{T}_{t+\Delta t} - \overline{T}_{t+2\Delta t}\right)/(12\,\Delta t).$$

Table C-1 lists the moving average period for both the temperature and rate of temperature change.

Table C-1 –Moving average period used to calculate rate of temperature change.

Heat Flux (kW/m^2)	Specimen#	Moving Average Period (sec)
6	31	120
7	23	120
7	24	120
8	19	120
8	20	120
9	21	60
9	22	60
9	30	60
10	17	60
10	18	60
12	15	30
12	16	30
15	14	30
15	28	30

<u>Legend Description</u>

(Orientations are given for the specimen placed in the cone and the observer standing in front looking down at the sample. Thus a location described as “right front” indicates the location is to the right of center and nearer the observer. For further specification of locations see Appendix A.)

Op_Py – Optical pyrometer

#.#mm – Thermocouple was mounted at #.# mm below sample surface

(TRF) – Surface mounted thermocouple at the right front of the sample

(TLB) – Surface mounted thermocouple at the left back of the sample

(1LM) – Thermocouple mounted in the first ply layer at the left middle of the sample

(1RM) – Thermocouple mounted in the first ply layer at the right middle of the sample

(2BR) – Thermocouple mounted in the second ply layer at the back right of the sample

(2FL) – Thermocouple mounted in the second ply layer at the front left of the sample

(3RB) – Thermocouple mounted in the third ply layer at the right back of the sample

(3LF) – Thermocouple mounted in the third ply layer at the left front of the sample

(4BL) – Thermocouple mounted in the fourth ply layer at the back left of the sample

(4FR) – Thermocouple mounted in the third ply layer at the front right of the sample

(BF) – Thermocouple mounted at the center of the sample between the back face and the insulation

(HB) – Thermocouple mounted at the center of the sample between the bottom of the steel holder and plate of the load cell

Time Rate of Temperature Change Profiles

6 kW/m^2 Heat Flux (1):

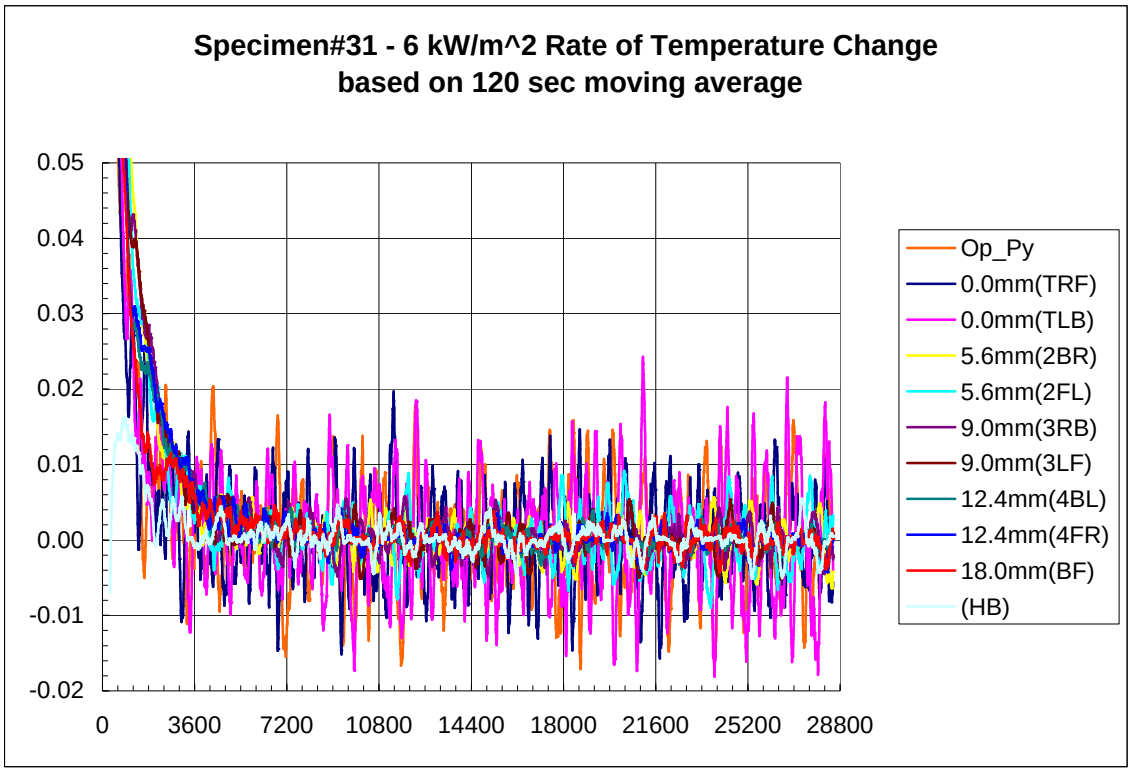

Figure C-1 – Time Rate of Temperature change for Specimen #31 exposed to a 6 kW/m^2 heat flux.

7 kW/m^2 Heat Flux (2):

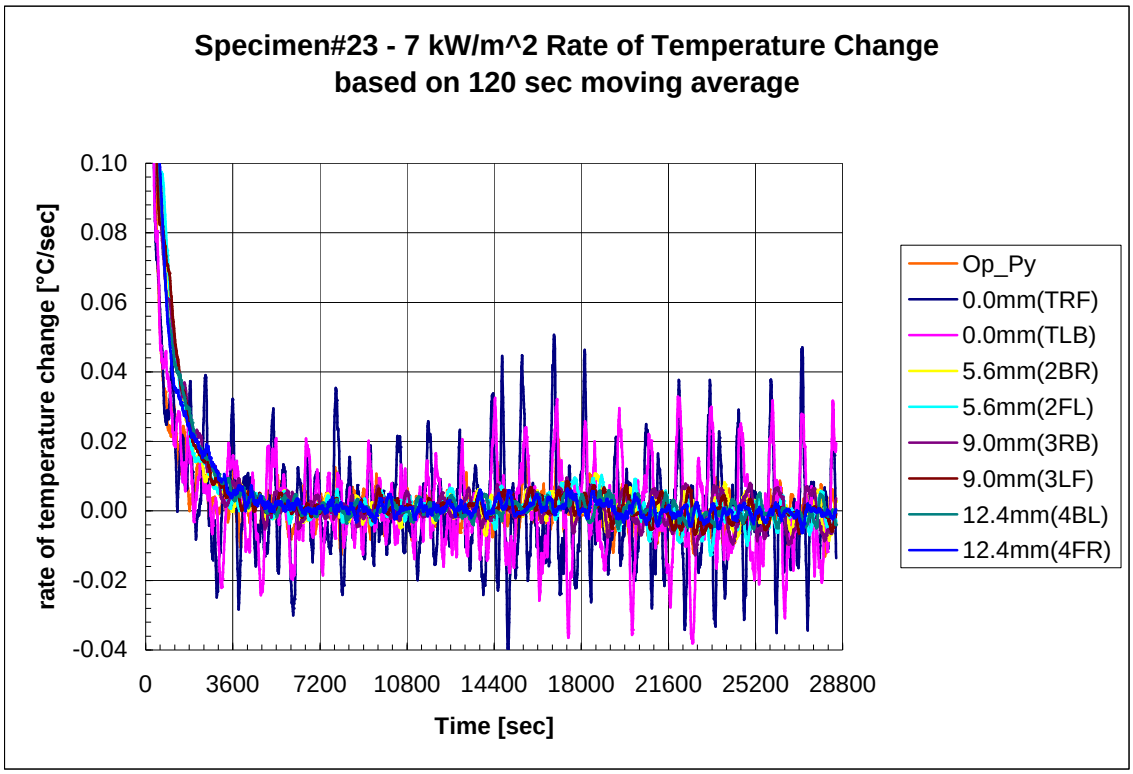

Figure C-2 – Time Rate of Temperature change for Specimen #23 exposed to a 7 kW/m^2 heat flux.

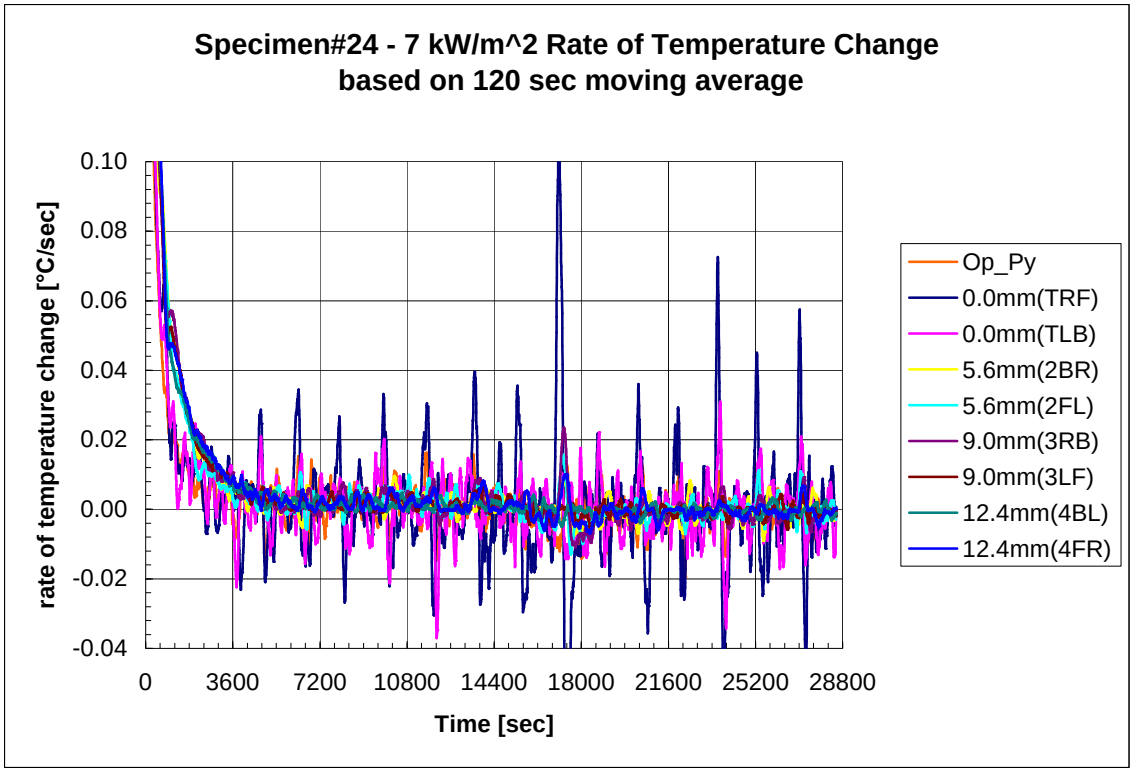

Figure C-3 – Time Rate of Temperature change for Specimen #24 exposed to a 7 kW/m^2 heat flux.

8 kW/m^2 Heat Flux (2):

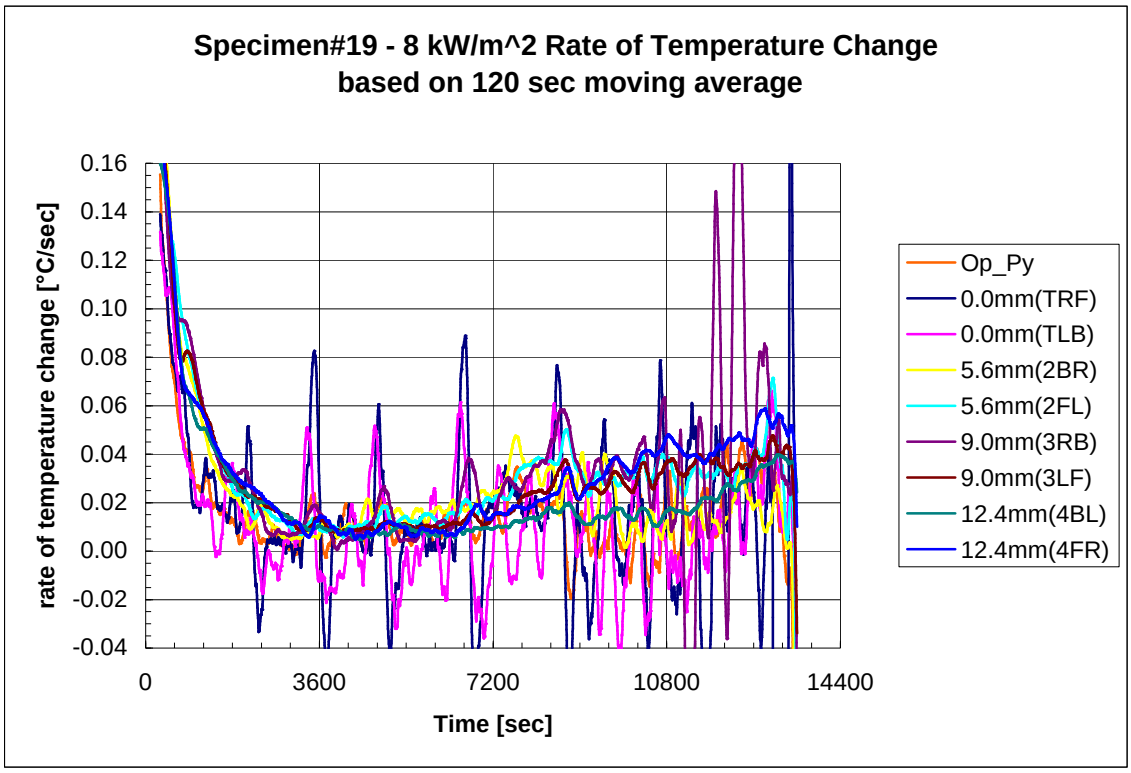

Figure C-4 – Time Rate of Temperature change for Specimen #19 exposed to an 8 kW/m^2 heat flux.

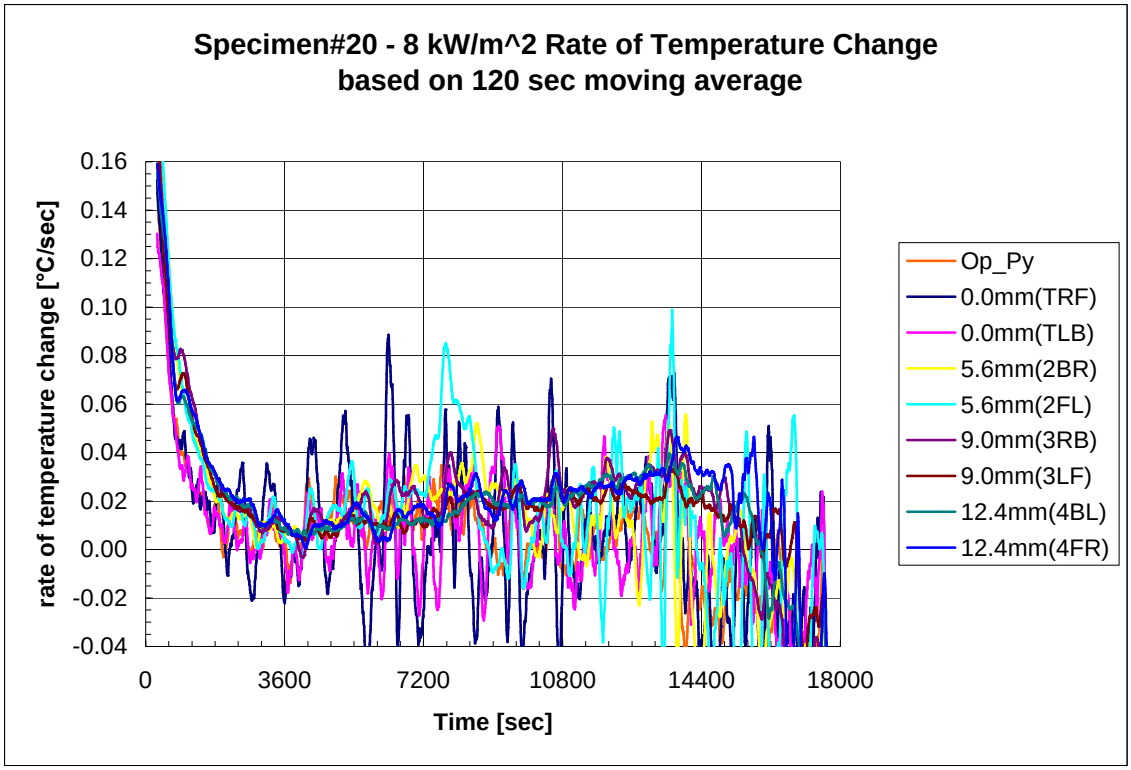

Figure C-5 – Time Rate of Temperature change for Specimen #20 exposed to an 8 kW/m^2 heat flux.

9 kW/m^2 Heat Flux (3):

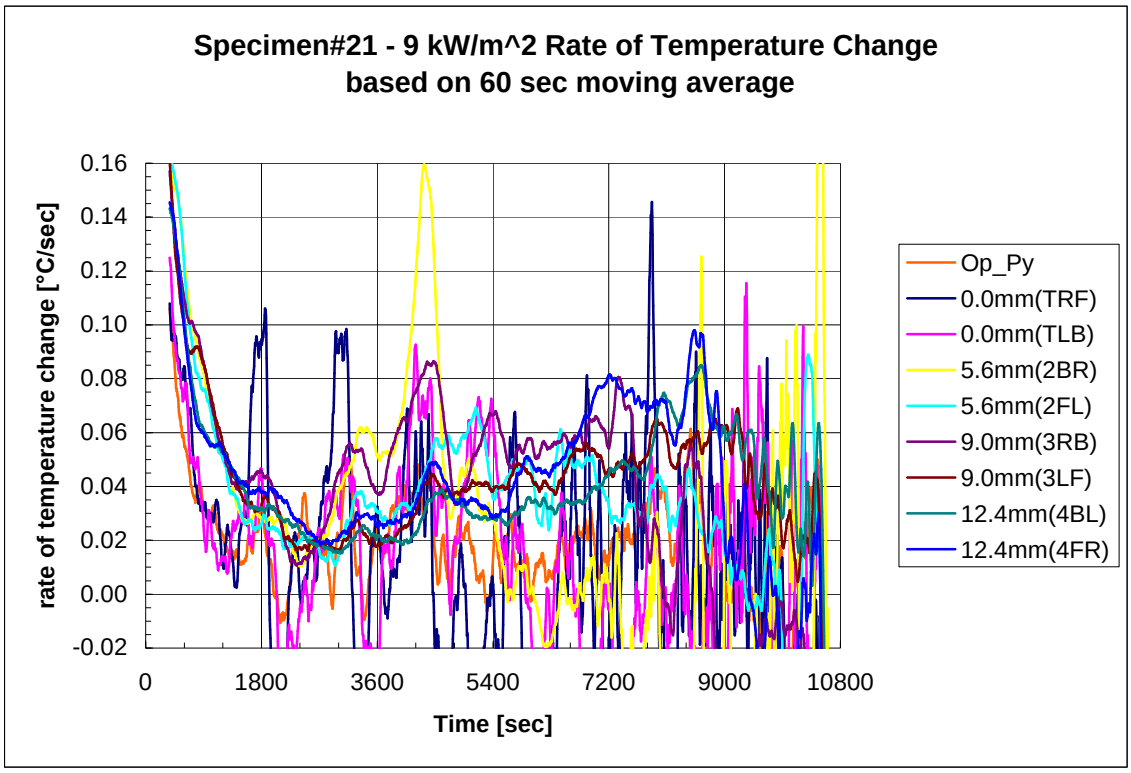

Figure C-6 – Time Rate of Temperature change for Specimen #21 exposed to a 9 kW/m^2 heat flux.

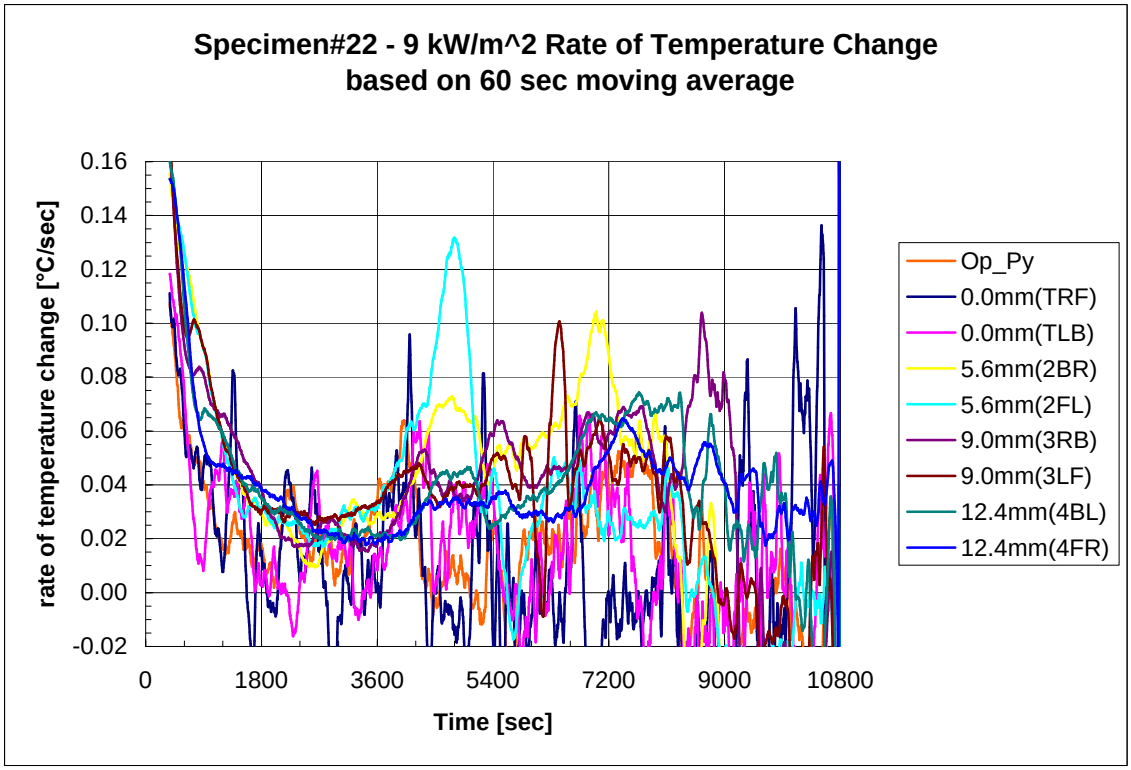

Figure C-7 – Time Rate of Temperature change for Specimen #22 exposed to a 9 kW/m^2 heat flux.

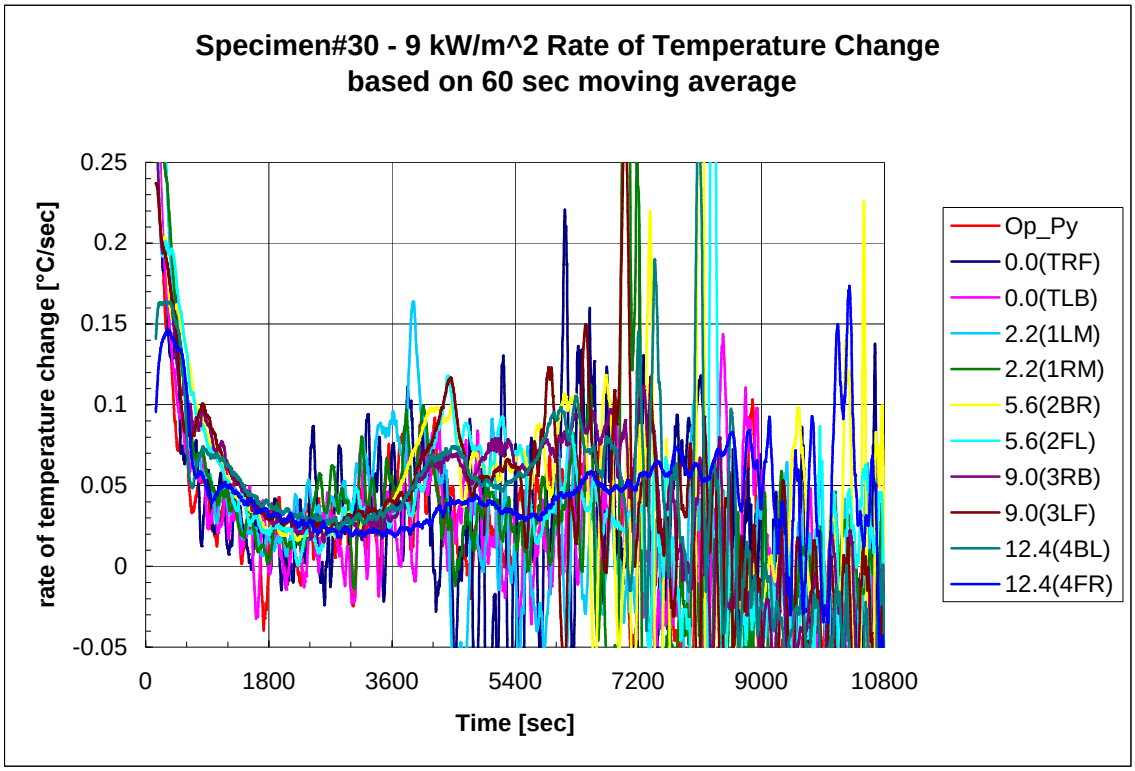

Figure C-8 – Time Rate of Temperature change for Specimen #30 exposed to a 9 kW/m^2 heat flux.

10 kW/m^2 Heat Flux (2):

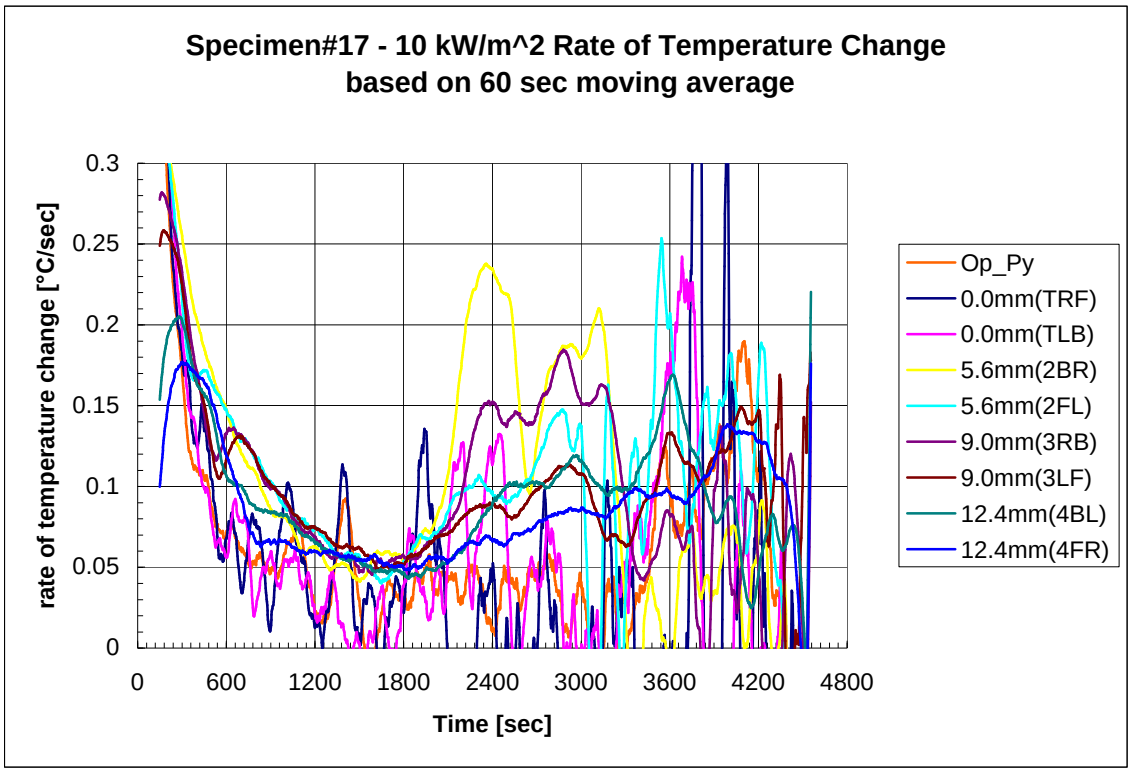

Figure C-9 – Time Rate of Temperature change for Specimen #17 exposed to a 10 kW/m^2 heat flux.

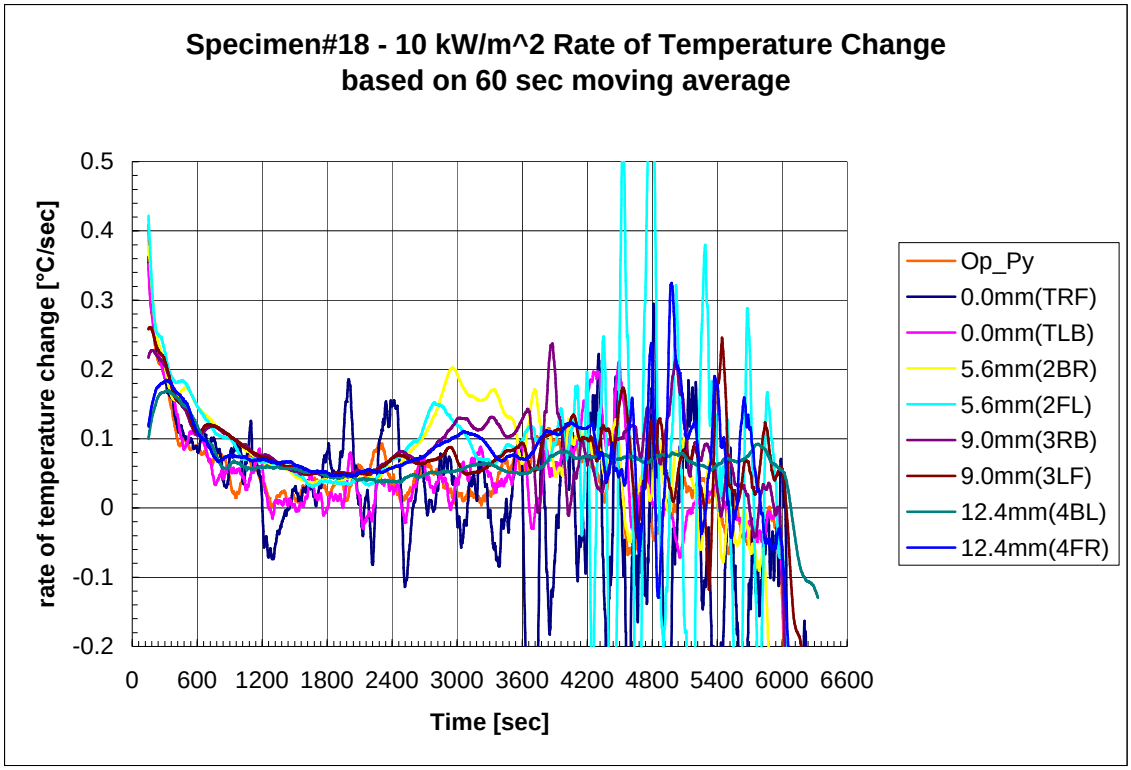

Figure C-10 – Time Rate of Temperature change for Specimen #18 exposed to a 10 kW/m^2 heat flux.

12 kW/m^2 Heat Flux (2):

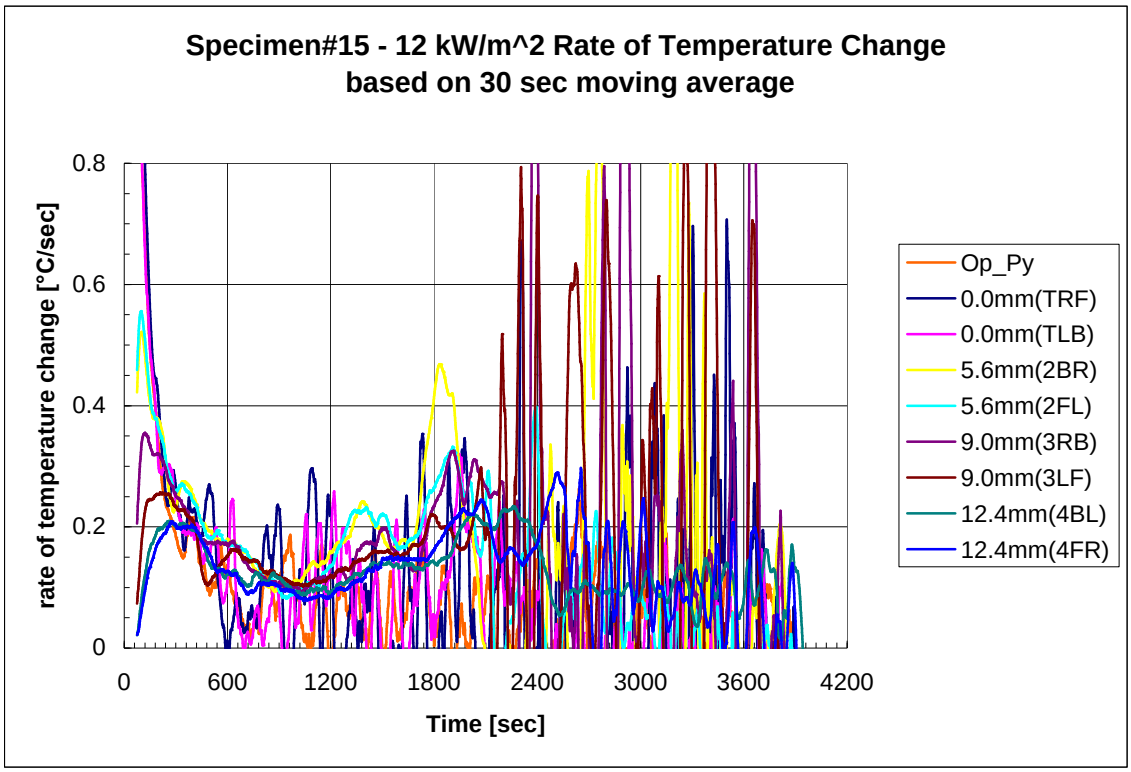

Figure C-11 – Time Rate of Temperature change for Specimen #15 exposed to a 12 kW/m^2 heat flux.

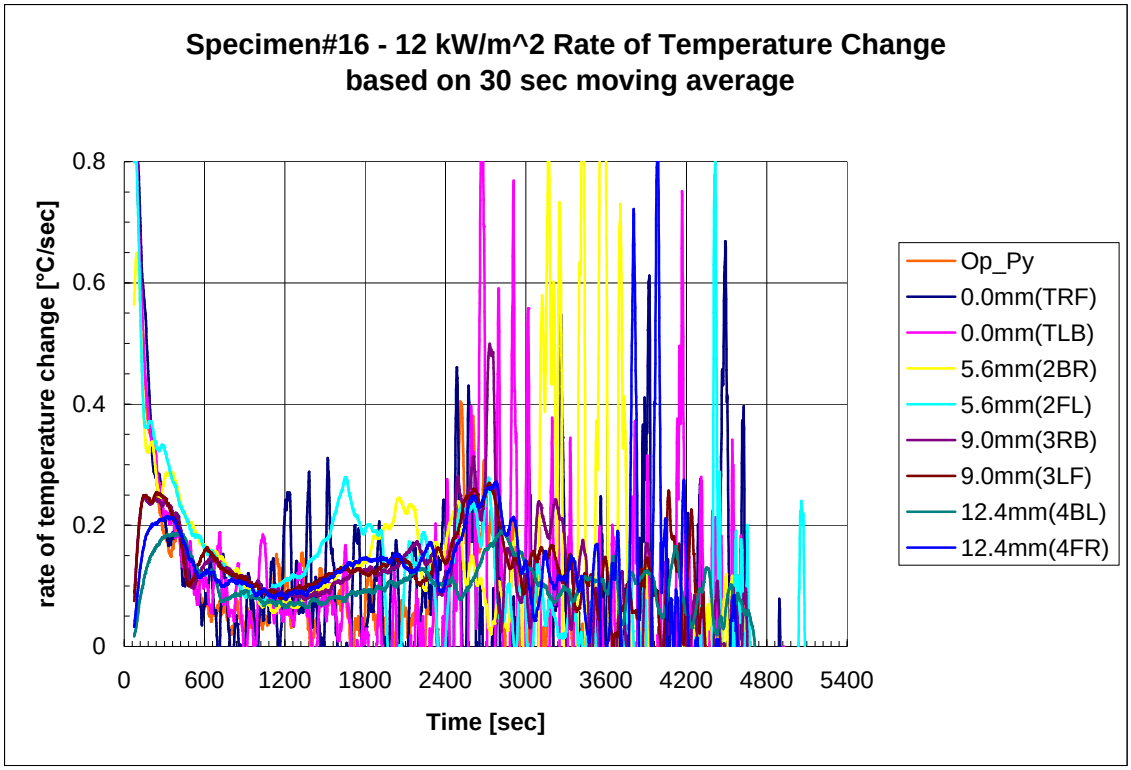

Figure C-12 – Time Rate of Temperature change for Specimen #16 exposed to a 12 kW/m^2 heat flux.

15 kW/m^2 Heat Flux (2):

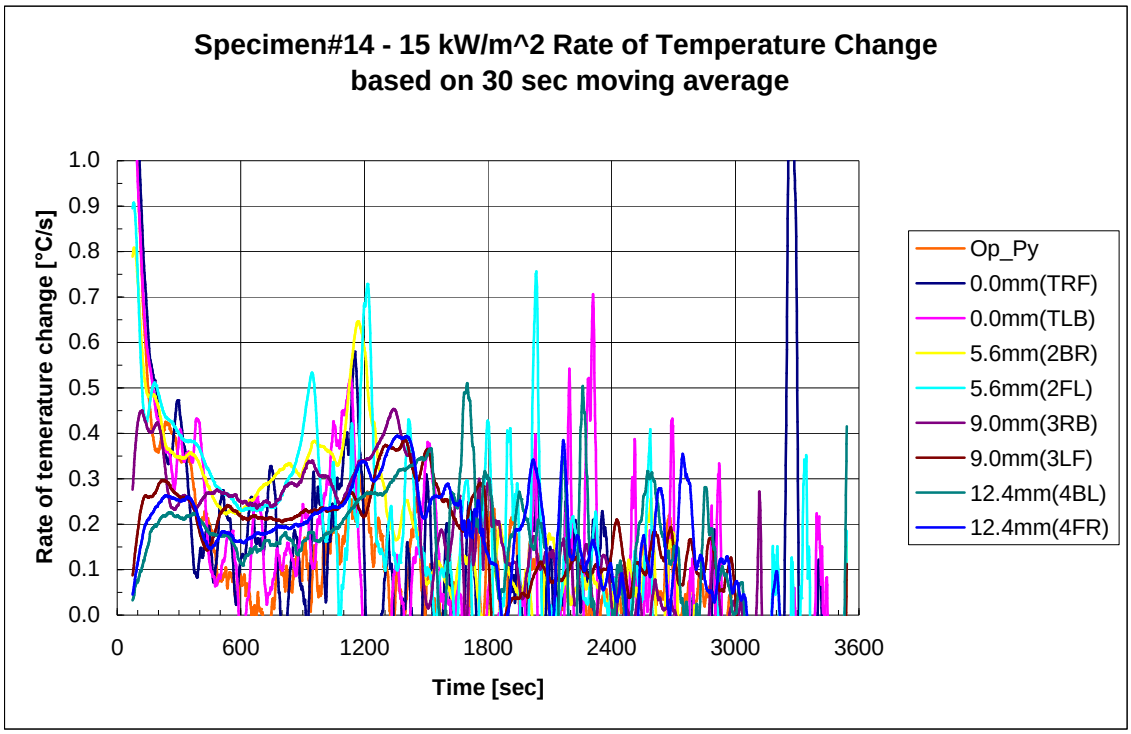

Figure C-13 – Time Rate of Temperature change for Specimen #14 exposed to a 15 kW/m^2 heat flux.

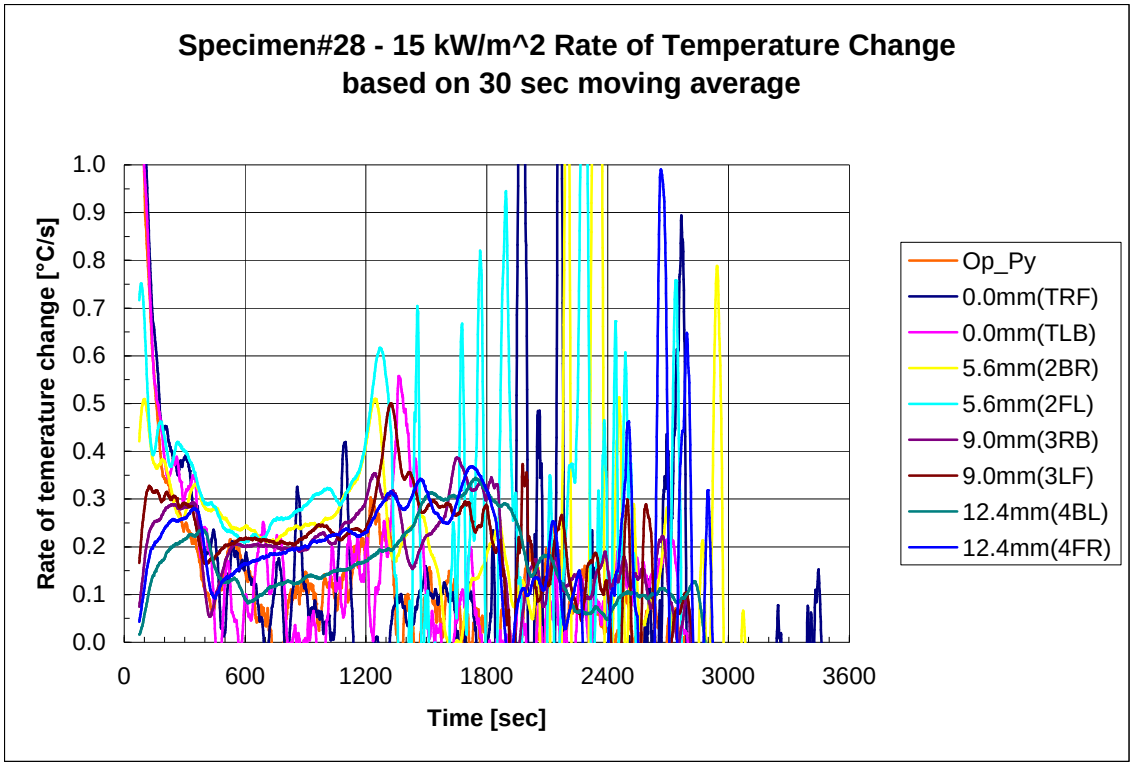

Figure C-14 – Time Rate of Temperature change for Specimen #28 exposed to a 15 kW/m^2 heat flux.

APPENDIX D – IGNITION TESTS THERMAL PROFILES

For each specimen exposed to a heat flux of 8 to 15 kW/m^2, the thermal profile is shown at the time of each of the following ignition criteria: time to observed glowing, time to 400°C, 370°C, 350°C, time to 5.6 mm depth thermocouple matches surface temperature and time to predominant self-heating. The depths are presented as non-dimensional depths below the surface based on the overall specimen thickness of 18 mm. The moving average period for the temperature is the same as for Appendix C. Both actual temperatures and non-dimensional temperatures are presented. The non-dimensional temperatures are relative to the surface temperature at the time of the ignition criteria. Overall thermal profiles for a heat flux take the conditions for individual specimen at a particular criterion and average those temperatures with the other specimen at that heat flux.

Legend Description

The numbers in the legend are the times in seconds and the corresponding Fourier numbers at which the criteria were achieved.

Thermal Profiles – Temperatures °C

8 kW/m^2 Heat Flux (2):

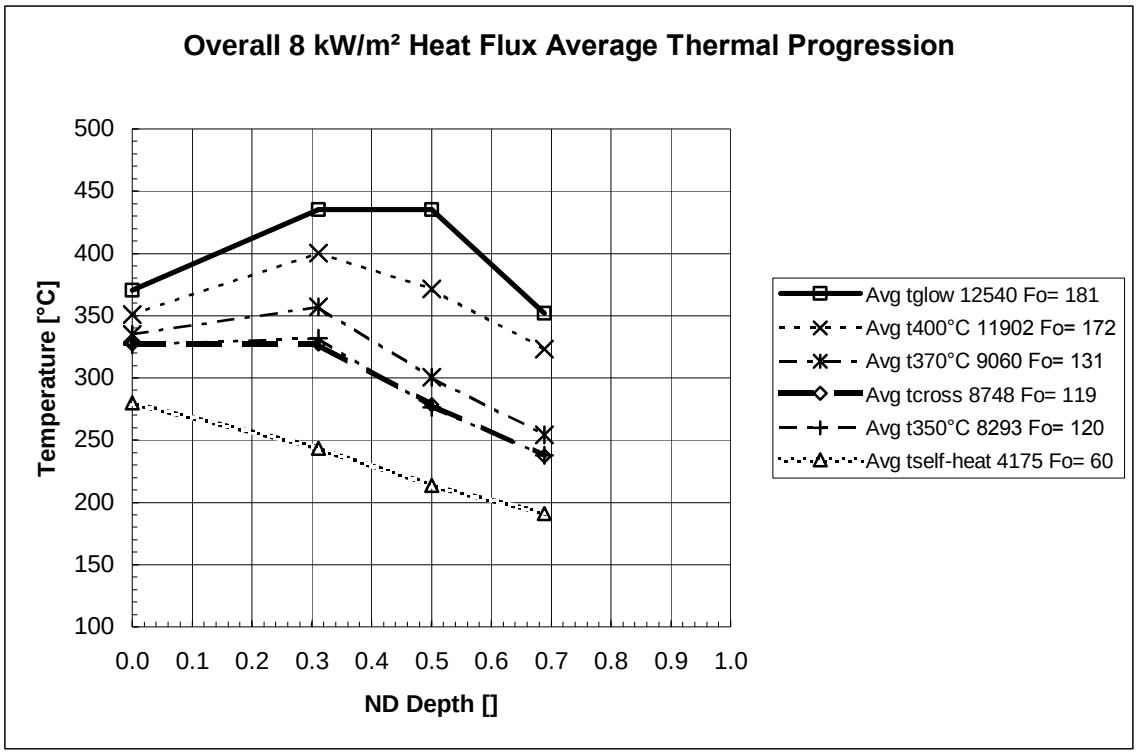

Figure D-1 – Average thermal profile progression for specimen subjected to an 8 kW/m^2 heat flux.

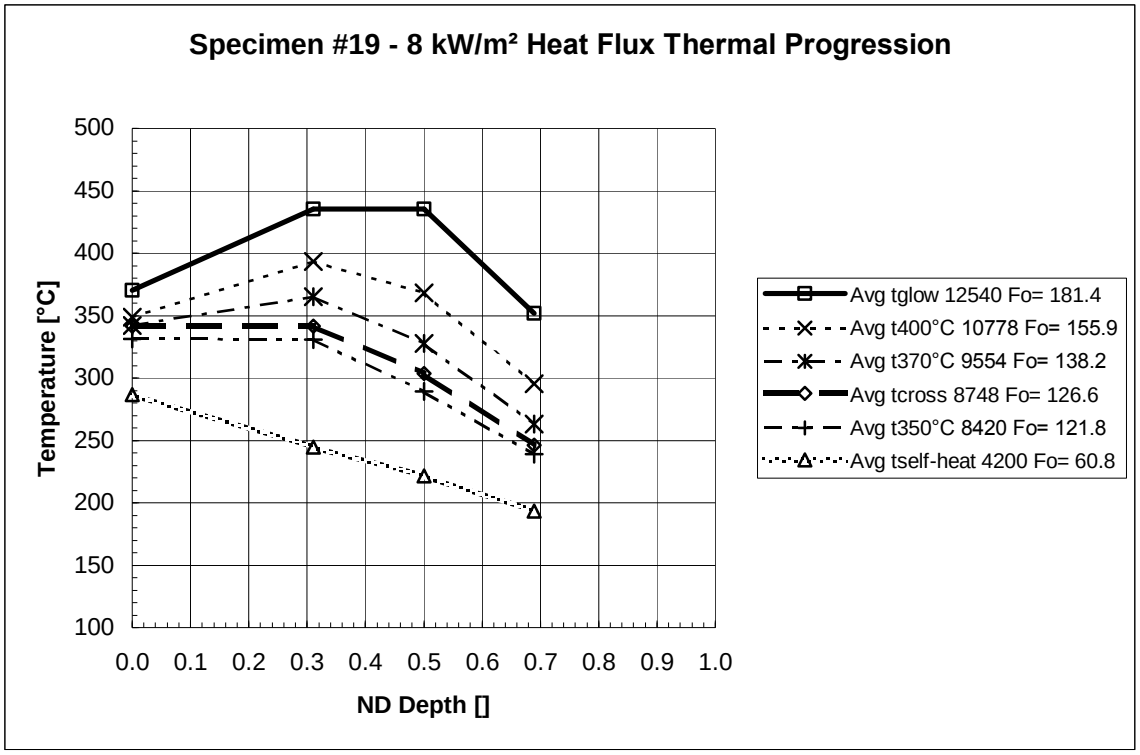

Figure D-2 – Thermal profile progression for specimen #19 subjected to an 8 kW/m^2 heat flux.

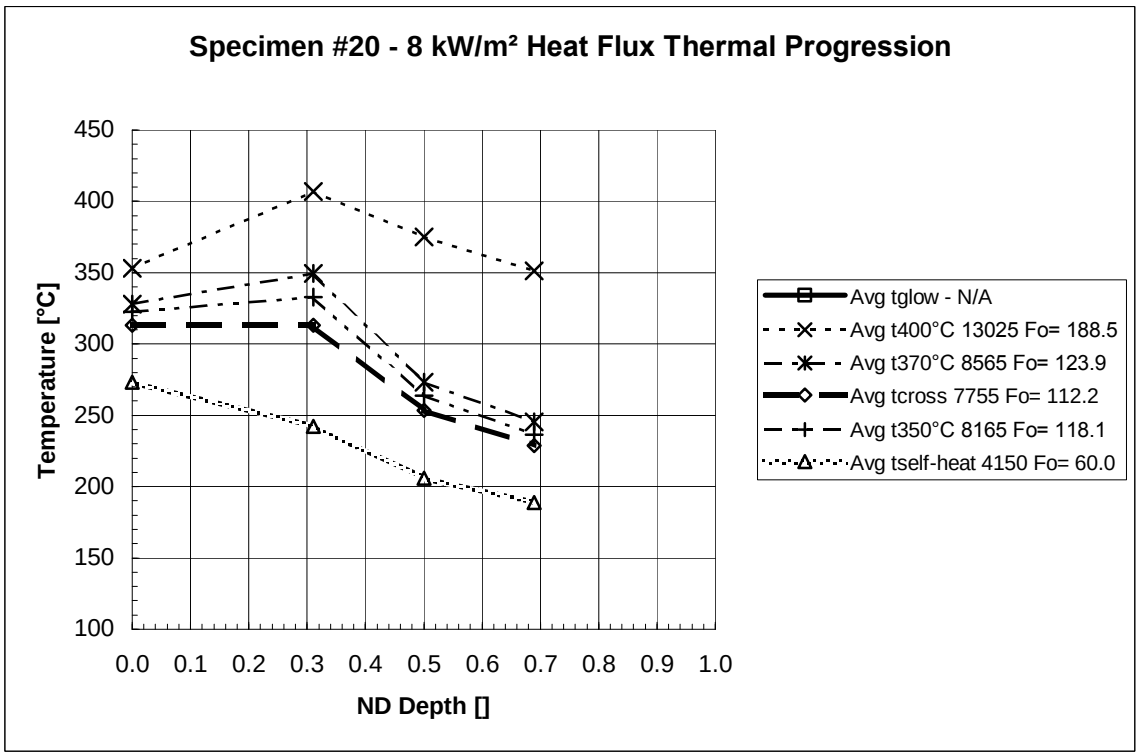

Figure D-3 – Thermal profile progression for specimen #20 subjected to an 8 kW/m^2 heat flux.

9 kW/m^2 Heat Flux (3):

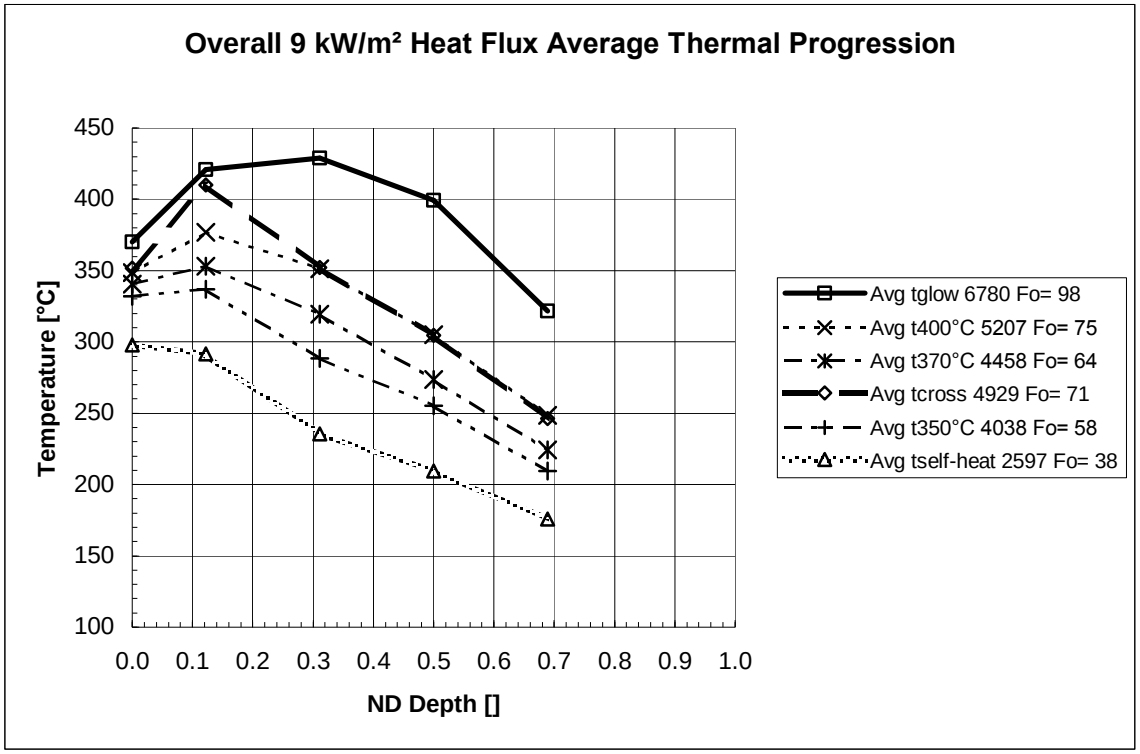

Figure D-4 – Average thermal profile progression for specimen subjected to a 9 kW/m^2 heat flux.

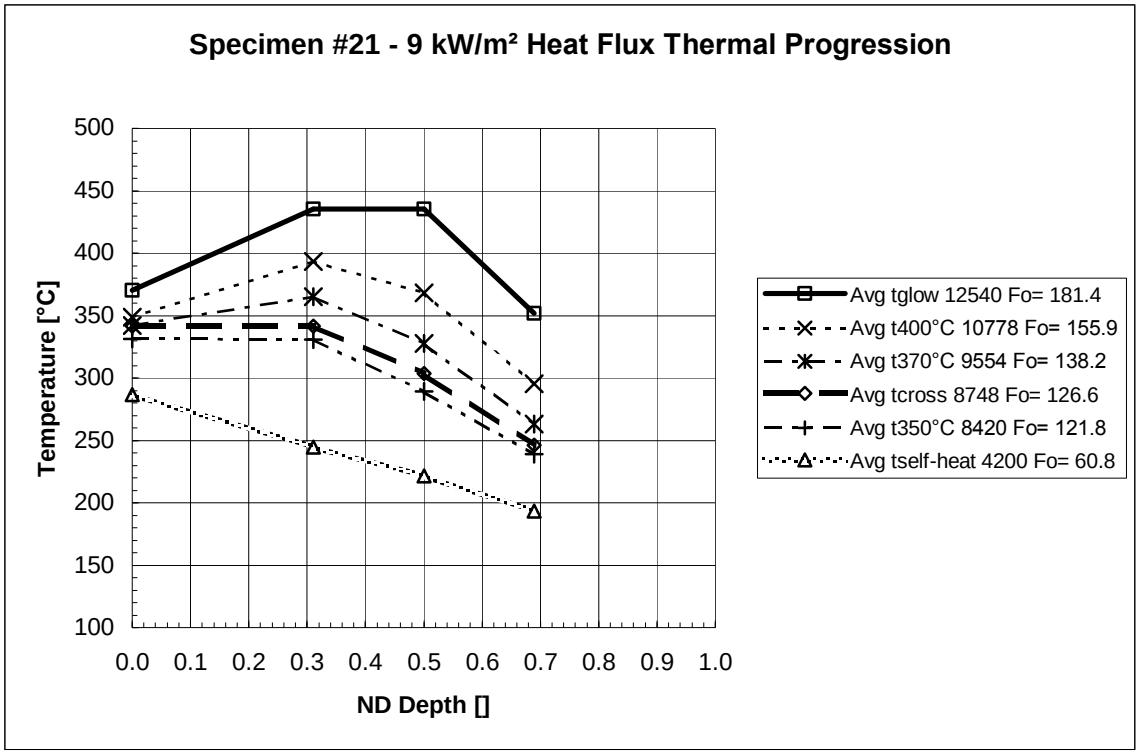

Figure D-5 – Thermal profile progression for specimen #21 subjected to a 9 kW/m^2 heat flux.

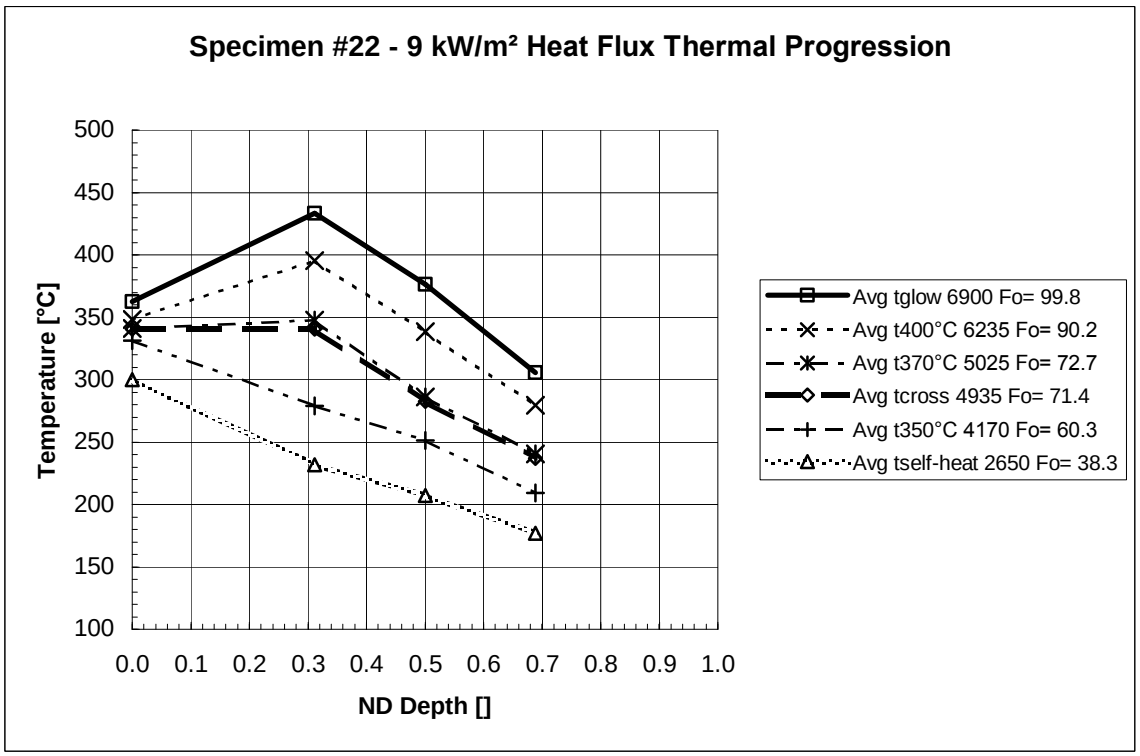

Figure D-6 – Thermal profile progression for specimen #22 subjected to a 9 kW/m^2 heat flux.

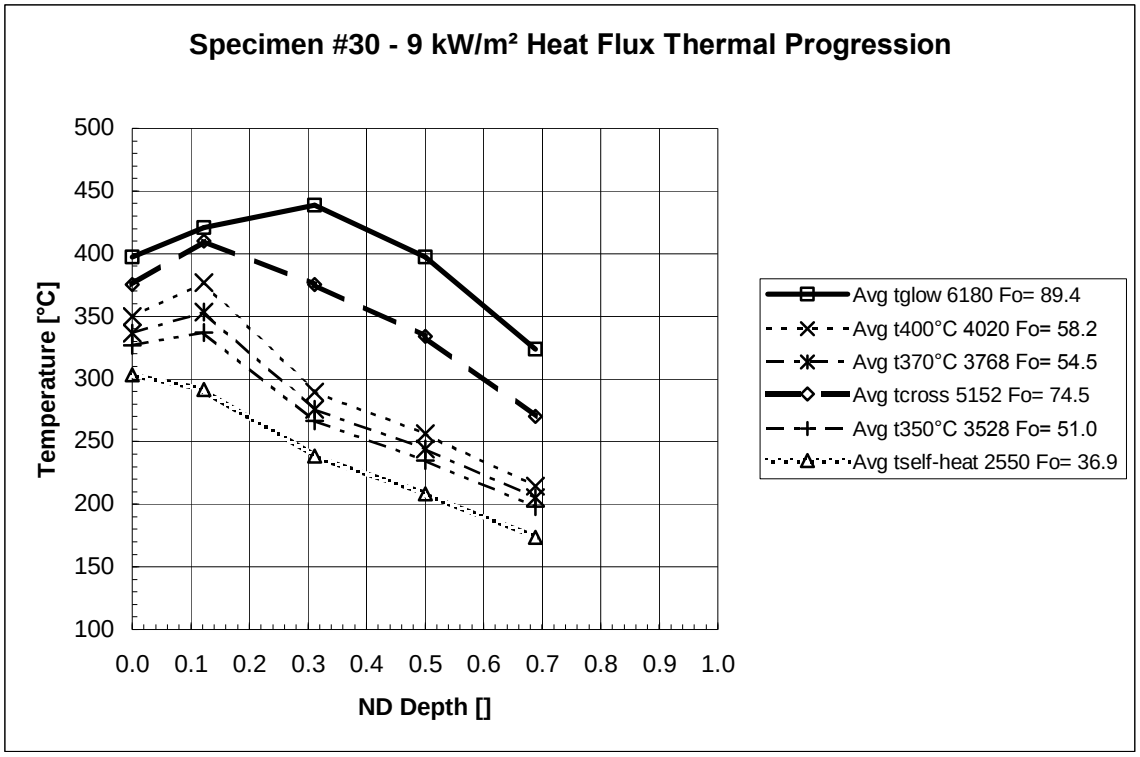

Figure D-7 – Thermal profile progression for specimen #30 subjected to a 9 kW/m^2 heat flux.

10 kW/m^2 Heat Flux (2):

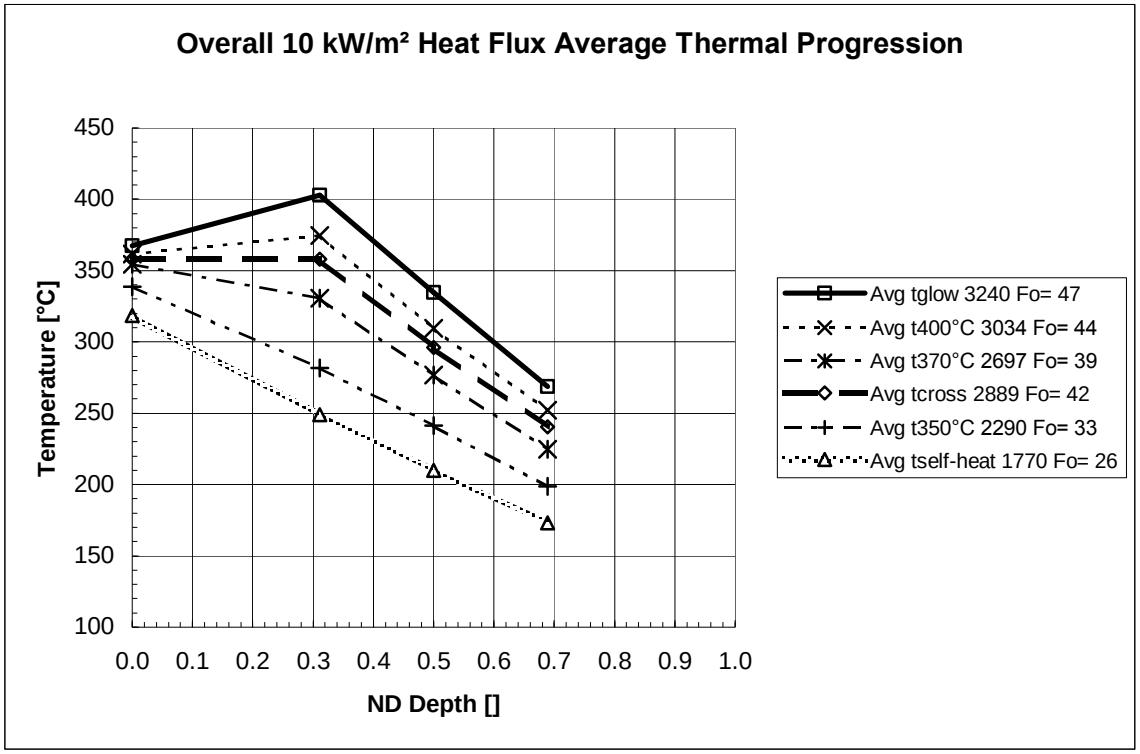

Figure D-8 – Average thermal profile progression for specimen subjected to a 10 kW/m^2 heat flux.

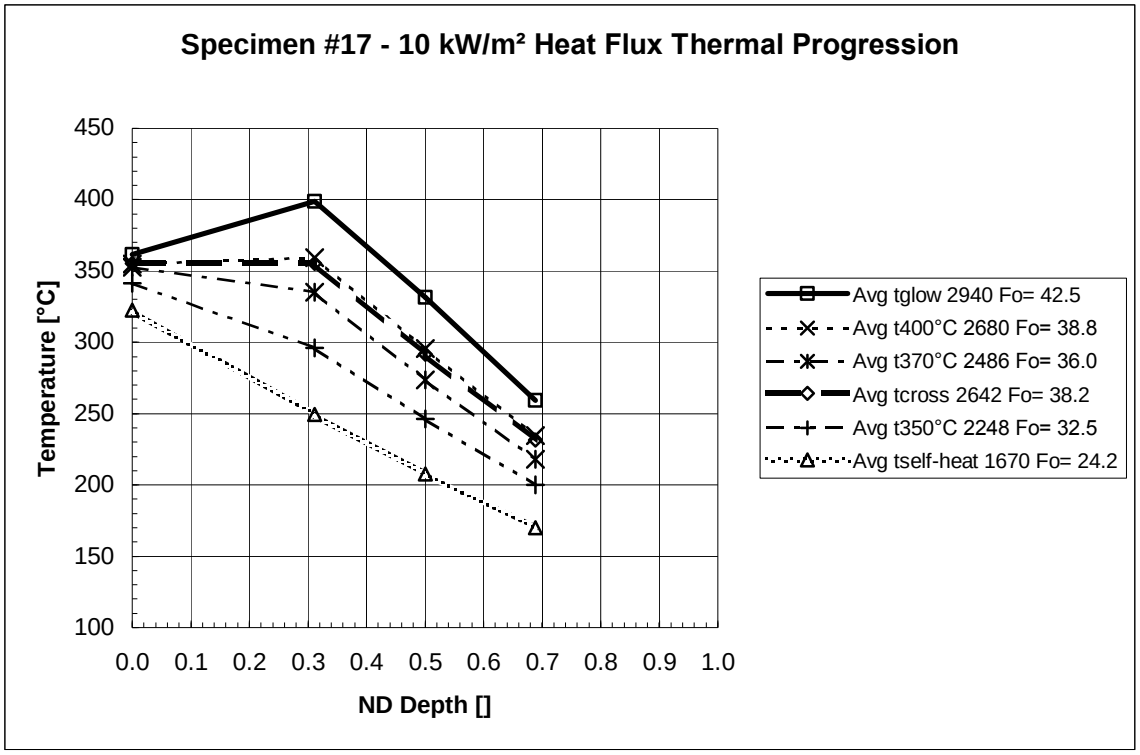

Figure D-9 – Thermal profile progression for specimen #17 subjected to a 10 kW/m^2 heat flux.

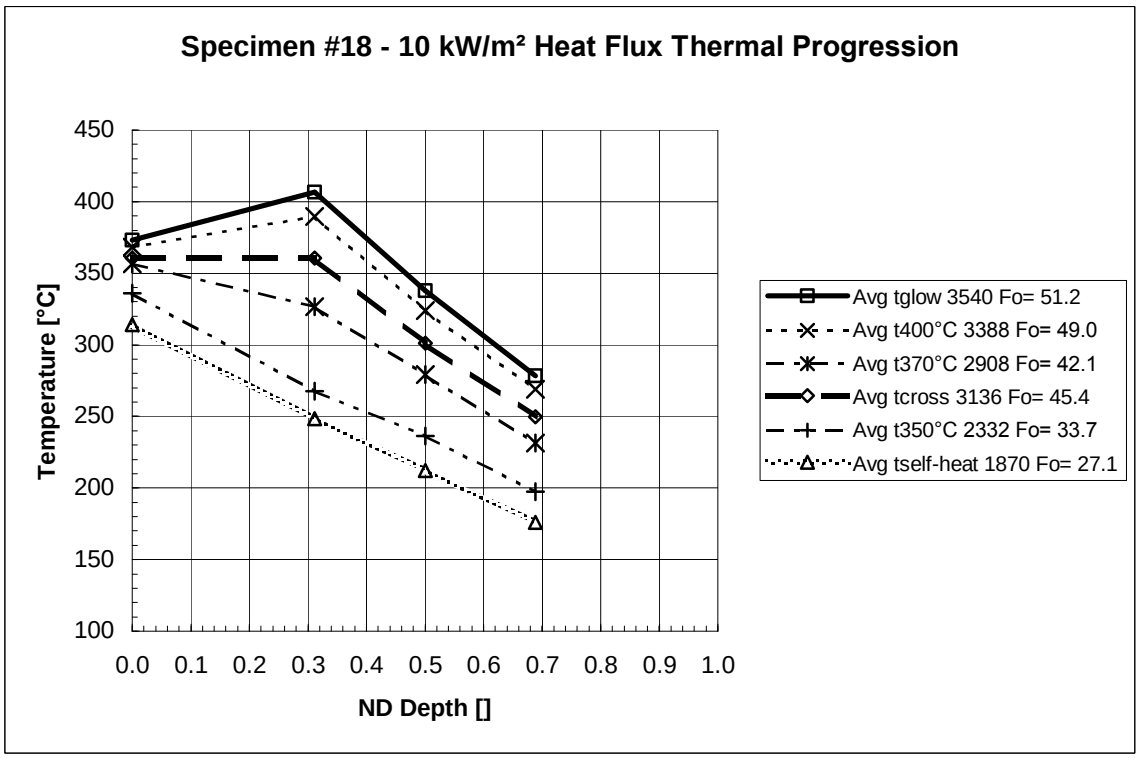

Figure D-10 – Thermal profile progression for specimen #18 subjected to a 10 kW/m^2 heat flux.

12 kW/m^2 Heat Flux (2):

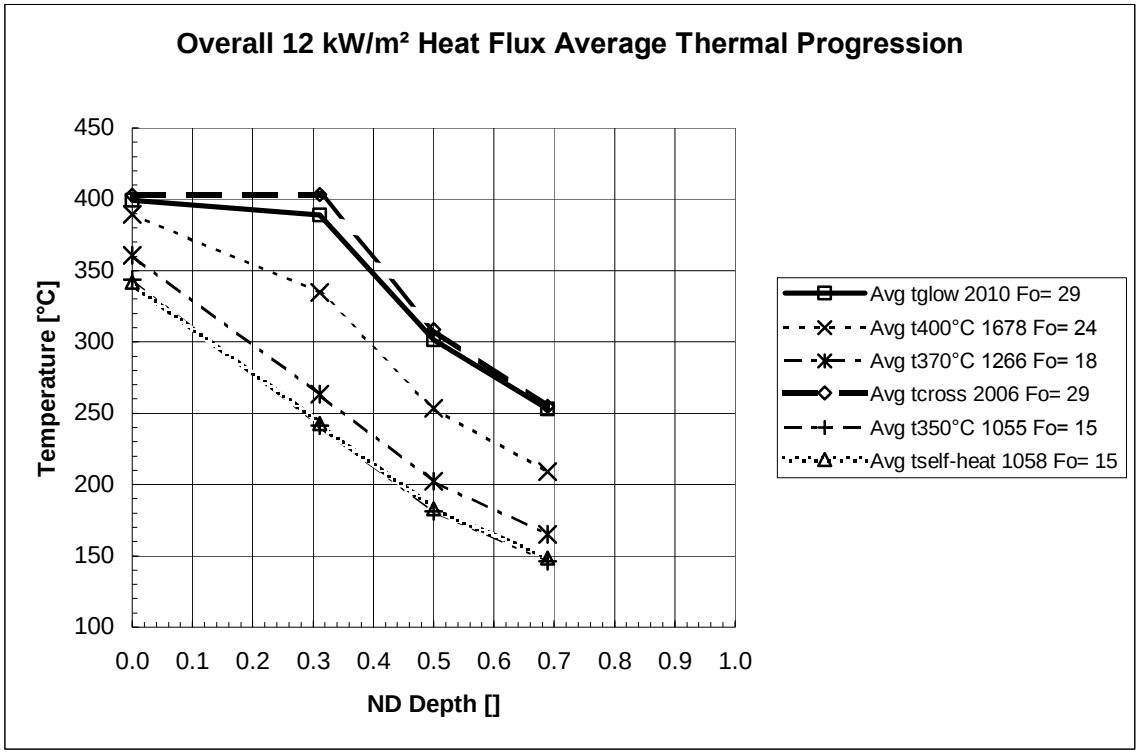

Figure D-11 – Average thermal profile progression for specimen subjected to a 12 kW/m^2 heat flux.

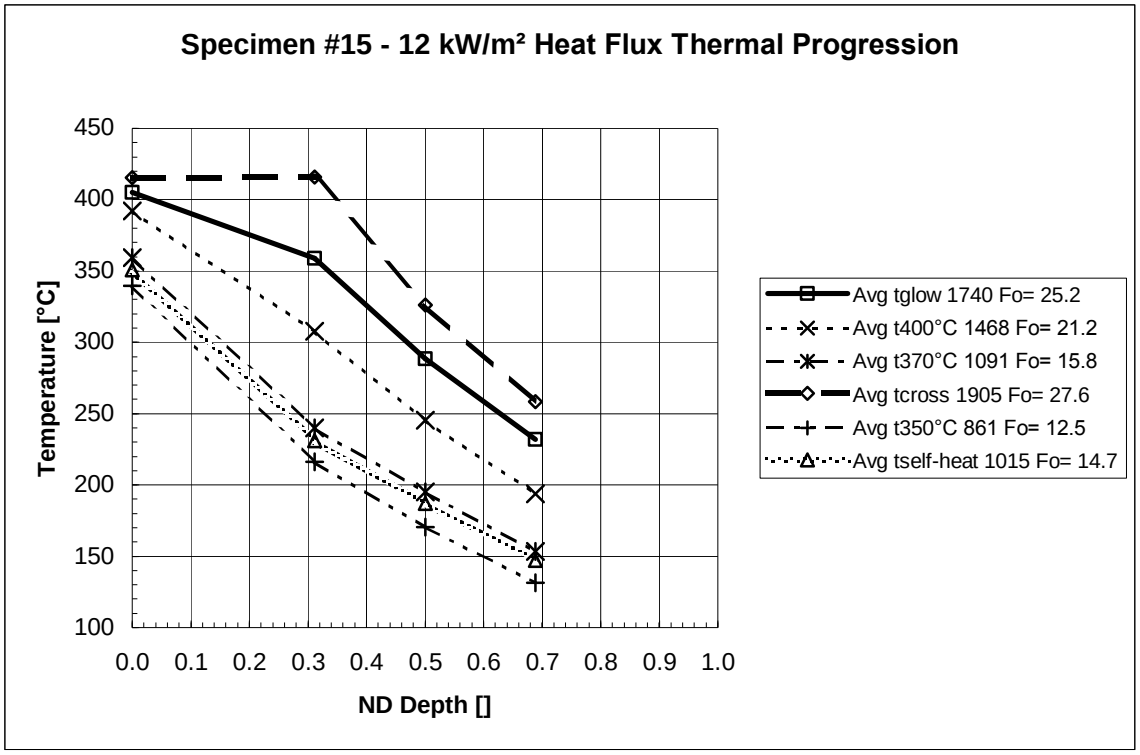

Figure D-12 – Thermal profile progression for specimen #15 subjected to a 12 kW/m^2 heat flux.

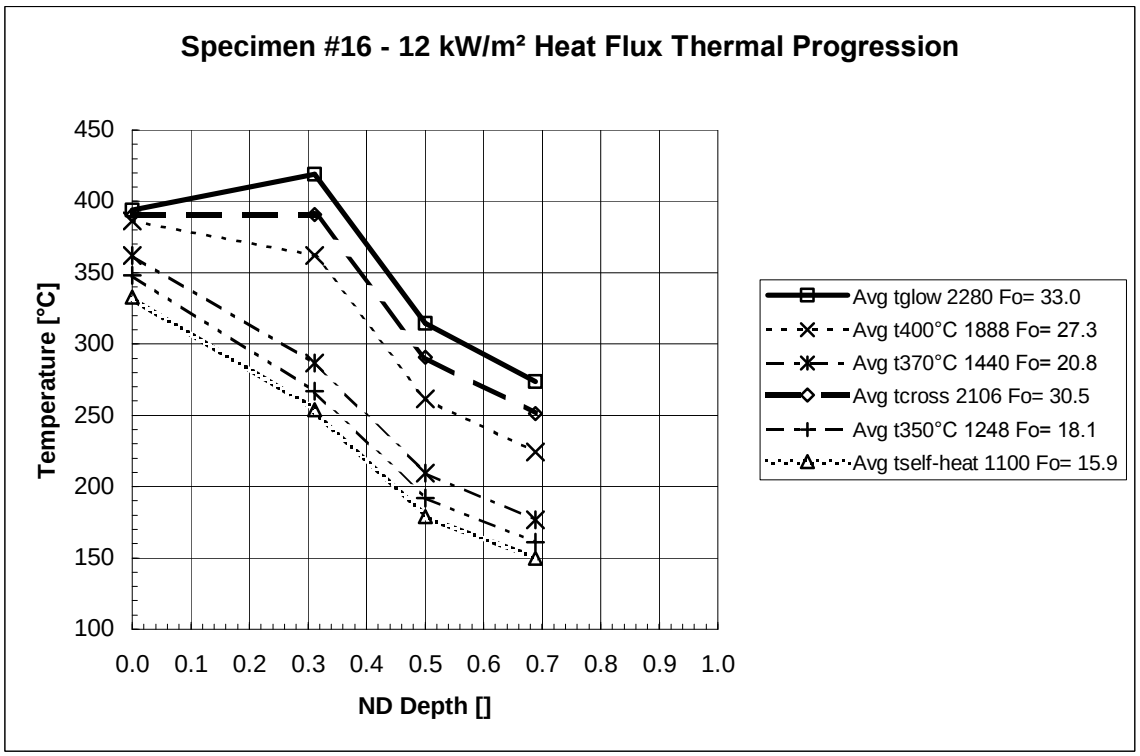

Figure D-13 – Thermal profile progression for specimen #16 subjected to a 12 kW/m^2 heat flux.

15 kW/m^2 Heat Flux (2):

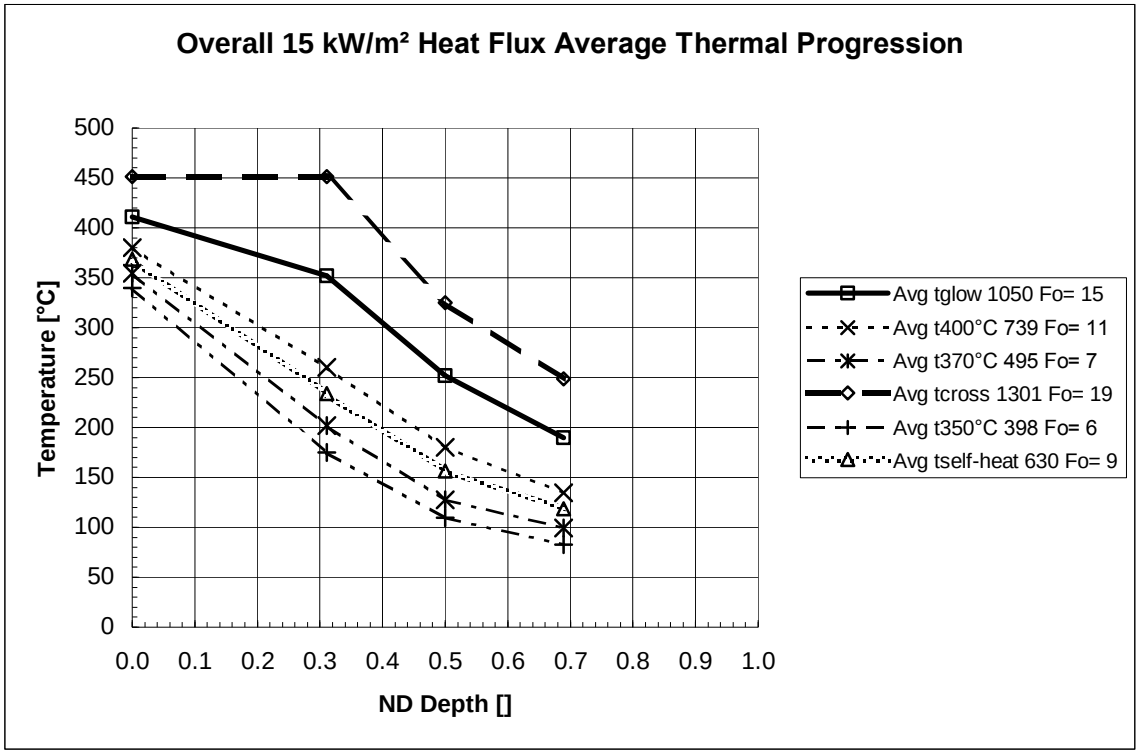

Figure D-14 – Average thermal profile progression for specimen subjected to a 15 kW/m^2 heat flux.

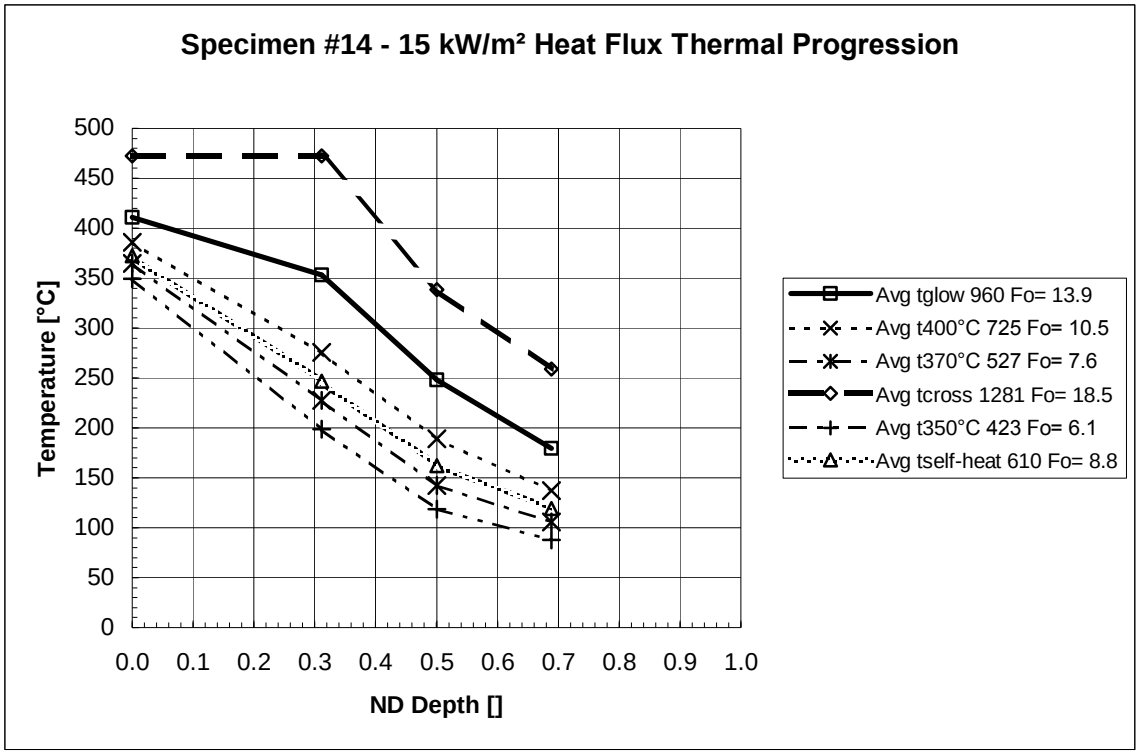

Figure D-15 – Thermal profile progression for specimen #14 subjected to a 15 kW/m^2 heat flux.

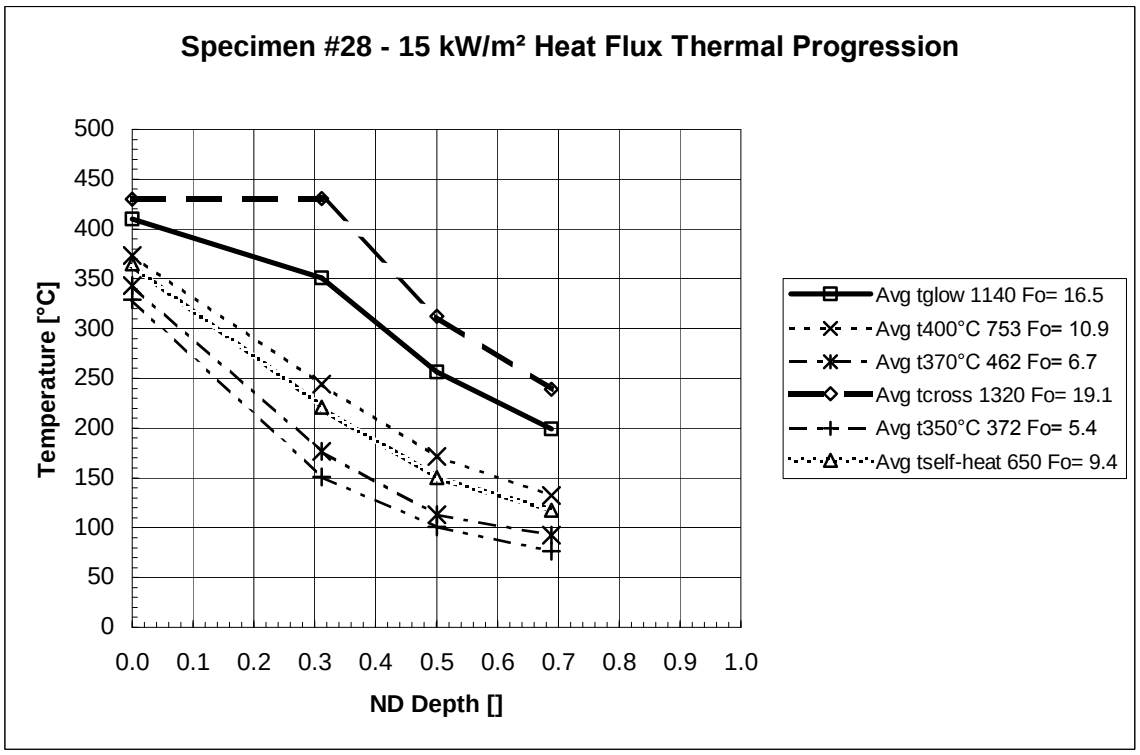

Figure D-16 – Thermal profile progression for specimen #28 subjected to a 15 kW/m^2 heat flux.

Thermal Profiles – Non-Dimensional Temperature Excess

8 kW/m^2 Heat Flux (2):

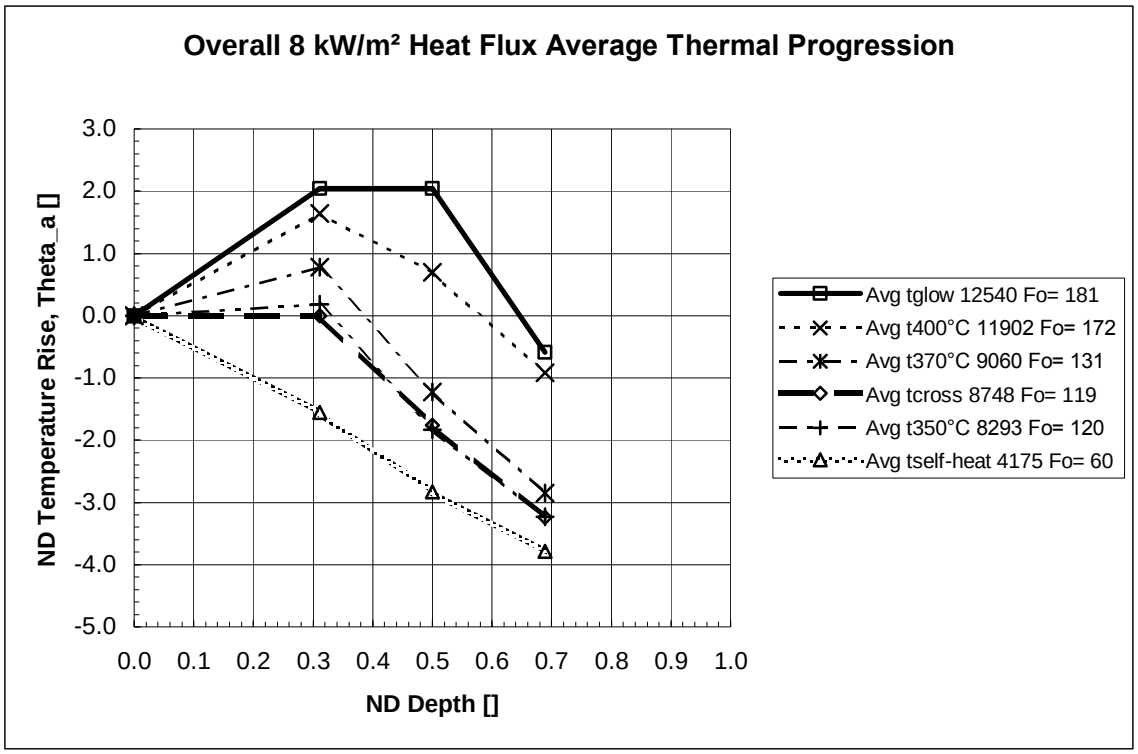

Figure D-17 – Average temperature excess (θ_a) profile progression for specimen subjected to an 8 kW/m^2 heat flux.

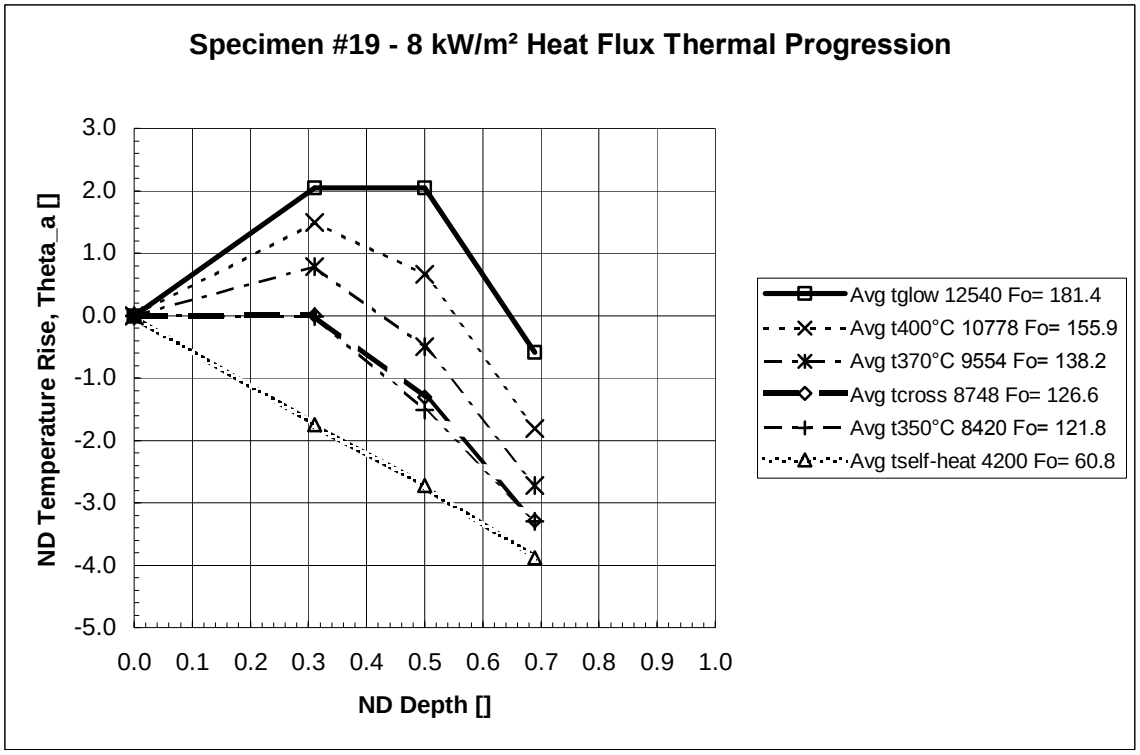

Figure D-18 – Temperature excess (θ_a) profile progression for specimen #19 subjected to an 8 kW/m^2 heat flux.

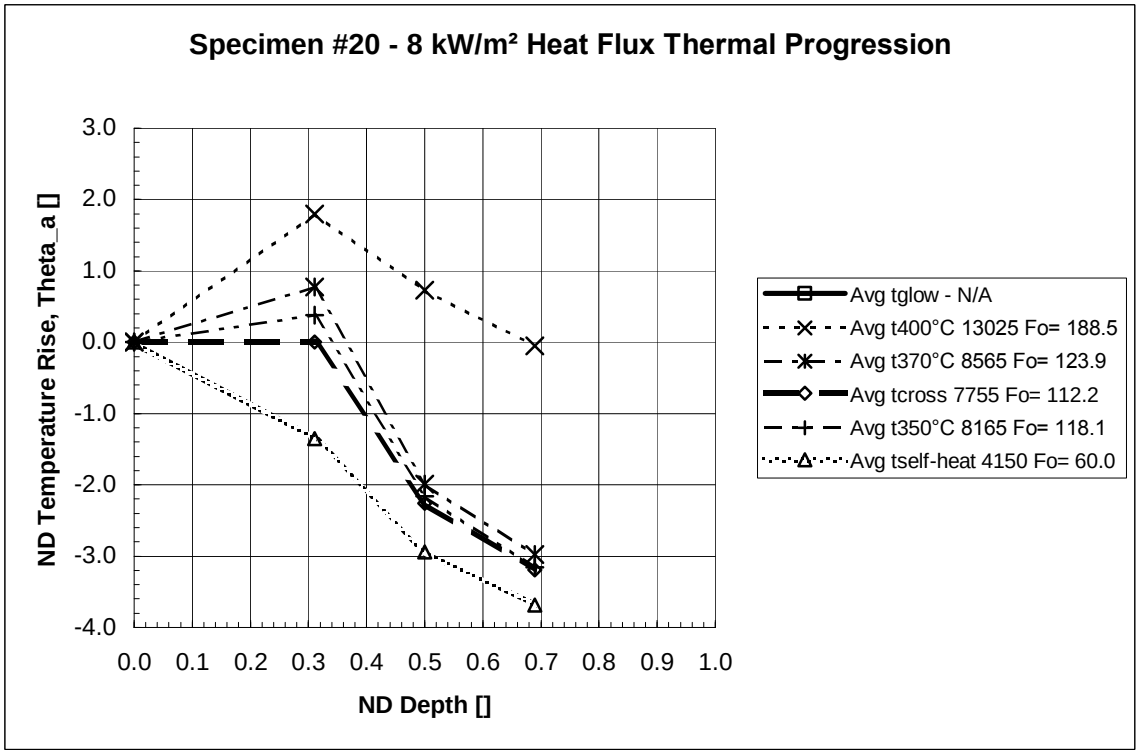

Figure D-19 – Temperature excess (θ_a) profile progression for specimen #20 subjected to an 8 kW/m^2 heat flux.

9 kW/m^2 Heat Flux (3):

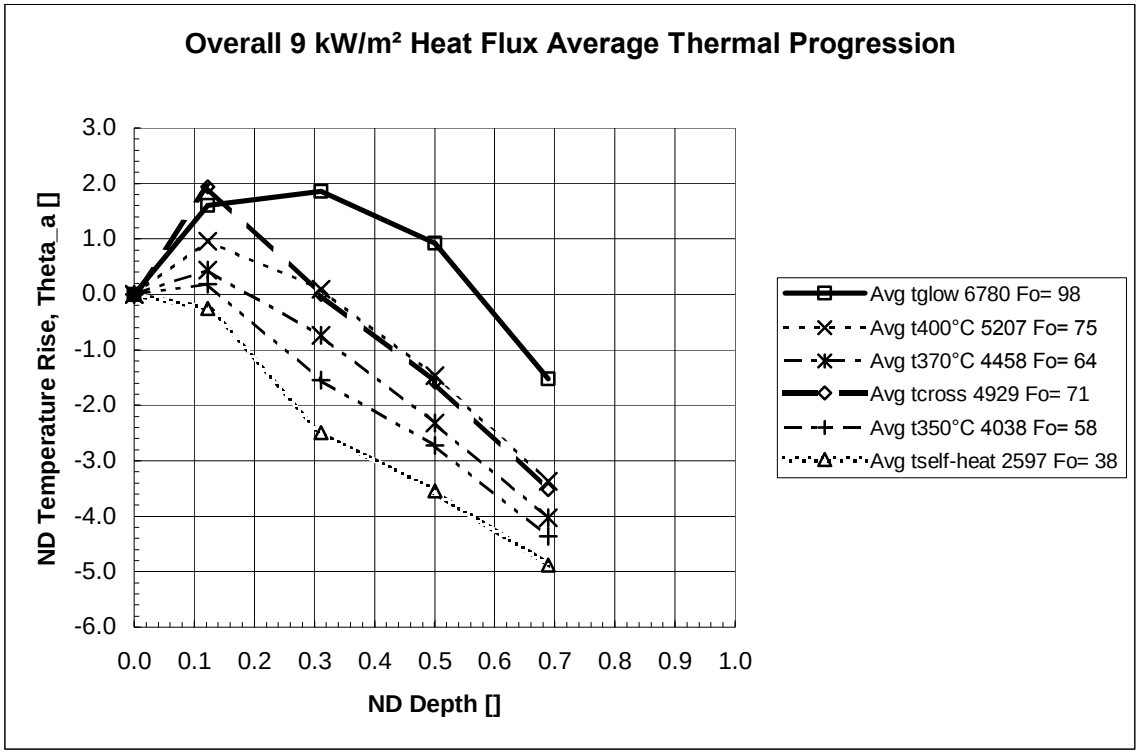

Figure D-20 – Average temperature excess (θ_a) profile progression for specimen subjected to a 9 kW/m^2 heat flux.

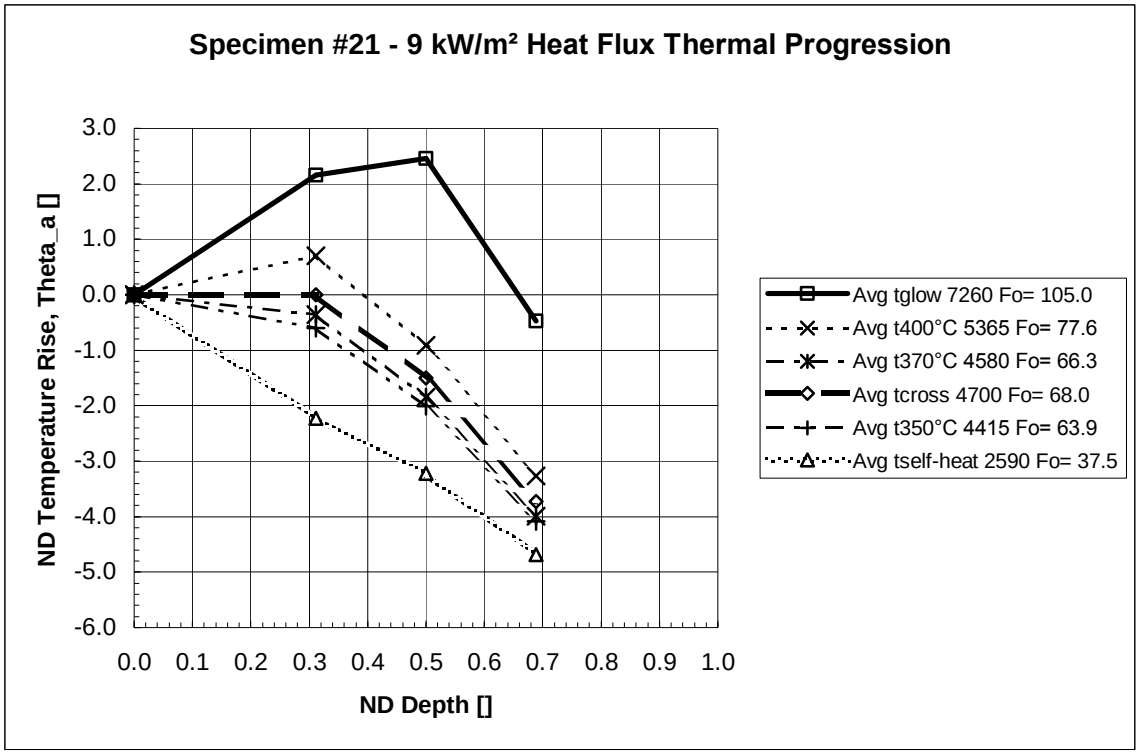

Figure D-21 – Temperature excess (θ_a) profile progression for specimen #21 subjected to a 9 kW/m^2 heat flux.

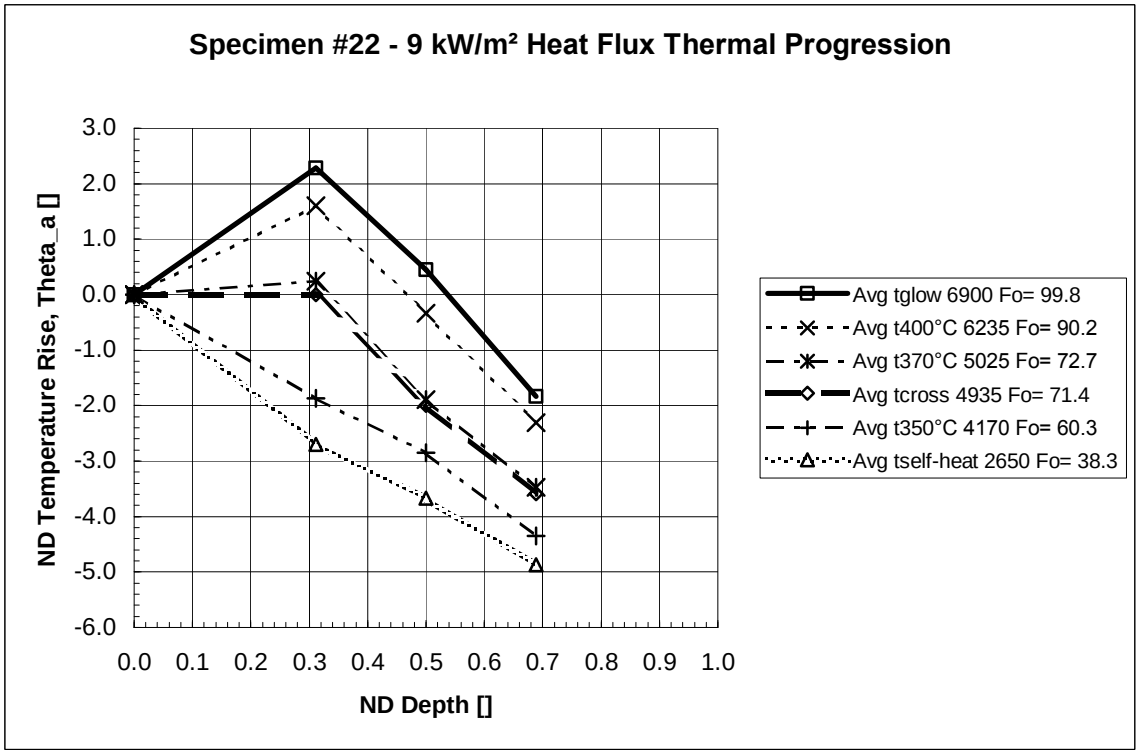

Figure D-22 – Temperature excess (θ_a) profile progression for specimen #22 subjected to a 9 kW/m^2 heat flux.

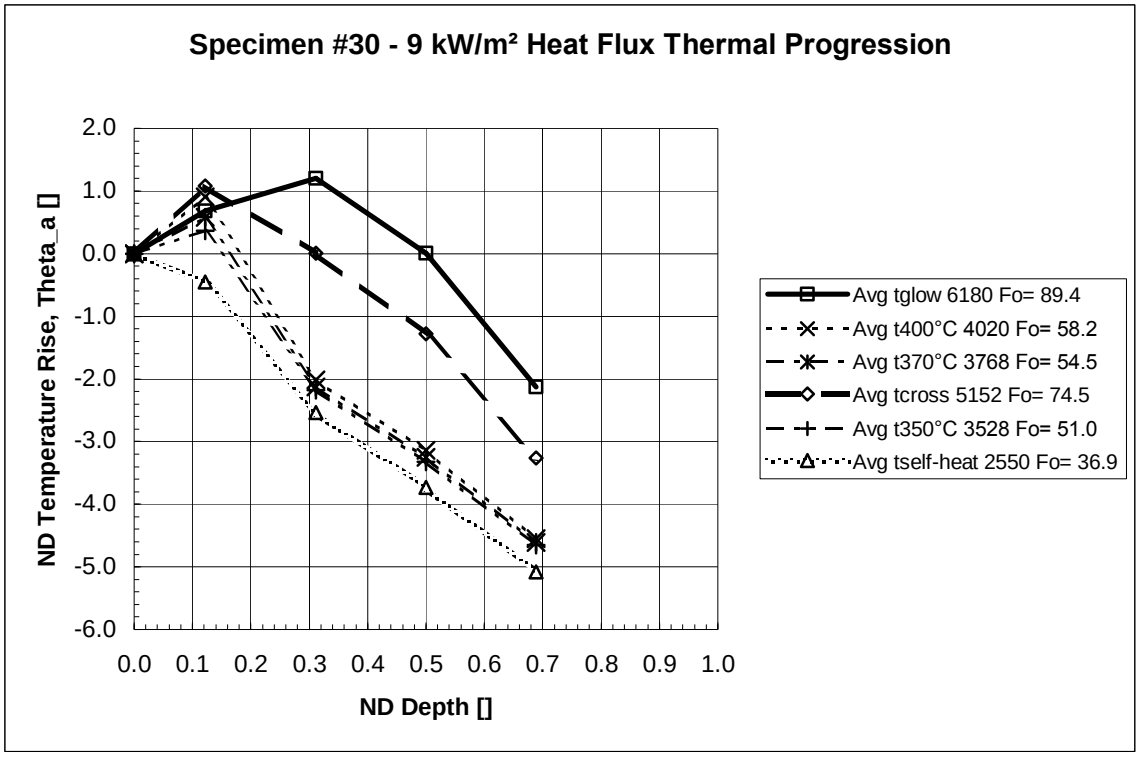

Figure D-23 – Temperature excess (θ_a) profile progression for specimen #30 subjected to a 9 kW/m^2 heat flux.

10 kW/m^2 Heat Flux (2):

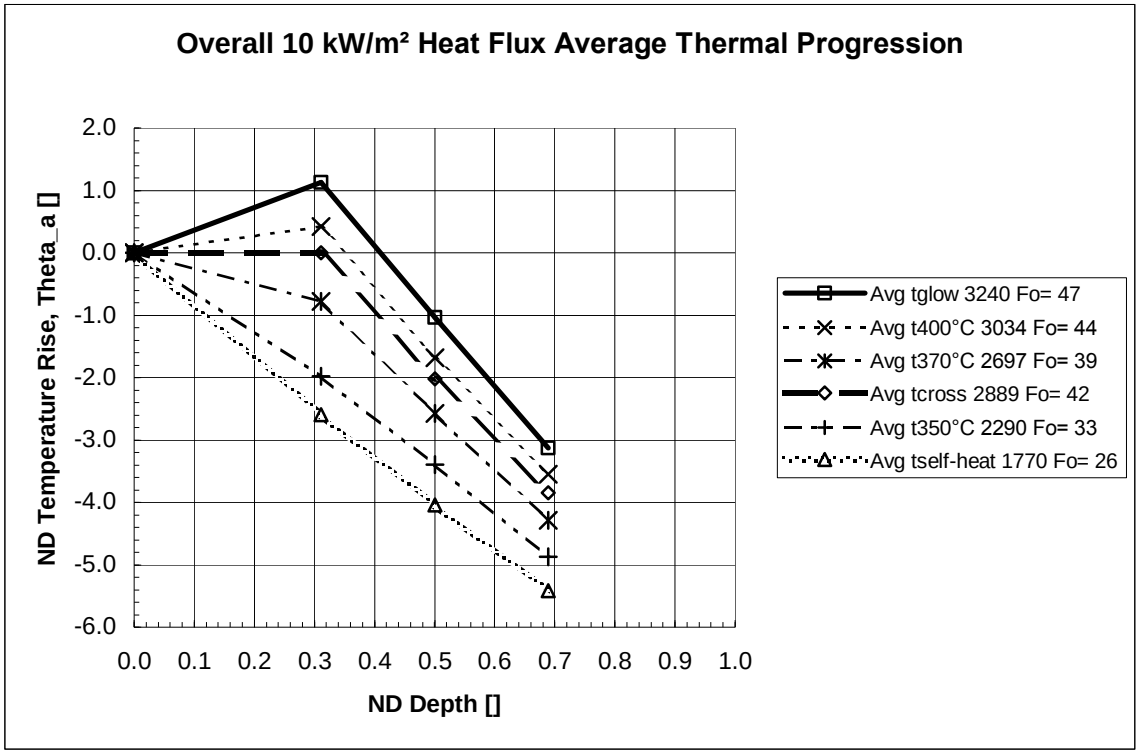

Figure D-24 – Average temperature excess (θ_a) profile progression for specimen subjected to a 10 kW/m^2 heat flux.

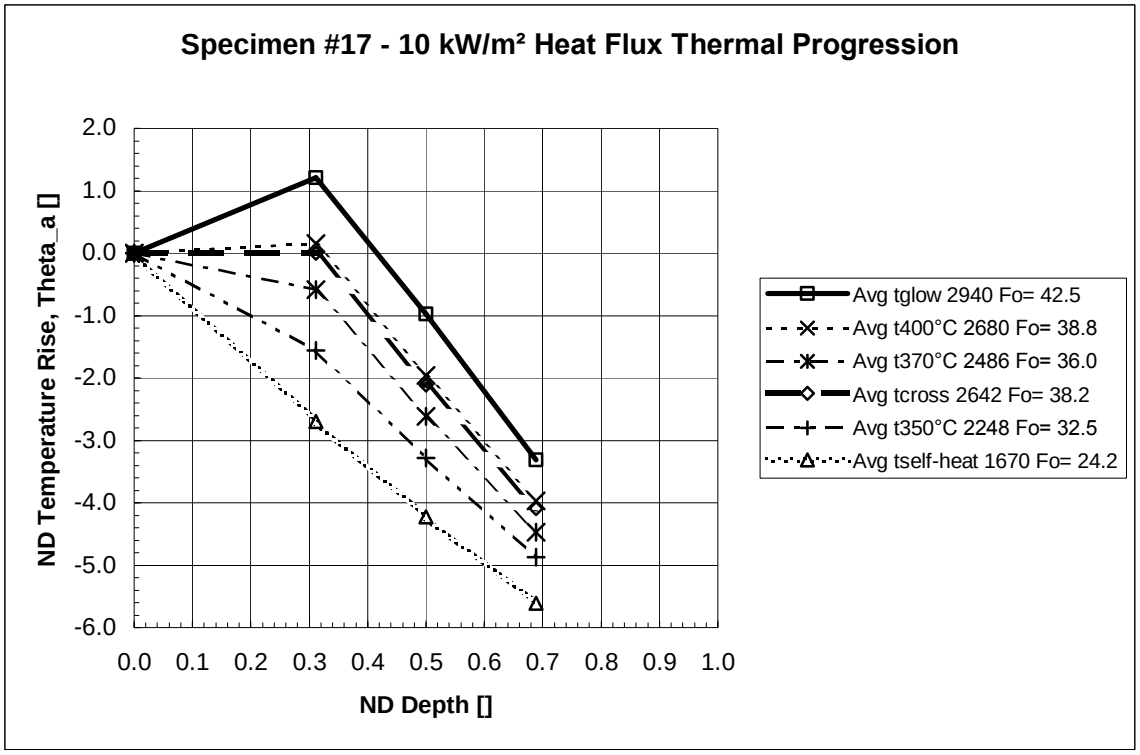

Figure D-25 – Temperature excess (θ_a) profile progression for specimen #17 subjected to a 10 kW/m^2 heat flux.

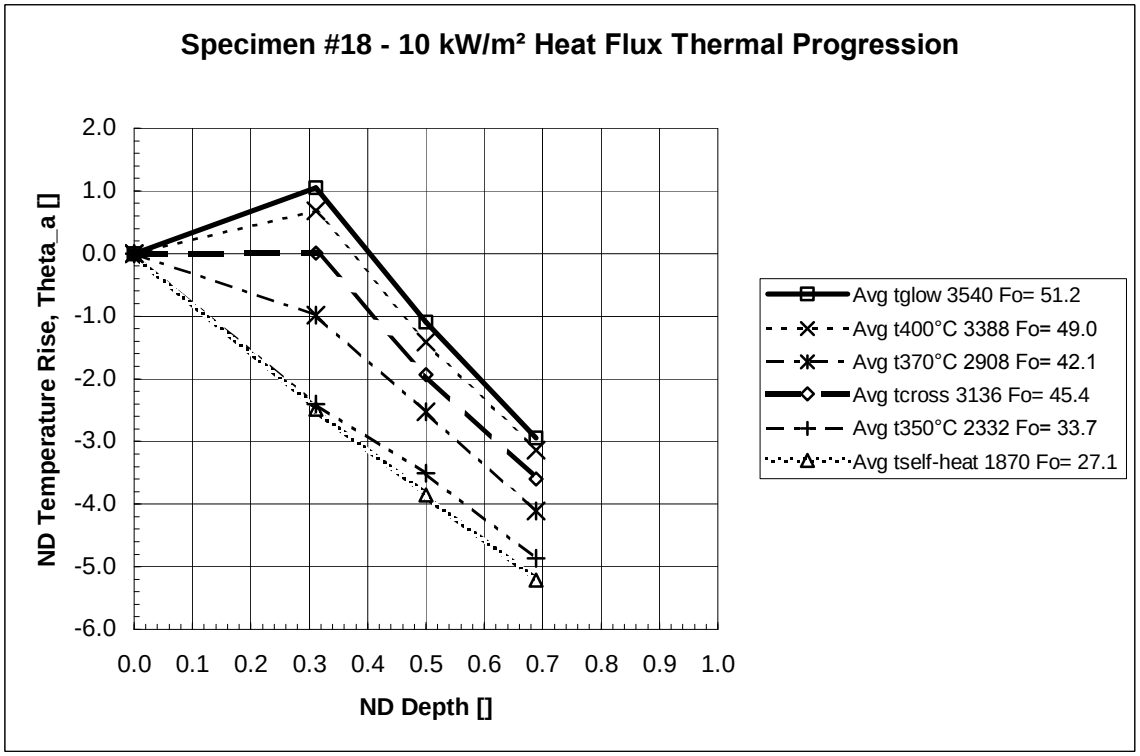

Figure D-26 – Temperature excess (θ_a) profile progression for specimen #18 subjected to a 10 kW/m^2 heat flux.

12 kW/m^2 Heat Flux (2):

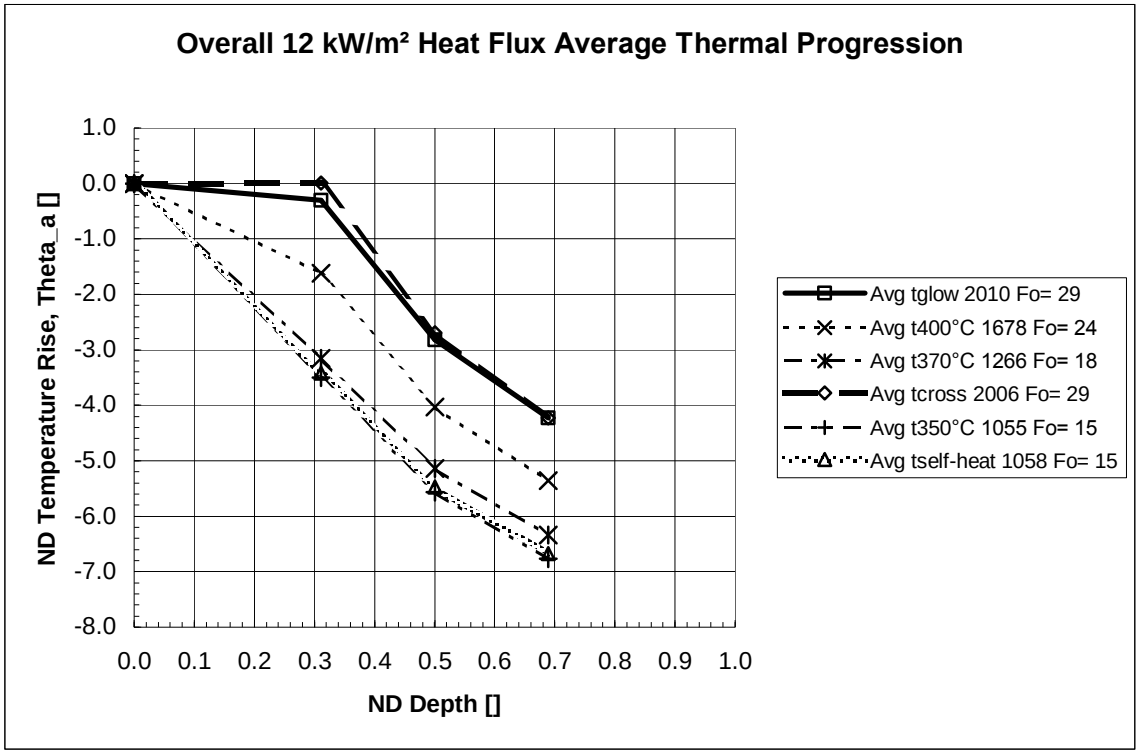

Figure D-27 – Average temperature excess (θ_a) profile progression for specimen subjected to a 12 kW/m^2 heat flux.

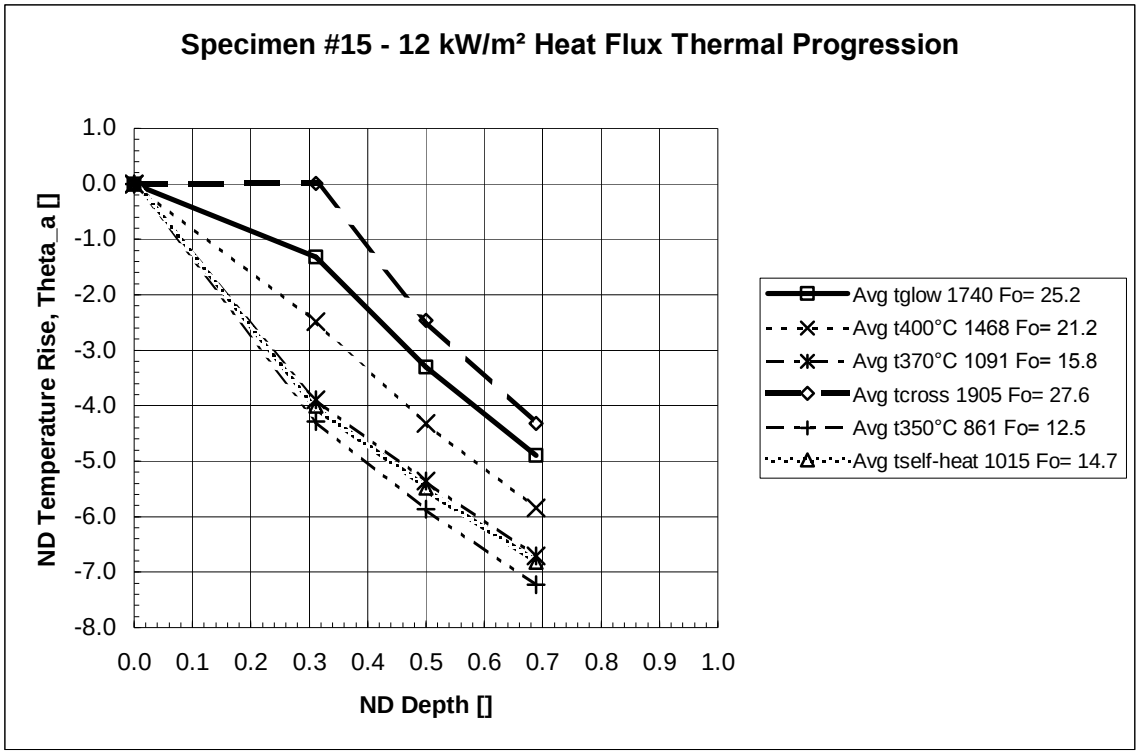

Figure D-28 – Temperature excess (θ_a) profile progression for specimen #15 subjected to a 12 kW/m^2 heat flux.

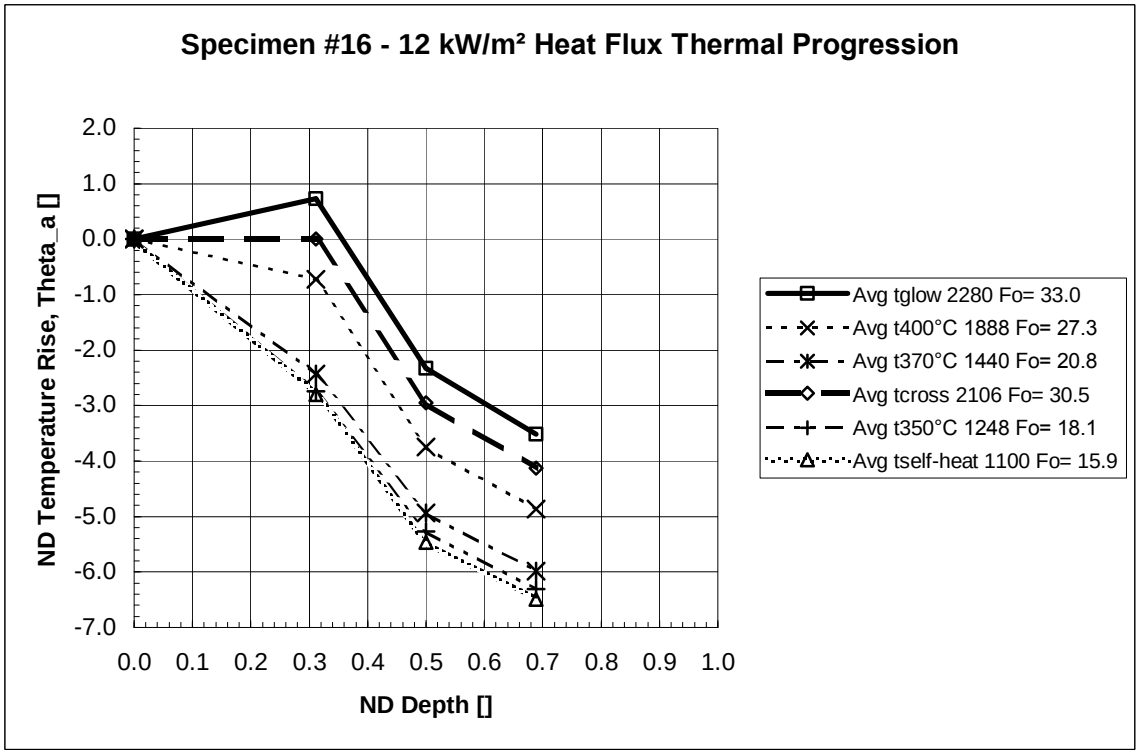

Figure D-29 – Temperature excess (θ_a) profile progression for specimen #16 subjected to a 12 kW/m^2 heat flux.

15 kW/m^2 Heat Flux (2):

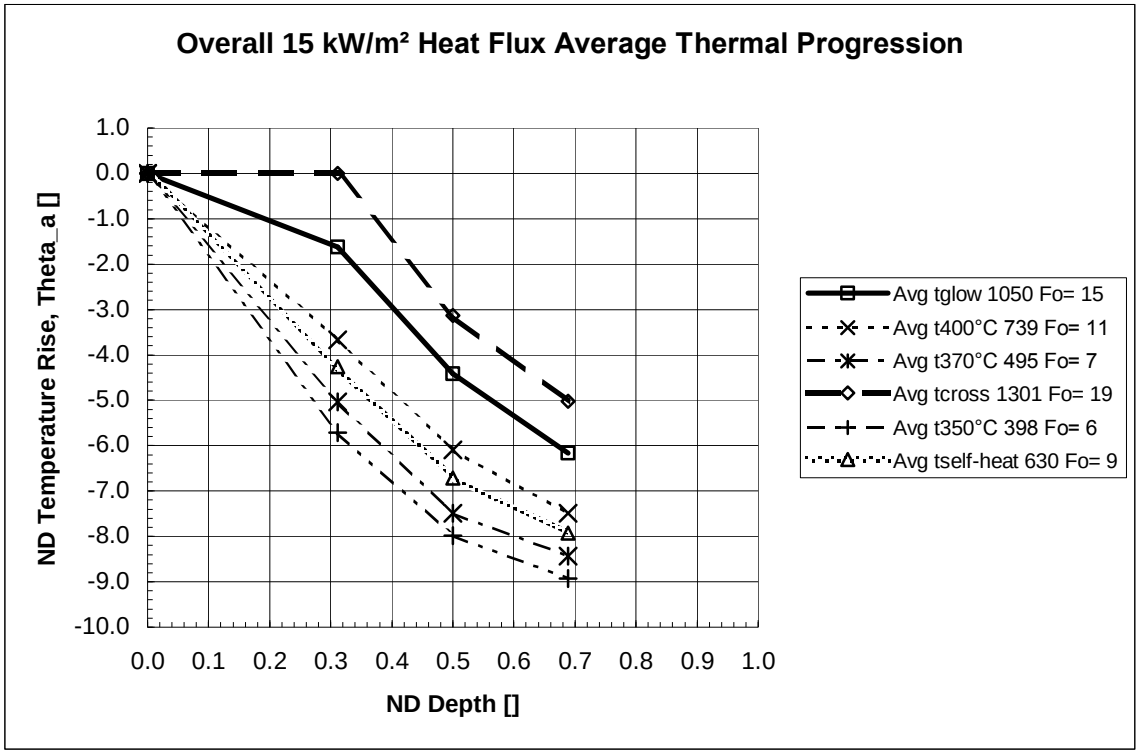

Figure D-30 – Average temperature excess (θ_a) profile progression for specimen subjected to a 15 kW/m^2 heat flux.

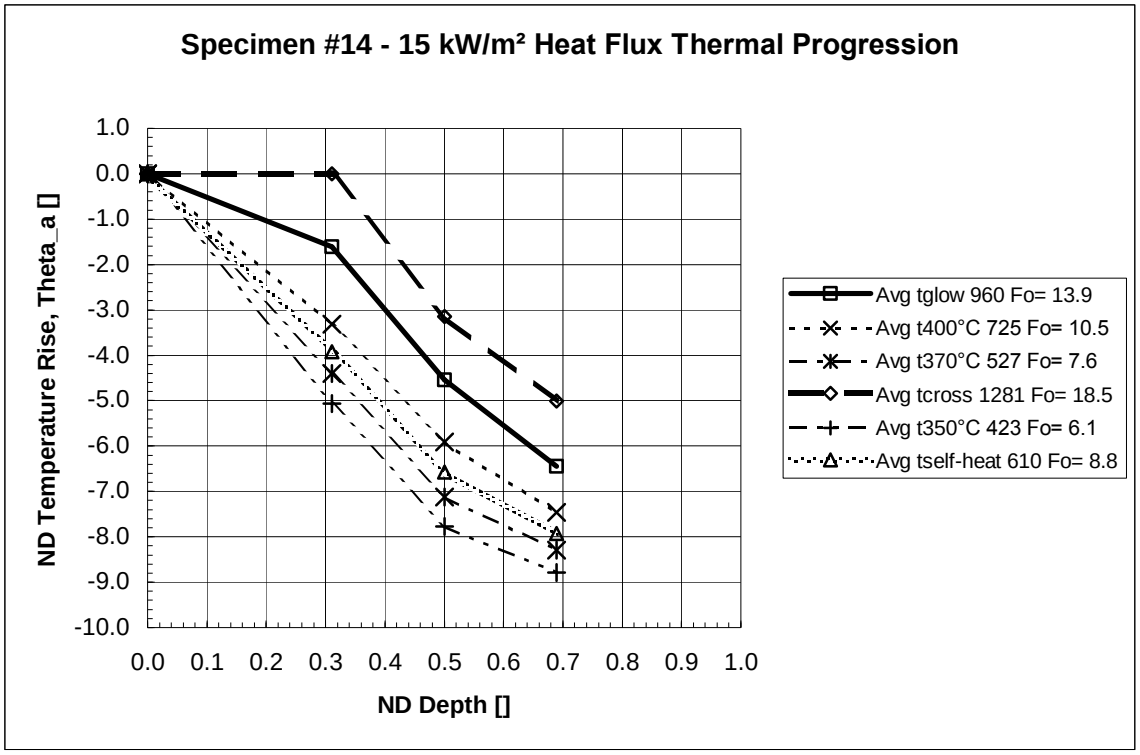

Figure D-31 – Temperature excess (θ_a) profile progression for specimen #14 subjected to a 15 kW/m^2 heat flux.

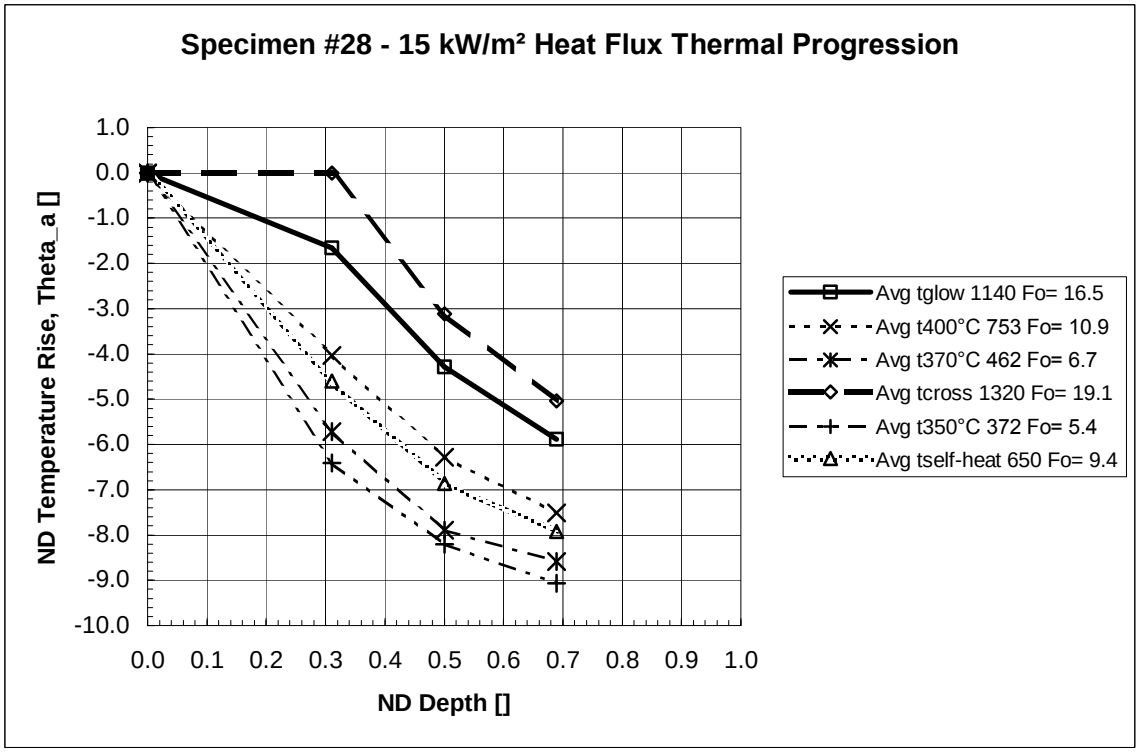

Figure D-32 – Temperature excess (θ_a) profile progression for specimen #28 subjected to a 15 kW/m^2 heat flux.

APPENDIX E – MASS LOSS RATE ANALYSIS

Mass Loss Rate Testing

The maple plywood specimens tested in the cone calorimeter weighed an average of 100 grams. Analysis of the mass loss rate data provides further insight into the behavior of wood exposed to low levels of radiant heating. The mass loss rate was calculated from the numerical differentiation of the moving average load cell mass data and is of the form,

$$\dot{m}_t = \left(-\bar{m}_{t-2\Delta t} + 8\bar{m}_{t-\Delta t} - 8\bar{m}_{t+\Delta t} + \bar{m}_{t+2\Delta t}\right)/(12\,\Delta t).$$

A moving average was chosen to smooth the noise in the load cell mass data and still reflect the behavior of the specimen. The period used for the moving average ranged from 75 seconds for 12 and 15 kW/m^2 heat flux calculations up to a maximum of 750 seconds for the 6 kW/m^2 heat flux calculation.

The mass loss rate over time for each specimen tested in the cone calorimeter is shown in figure E-1. Specimen subjected to the highest heat flux experienced the highest mass loss rates.

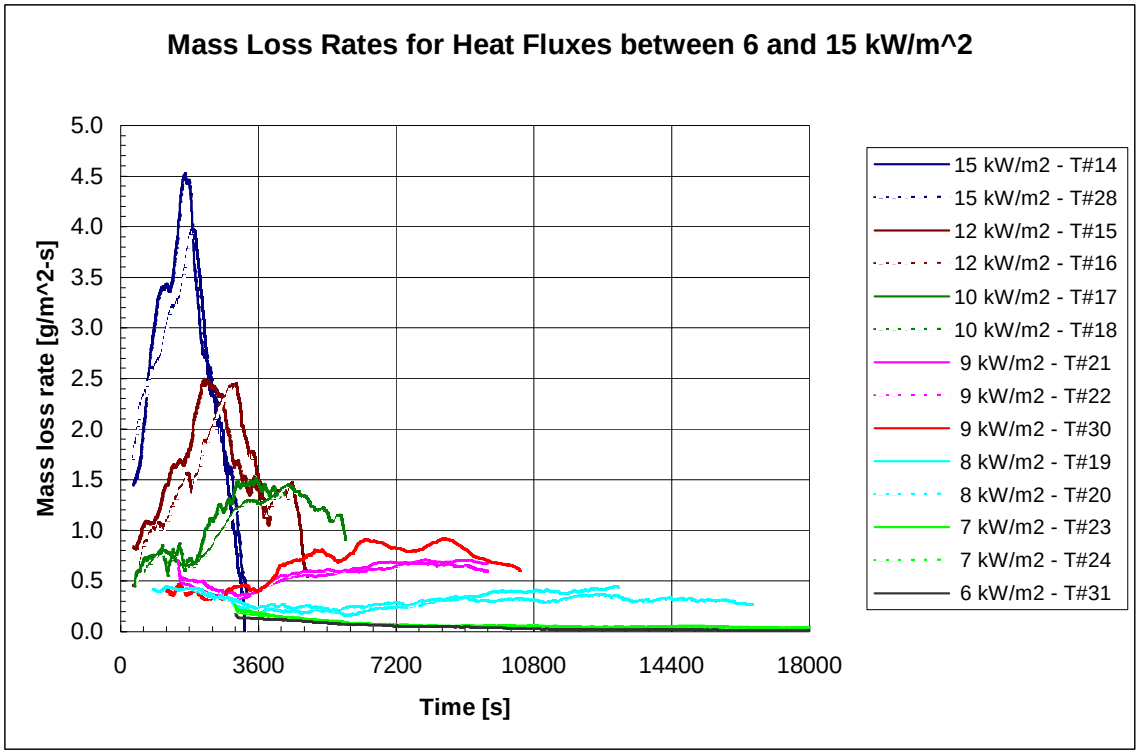

Figure E-1 – Mass loss rate for each of the maple plywood ignition tests, 6-15 kW/m^2 heat flux in the cone calorimeter.

Mass Loss Rate Analysis

The maximum mass loss rate for specimens exposed to 6 or 7 kW/m^2 heat flux experienced the highest mass loss rate near the beginning of the test. This is a result of the evaporation of moisture from within the wood and not from significant decomposition of the wood or formation of char. The evaporation of moisture was also observed in the mass loss rate data for specimen exposed to 8 to 10 kW/m^2 heat flux. Initial mass loss rates reach a small peak early in the test before increasing again to the maximum mass loss rate experienced during smoldering.

The decrease in mass loss rate after the peak may be attributable to two mechanisms. The first was the loss of available mass to burn, specifically when burning reached the backside or edges of the specimen. The second was the decrease in the effective heat

flux as the surface regressed away from the cone heating element during the burning process.

Table E-1 presents the times to maximum mass loss rate and observed glowing as well as the associated mass loss rates for each test. A comparison of the times shows the mass loss rate was a lagging indicator of smoldering. The difference in mass loss rates was an order of magnitude between the 8 and 15 kW/m^2 tests even though exposure at both heat fluxes resulted in smoldering. The largest peak burning rate achieved in the smoldering ignition tests was 4.5 g/m^2-s for specimen#14 exposed to a heat flux of 15 kW/m^2. By comparison, Drysdale [1] reports peak flaming burning rates of 13 g/m^2-s for wood based on the work of Tewarson and Pion (1976).

Due to the large differences with respect to heat flux and the lagging nature of the quantity, mass loss rate does not provide a useful tool for determining smolder initiation.

Table E-1 – Times of maximum mass loss rate and observed glowing and associated mass loss rates.

Heat Flux [kW/m^2]	Specimen#	Time of Max. Mass Loss Rate [sec]	Time of Observed Glowing [sec]	Max. Mass Loss Rate [g/m^2-s]	Mass Loss Rate at Observed Glowing [g/m^2-s]
6	31	Early	-	0.17	-
7	23	Early	-	0.25	-
7	24	Early	-	0.25	-
8	19	12930	12540	0.45	0.41
8	20	12470	-	0.42	-
9	21	7950	7260	0.71	0.68
9	22	7775	6900	0.70	0.61
9	30	8476	6180	0.92	0.85
10	17	3522	2940	1.52	1.31
10	18	4386	3540	1.45	1.29
12	15	2180	1740	2.49	1.75
12	16	3020	2280	2.45	1.87
15	14	1682	960	4.53	3.25
15	28	1903	1140	3.97	2.86

REFERENCES

[1] Drysdale, D., An Introduction to Fire Dynamics, Second Edition, John Wiley & Sons, Chichester, England, 1998.

APPENDIX F – CHAR DEPTH ANALYSIS

Wood decomposes to char when exposed to radiant heat, starting at the surface and progressing through the depth of the material. The decomposition to char significantly alters the thermal properties, providing additional thermal insulation. As compared to wood, char has a reduced density and thus thermal conductivity as well as a reduced specific heat. However, permeability is increased, providing an avenue for increased oxygen diffusion throughout the char and to the smolder front. Oxygen access is further accommodated by the formation of cracks within the char. With respect to smoldering of wood, the smolder reaction is primarily driven by char oxidation due to the relatively low permeability of the material [26]. Therefore smoldering does not occur till after a char layer has formed. Char depth testing provides both an understanding of where and at what temperature char forms and thus allows further insight into where smoldering ignition may occur.

Char Depth Testing

To better understand the decomposition, char depth testing was performed at an incident heat flux sufficient for charring in a reasonably short time and yet at a low enough level that char is formed, in part, due to self-heating and not just from the radiant heating. Instrumented tests, specimens#21 and #22, at an incident heat flux of 9 kW/m^2, provided characteristic data for devising the char depth tests. Surface charring, evidenced by blackening of the surfaces, was complete at around 1680 seconds (28 minutes) with first cracks observed around 2280 seconds (38 minutes). While glowing was observed at 7200 seconds (2 hours), analysis of thermocouple data showed significant changes in sub-surface thermal activity between 2700 and 4200 seconds (45-70 minutes). Therefore,

char depth test samples were each exposed to a heat flux of 9 kW/m^2 for 2100, 2700, 3300 and 3900 seconds. The optical pyrometer was used for surface temperature measurements during the testing.

After each test, the actual char depth was determined by scraping the char from the remainder of the sample with a stiff wire brush. Scrapes were made at 45-degree angles to the plywood grain to reduce the possibility of gouging of the surface. The bottom of the char layer was reached when little to no decomposition particles were removed with each scrape as unpyrolized wood is not very susceptible to damage from the wire brush. Results are presented in Table F-1.

Table F-1 – Results of Char Depth Testing at a heat flux of 9 kW/m^2.

Test Duration [sec]	Char Yield [%]	Char Depth [% (mm)]	End of Test Surface Temperature [°C]
2100	18	9.5 (1.7)	308
2700	26	25.9 (4.7)	318
3300	28	44.1 (7.9)	361
3900	28	44.1 (7.9)	361

The char yield is the ratio of the mass of char created per unit mass of wood decomposed (final weight minus the scraped weight to the initial weight minus the scraped weight). Drysdale [25] reports wood burned or heated over 450 °C typically yields 15-25% char. However, the actual yield depends on both the temperature and rate of heating. Therefore, the char depth test char yields were reasonable.

Char Depth Analysis

The char depth is the maximum depth of the char as compared to the original thickness of the sample. The end of test surface temperature reflects the surface

conditions at the targeted time and provides a point of comparison to the ignition test data.

As expected, the char depth was greater for the longer duration tests. It should be noted that the entire sample does not decompose to char down to the char depth. If the sample dimensions were sufficiently large to approximate an infinite plane slab, then the char depth would be expected to be nearly uniform. But for the 0.1 x 0.1 m square samples tested in the cone calorimeter, charring was more prevalent near the center of the sample with less near the edges, primarily due to lower temperatures from heat losses out the sample sides. Since the sample center provides the closest approximation to the infinite slab, the use of the maximum char depth, occurring at the sample center, is appropriate.

The char depth for the 3300 and 3900-second tests were the same. Post-test observations of the two samples revealed similar amounts of decomposition. The primary difference being the 65-minute sample had three moderate sized cracks while the 3300-second sample had one moderate and one large crack. Within the larger crack, the availability of more air likely allowed self-heating to progress further in the shorter time. An examination of the time-temperature history, figure F-1, shows higher surface temperatures for the 3300-second specimen than for the 3900-second sample. Given that the time to self-heating as the dominant mechanism for the instrumented 9 kW/m^2 tests occurred between 2550 and 2650 seconds, it is within reason that significant self-heating initiated sooner resulting in deeper char depth penetration in the shorter time frame.

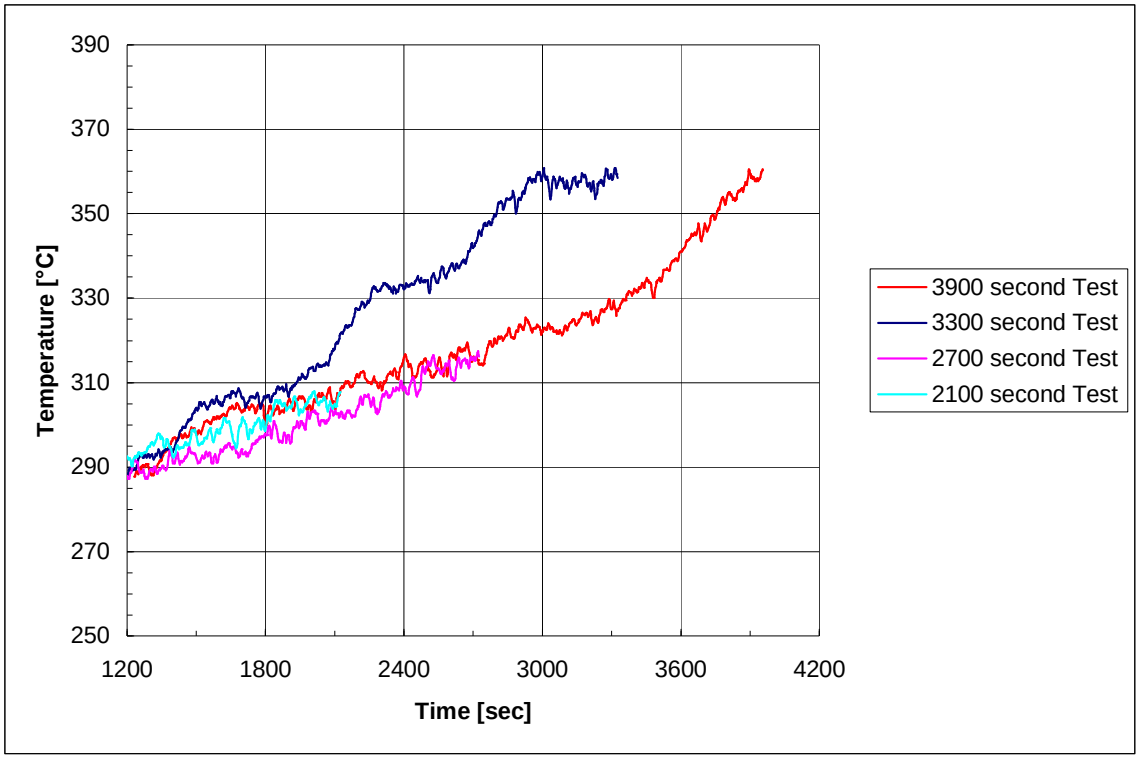

Figure F-1 – Char depth testing surface temperatures, timed exposure at 9 kW/m^2 heat flux

While thermocouples were not installed in the char depth test samples, a comparison can be made with temperature data from the three instrumented ignition tests at the same heat flux. A sense of the char front temperature may be determined by looking at the temperature profile of the ignition tests at the times of the char depth tests. The char front temperature is derived from interpolation between recorded depth temperatures. Figures F-2 through F-4 overlay the interpolated char front temperatures and char test surface temperatures on the ignition test time-temperature profiles.

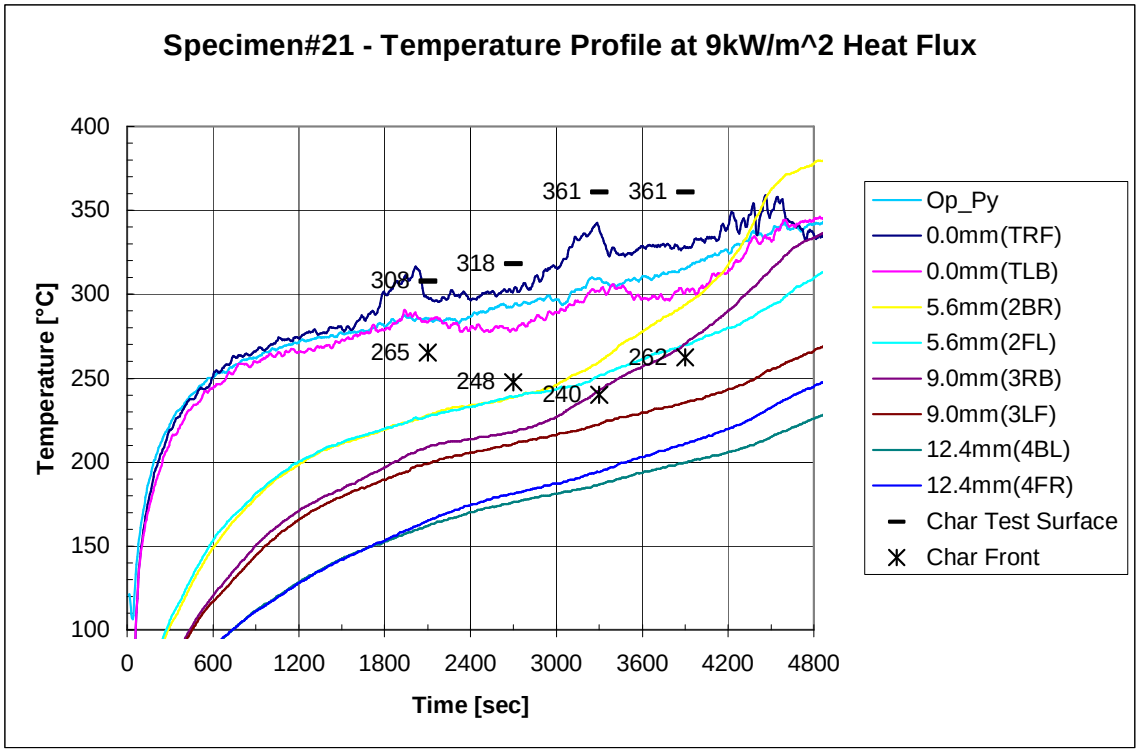

Figure F-2 – Char test surface temperatures and derived char front temperatures compared to the time-temperature profile for ignition test specimen#21, at 9 kW/m^2 heat flux.

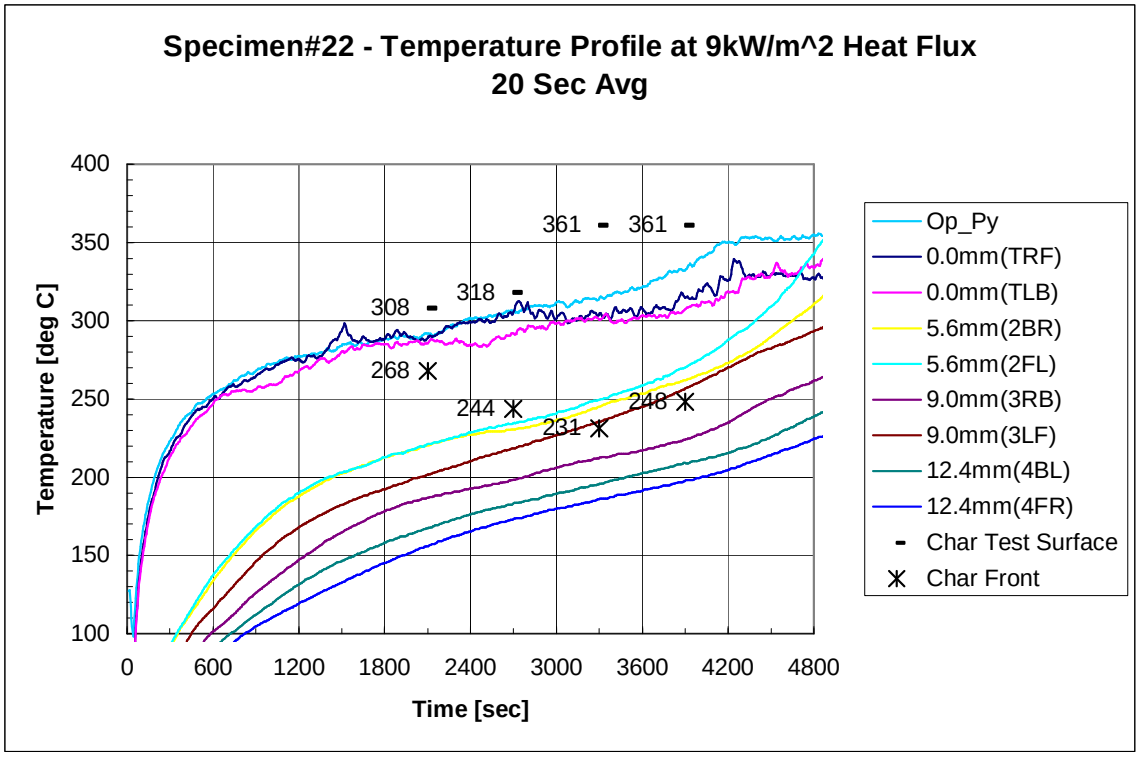

Figure F-3 – Char test surface temperatures and derived char front temperatures compared to the time-temperature profile for ignition test specimen#22, at 9 kW/m^2 heat flux.

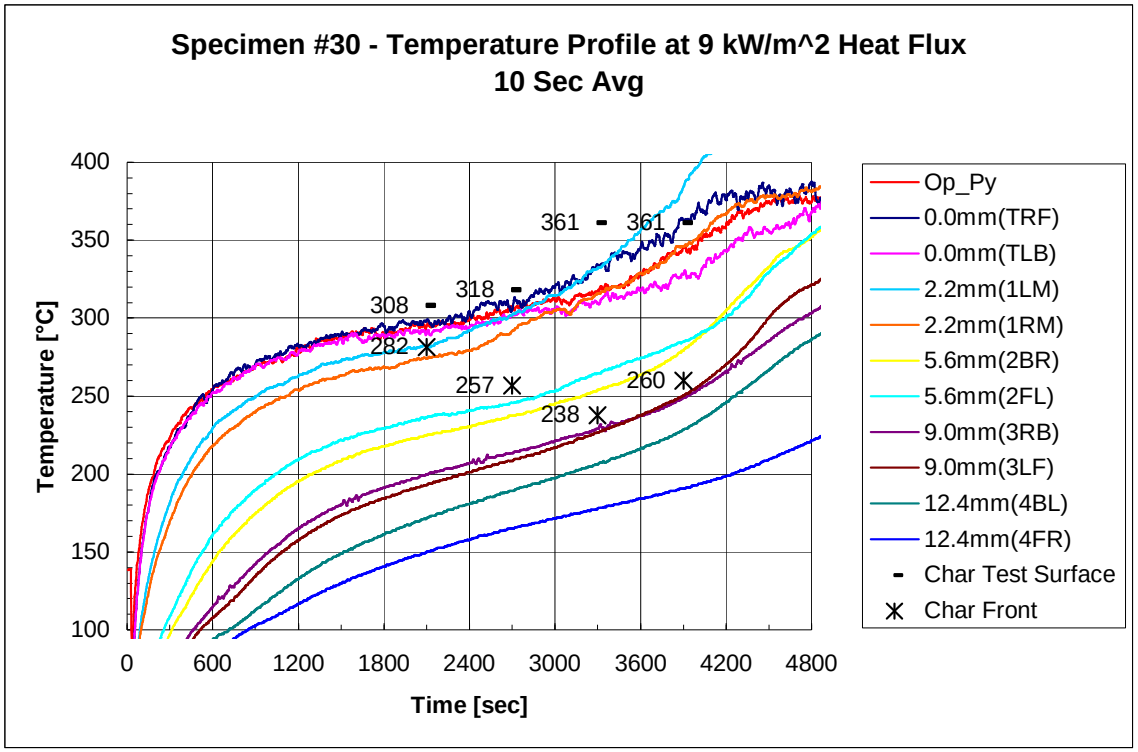

Figure F-4 – Char test surface temperatures and derived char front temperatures compared to the time-temperature profile for ignition test specimen#30, at 9 kW/m^2 heat flux.

If the char depth tests are any indication of the behavior observed in the ignition tests, it can be seen in the above figures that the rate of change of the temperatures recorded at depth increased around the time the derived char front passed. Thus the increased thermal behavior at depth at these times is attributable to the char front.

Between the three ignition tests, the derived char front temperatures compare favorably. The surface temperatures for all the char depth tests were hotter than for the ignition tests. As such, the actual char front temperatures may have been lower than the derived temperatures. The comparisons are shown in table F-2.

Table F-2 – Comparison of derived char front temperatures for the 9 kW/m^2 ignition tests.

Char Test Duration [sec]:	2100	2700	3300	3900
Char Test Surface Temperature [°C]:	308	318	361	361
Ignition Test Surface Temperature [°C]:				
Specimen #21	289	292	316	315
Specimen #22	289	301	306	318
Specimen #30	294	305	320	345
Char Front Depth [% (mm)]:	9.5 (1.7)	25.9 (4.7)	44.1 (7.9)	44.1 (7.9)
Derived Char Front Temperature [°C]:				
Specimen #21	265	248	240	262
Specimen #22	268	244	231	248
Specimen #30	282	257	238	260

Long Duration Sub-Critical Heat Flux Char Formation

Additional char depth measurements were made from long duration sub-critical ignition tests, specimens#31, #23 and #24 (6 and 7 kW/m^2). Table F-3 presents the results.

Table F-3 – Long duration (8 hour) sub-critical char depth data

Specimen# (Incident HF)	Char Depth [% (mm)]	Char Depth Temperature Range [°C]	Maximum Surface Temperature [°C]
#31 (6 kW/m^2)	23.9 (4.3)	199*	237
#23 (7 kW/m^2)	52.6 (9.5)	200-218	267
#24 (7 kW/m^2)	38.0 (6.8)	201-216	270

*Temperature interpolated between surface and 5.6 mm layer data.

The difference in char depth between the two 7 kW/m^2 samples was due to a deeper conical shaped char formation for specimen #23 versus a shallower bowl shaped char formation for specimen #24. This char pattern was consistent with fewer, but deeper cracks in specimen #23 and more, but shallower cracks in specimen #24. No reason for the difference in cracks and thus char formations can be found beyond the natural differences between two pieces of wood.

The above long duration sub-critical cone calorimeter data relates the local temperatures to that of the char front at various depths. From this limited data, the char front was estimated to form at depths passing between 200 and 220 °C. These temperatures were significantly less than those observed in the super-critical test data. For a super-critical heat flux, the thermal decomposition of the specimen continues till insufficient reactants remain exposed to the super-critical heat flux. For the sub-critical case, the charring continues till the temperature at depth is insufficient for the Arrhenius-type reaction to occur.

REFERENCES

[1] Ohlemiller, T.J., "Smoldering Combustion," In The SFPE Handbook of Fire Protection Engineering, 2nd Ed., National Fire Protection Association, Quincy, MA, 1995.

[2] Drysdale, D., An Introduction to Fire Dynamics, Second Edition, John Wiley & Sons, Chichester, England, 1998.

APPENDIX G – CALIBRATION TESTS

Prior to smolder testing, a series of scoping tests were run utilizing both the optical pyrometer and thermocouples mounted to the sample surface. These tests served two purposes. First, they allowed for comparison of optical pyrometer temperature data with thermocouple data. Second, they showed the variability of the heating of the wood surface with position and between samples.

Optical Pyrometer to Thermocouple Calibration

The optical pyrometer was calibrated to a thermocouple butt-welded to a steel plate sprayed with an optical black coating (0.96 emissivity) produced by Medtherm Corporation, Huntsville, Alabama. Optical pyrometer temperature measurements were within 2 °C of the thermocouple at tested elevated temperatures up to 400 °C during periods of changes in surface temperatures up to 10 degrees per minute. During periods of significant temperature changes, 10 degrees per minute or greater, the difference was as much as 10 °C, but differences around 5 °C were more typical. Because of the extended time periods associated with low heat flux ignition testing, the differences between optical pyrometer and thermocouple performance were not considered significant.

Surface Heating Uniformity

Surface temperature uniformity tests were performed using four thermocouples mounted to the surface of a maple plywood specimen and the optical pyrometer. Three tests, utilizing the specimen preparation shown in Appendix A were subjected to a 15 kW/m^2 incident heat flux in the cone calorimeter. The beads of the four thermocouples were attached to the surface of the sample at the corners of the central 5 x 5 cm area.

Thermocouple temperatures were compared during the relatively steady-state period after initial slab heating and before bonding of the wire with the surface was compromised due to degradation and regression of the surface resulting in a release of a thermocouple from the surface. Table G-1 shows the average temperatures from the four thermocouples and the optical pyrometer over this time period for each of the three tests. Full time-temperature curves of the three tests are shown in Figures G-1 through G-3.

Table G-1 – Average surface temperatures [°C] during surface uniformity tests

Test (time period – minutes)	Front Left	Back Left	Back Right	Front Right	TC Avgerage*	Optical Pyrometer
#8 (5-18.5)	352	363	405*	364	360	359
#12 (5-14.5)	359	360	387	351	364	364
#13 (5-13.7)	357	324	296*	380	354	354

*Specific thermocouple values not included in average. All temperatures in °C.

While individual thermocouples do not necessarily match each other, across the surface the average temperatures match those of the optical pyrometer. This is reasonable as thermocouples are point source measurements while the optical pyrometer is an area-based measurement. This also shows that averages of multiple thermocouples may be used to interpret conditions beyond the immediate vicinity of individual thermocouples. The outlier temperature for the back right of specimen #8 is due to the cone-heating element not being level. Subsequent tests were performed after leveling the element. For specimen #13, the thermocouple wire was inadequately bonded to the surface, resulting in a release of the back right thermocouple within three minutes of exposure to the heat flux.

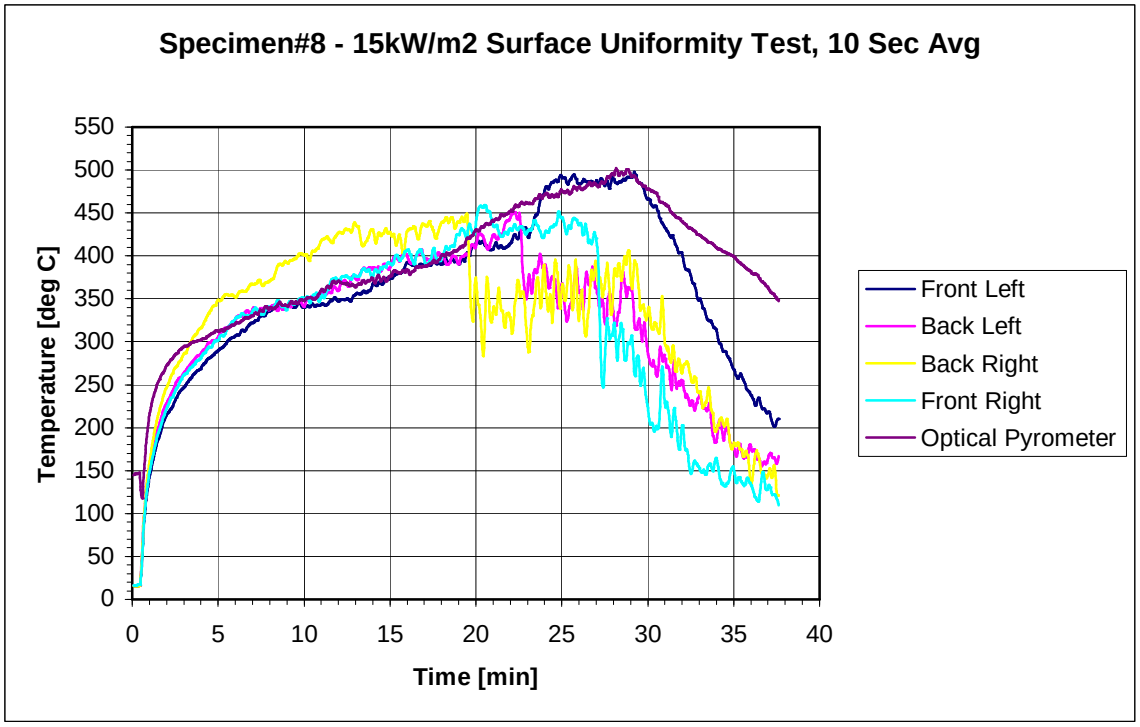

Figure G-1 – Time-Temperature plot of 15 kW/m^2 surface uniformity test, Specimen #8.

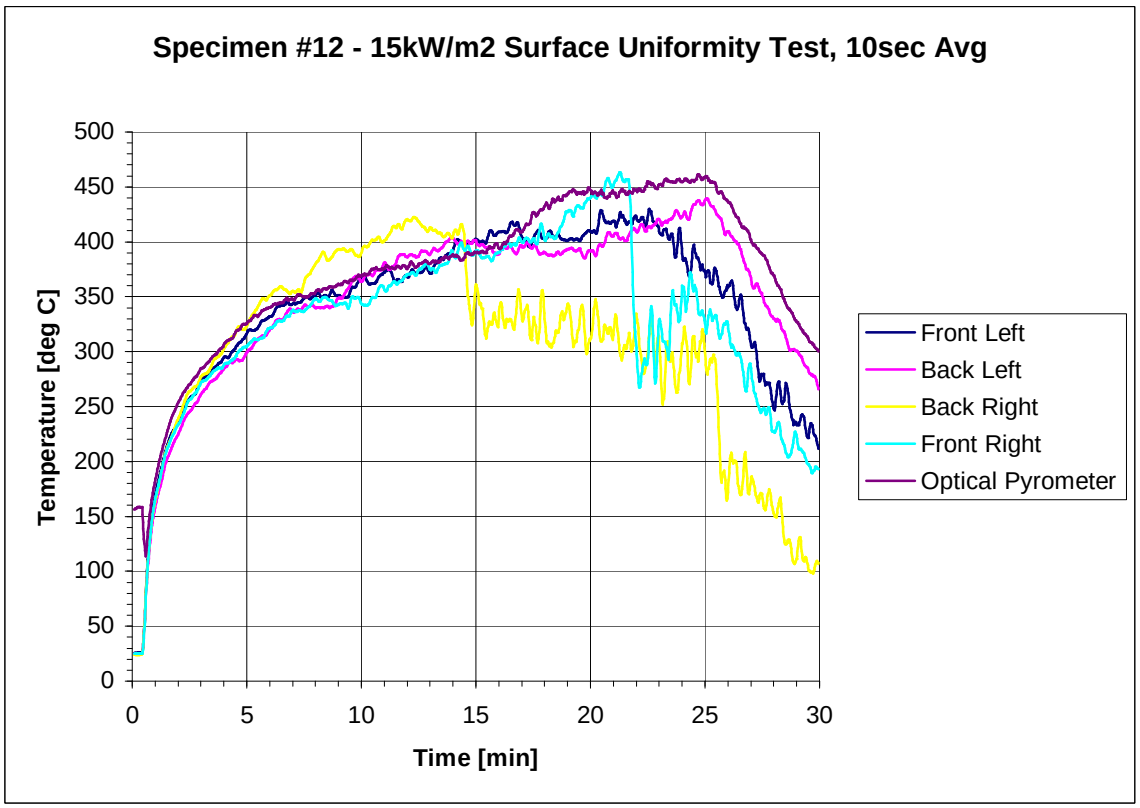

Figure G-2 – Time-Temperature plot of 15 kW/m^2 surface uniformity test, Specimen #12.

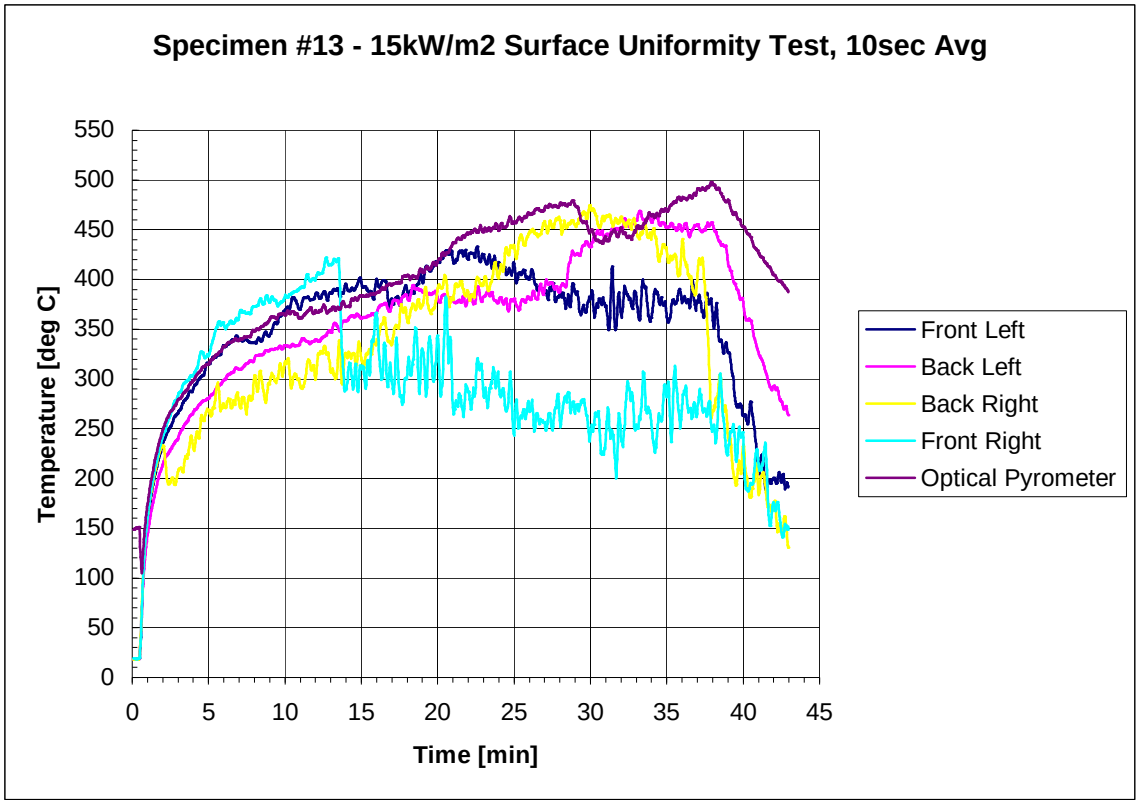

Figure G-3 – Time-Temperature plot of 15 kW/m^2 surface uniformity test, Specimen #13.

APPENDIX H – COMPUTER MODELING WITH HEATING

Heat Engineering And Transfer In Nine Geometries (HEATING) 7 [1] is a multidimensional finite difference heat conduction analysis code system distributed by the Radiation Safety Information Computational Center of the Oak Ridge National Laboratory. Version 7.3beta is run on a Pentium 4 platform with a Windows XP operating system. Among other capabilities, HEATING can solve three dimensional conduction problems involving multiple materials with both time and temperature dependent properties. Temperature dependent heat generation rates are modeled as well as temperature and position dependent surface-to-environment natural and forced convection, prescribed heat flux, and radiation exchange. Both steady state and transient problems are solved.

Significant input parameters include the dimensions of the materials to be modeled along with the potentially non-uniform grid mesh size, material thermal properties (density, thermal conductivity and specific heat), incident heat flux and temperature dependent radiative and convective cooling parameters for the top, sides and bottom surfaces.

Model Inputs

A modified layout of the sample configuration used in the cone calorimeter is modeled. The physical dimensions of the wood sample as well as the ceramic fiber blanket and base of the steel holder are modeled. The holder sides are not modeled due to platform related computation time limitations. Database thermal properties for carbon steel, type 1020, are used. Thermal properties for the ceramic fiber blanket are used as supplied by the manufacturer with temperature dependent conductivity and specific heat.

Thermal properties for virgin maple are a best fit between experimentally derived and literature data. Measuring the dimensions and weight of samples yielded a calculated density of 520 kg/m^3 with lower and upper bounds of 510 and 550 kg/m^3. Wood conductivity was determined from sub-critical cone tests to steady state utilizing the temperature profiles across both the wood and ceramic fiber blanket. Wood specific heat is the values from Lee as reported by Atreya [2]. Atreya also provided temperature dependency data for the above thermal properties. Up to the temperature at which the wood begins decomposition to char, this temperature dependency is modeled.

While char formation is not strictly a function of temperature, model limitations make this a reasonable approximation. From sub-critical char depth testing, 200 °C is an appropriate transition initiation temperature. The temperature at which the transition to char is complete is unclear. Since it is wood transformed to char that smolders, the temperature at which the transition completes is important. However, it may not be necessary for the wood to char in its entirety for initiation of smolder within char. Experimental data shows the temperature inflection, a sign of smolder initiation, varies with both incident heat flux and depth. The inflection points generally occur at lower temperatures with depth and lower heat fluxes. They range from a low around 250, seen in the second and third layers of specimen at 9 kW/m^2, to over 400 °C, seen on the surface at 15 kW/m^2. Therefore, completion temperatures of 300 and 400 °C are modeled to investigate the sensitivity of this uncertainty. The difference in char transition completion temperatures affects the thermal properties as well as heat generation rates with higher properties and rates at the higher of the completion temperatures. As will be seen below, the result is competing mechanisms between the

effects of decreased insulation and the increase in heat generation rates. Above these temperatures, thermal properties data for char are used as reported by Atreya [2]. Lacking better data, a linear transition between wood and char properties is modeled.

An important effect of the formation of char is the blackening of the sample surface. The result is an increase in sample emissivity. Babrauskas [3] suggests the emissivity of wood ranges from 0.76 for virgin wood to near unity for char. Therefore, the modeled emissivity varies from 0.76 below 100 °C to 0.96 at 250 °C and above.

Heat generation within the wood is modeled as an Arrhenius-type temperature dependent function based on kinetic data from one of several sources. Figure H-1 shows the heat generation rates for sawdust data from Bowes [4], Chong [5] and modified Bowes values.

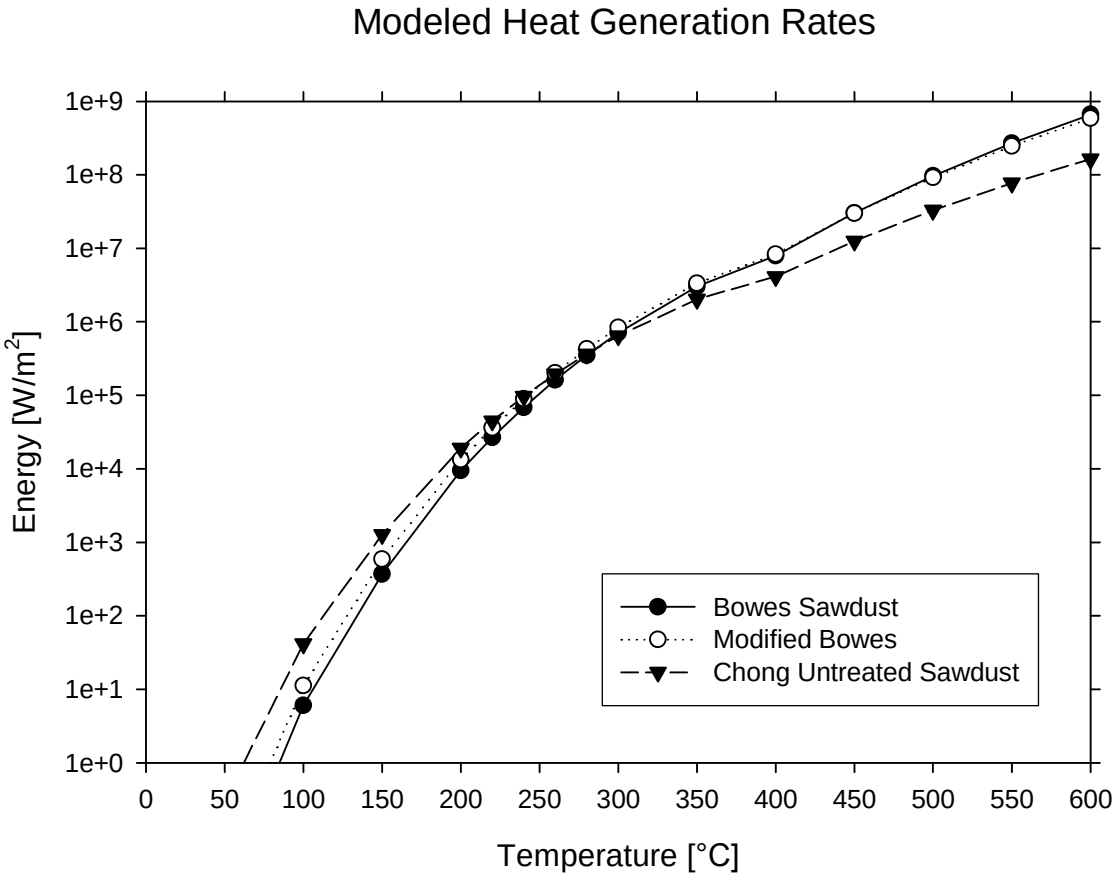

Figure H-1 – Modeled heat generation rates

Table H-1 summarizes the activation energy, E, and the theoretical heat release per unit mass, QA. The Bowes and Chong sets are reported values [4,5]. The activation energy for the modified Bowes set is an average between the reported value for sawdust and a general value for oxidative self-heating of carbonaceous materials. The modified Bowes QA is simply an average between the values of Bowes and Chong for sawdust. Note that despite the large differences in reported values, the heat generation rates are quite similar.

Table H-1 – Kinetics data

Source	E [J/kg-mol]	QA [J/kg-s]
Bowes sawdust [1]	1.08×10^{8}	1.54×10^{13}
Modified Bowes	1.04×10^{8}	7.86×10^{12}
Chong untreated sawdust [20]	0.90×10^{8}	3.19×10^{11}

Along with the prescribed incident heat flux, boundary conditions include a radiative heat transfer coefficient to the environment and convective cooling from the top, sides and bottom surfaces. The top surface is modeled using the correlations for cooling of a horizontal plate with the hot face up [6]. It is the same as that used for the Bowes theoretical modeling. Likewise, appropriate correlations from the same source are used for the bottom and sides of the holder. Note that even though the actual sides of the holder are not physically modeled, the radiative properties of steel are modeled.

The above three sets of kinetics data comprise the primary sets run through a suite of tests at different incident heat fluxes and compared to experimental results. The suite includes the steady state temperature profile at depths and locations consistent with experimental tests at 6 kW/m^2, determination of critical heat flux and transient runs at 9 and 15 kW/m^2 for times to elevated temperatures as a gauge of thermal runaway.

Results

Because the model does not handle cracking, shrinkage and mass loss due to pyrolysis, there is no built in mechanism to prevent heat generation beyond the limits of a physical specimen. The result is thermal runaway yielding temperatures in excess of 1000 °C. The highest incident heat flux that results in a steady-state solution is considered the critical heat flux. For heat fluxes above critical, transient simulations are run to determine the time at which thermal runaway occurs.

Table H-2 is a comparison of temperature data at depth for a 6 kW/m^2 incident heat flux for both simulations and experimental data. While the steady state solution technique (point-successive-overrelaxation iteration) provides good agreement with the steady state temperatures of the transient simulations for the upper layers, the transient

simulations yield better agreement with experimental data. It is unclear why the simulations yield surface temperatures 15 °C lower than those recorded from the experimental test. Possibly, the heat losses from the surface are over predicted in the simulations. But this should also result in cooler sub-surface temperatures, which it doesn't. Another possibility is that the cracking of the sample surface, while minor, provides a radiation feedback mechanism within the surface crack resulting in elevated surface temperatures. This hypothesis was not investigated further.

Table H-2 – Temperature profiles for sub-critical 6 kW/m^2 tests

	Surface	First Layer	Second Layer	Third Layer	Fourth Layer	Fifth Layer	Bottom Surface	Back of Holder
Experimental Specimen #31	235	-	187	170	152	-	120	61
Bowes SS	219	201	185	162	140	123	109	51
Bowes Transient SS	219	203	187	165	143	127	114	58
Chong SS	221	205	188	166	142	125	111	50
Chong Transient SS	223	207	191	169	147	130	117	59
Modified Bowes SS	220	202	186	163	140	123	109	50
Modified Bowes Transient SS	221	204	188	167	145	128	115	58
"-" No data available								

Table H-3 shows the critical incident heat flux predicted by Bowes theory as well as that required for thermal runaway for the three sets of kinetics simulated. For the simulations, the critical flux is taken as the highest incident heat flux for which thermal runaway does not occur. The critical flux from the simulations for transition to char complete by 400 °C compare favorably to Bowes theory with Chongs' kinetics data showing the least favorable agreement at 0.8 kW/m^2 higher than predicted. For transition to char complete by 300 °C, the critical heat flux is between 1.0 and 1.3 kW/m^2 higher than theoretical predictions.

Table H-3 – Critical incident heat flux

Calculation method (wood to char transition temperatures [°C])	Critical incident heat flux [kW/m^2]
Bowes Theory – Sawdust (N/A)	6.8
Bowes Theory – Modified Bowes (N/A)	6.4
Bowes Theory – Chong Untreated Sawdust (N/A)	6.0
Bowes SS (200-300)	7.8
Modified Bowes SS (200-300)	7.4
Chong SS (200-300)	7.3
Bowes SS (200-400)	7.2
Modified Bowes SS (200-400)	6.9
Chong SS (200-400)	6.8

Table H-4 compares the time to reach 300, 350 and 400 °C for both experimental and simulation results at 15 kW/m^2. The times to these temperatures give an indication of the progression of thermal runaway with 400 °C considered initiation of smolder. Two observations are apparent in the data. First, the simulations reach elevated temperatures significantly sooner than experimental specimen. Second, the time between 350 and 400 °C is relatively short, between thirty seconds and one minute, indicating thermal runaway and thus initiation of smolder. Experimental results are not so predictable. Examination of surface and optical pyrometer temperature data for the two cone tests shows inflection temperatures between 390 and 450 °C. So while both simulation and experimental data support initiation of thermal runaway before 400 °C, the times to these temperatures are significantly different.

Table H-4 – Times to elevated temperatures at 15 kW/m^2

Time to surface temperature at 15 kW/m^2:	300 °C [min]	350 °C [min]	400 °C [min]
Specimen #14	4.4	7.1	14.6
Specimen #28	4.9	8.0	17.4
Bowes Transient(300)	1.5	3.1	3.6
Mod. Bowes Transient(300)	1.4	3.0	3.4
Chong Transient(300)	1.4	3.5	4.5
Bowes Transient(400)	1.5	2.8	3.1
Mod. Bowes Transient(400)	1.5	2.6	3.0
Chong Transient(400)	1.5	3.0	3.9

Comparing the differences in times to elevated temperatures between char completion temperature cases shows that while the 300 °C completion cases reach 300 °C at the same time or sooner than the 400 °C completion cases, they reach 350 and 400 °C later. By 300 °C, an increase in surface temperature due to the higher heat generation rates for the higher completion cases are already overtaking the higher surface temperature due to the higher surface insulation of the char in the lower completion case. When the surface temperature reaches 300 °C, the temperature in the first layer is 167 °C for the lower completion cases and 170 °C for the higher completion cases. Since heat generation is not significant below 200 °C, this indicates the reaction takes place entirely at the surface.

Table H-5 compares the time to reach 300, 325 and 350 °C for both experimental and simulation results at 9 kW/m^2. As expected, the times to elevated temperatures are longer for 9 kW/m^2 than for 15 kW/m^2. Like the 15 kW/m^2 results, the simulations yield poor agreement with experimental results with the simulations reaching temperatures significantly sooner than for cone calorimeter tests. At 9 kW/m^2, both second layer temperatures for specimen #21 and first layer temperatures for specimen #30 reached 350 °C earlier than surface measurements, indicating sub-surface self-heating overtaking surface heating. Similar results were seen in the simulations where first layer temperatures reached 350 °C around the same time as the surface or a little sooner. While the 15 kW/m^2 simulations showed a marked increase in rate of temperature change between 350 and 400 °C, the 9 kW/m^2 simulations marked increase in rate of temperature change occurs between 325 and 350 °C. For all simulations, the higher char completion cases yielded earlier times to elevated temperature. By 300 °C, the heat generation rate already dominates thermal properties and thus the 400 °C completion cases reach 300 °C

first. Also, when the surface reaches 300 °C, the first layer temperatures are 289 and 281 °C for lower and higher completion cases, respectively. The higher completion case first layer temperature is lower due to the surface reaching 300 °C sooner. At this time in the lower completion cases, the first layer temperature is 26 °C lower than the surface as opposed to 19 °C in the higher completion cases.

Table H-5 – Times to elevated temperatures at 9 kW/m^2

Time to surface temperature at 9 kW/m^2:	300 °C [min]	325 °C [min]	350 °C [min]
Specimen #21	52	69	86/ 74 (L2)
Specimen #22	40	61	69
Specimen #30	40	58	67/ 59 (L1)
Bowes Transient(300)	26.2	28.2	28.3
Mod. Bowes Transient(300)	22.1	23.5	23.6
Chong Transient(300)	23.9	26.6	26.9
Bowes Transient(400)	18.5	19.4	19.6
Mod. Bowes Transient(400)	16.2	16.9	17.1
Chong Transient(400)	17.3	18.6	18.9

In summary, simulation results compare favorably to experimental data for sub-critical incident heat flux temperature profiles, excepting surface temperatures. Simulation results also compare favorably to theoretical predictions of critical incident heat fluxes. At the lower heat flux, 9 kW/m^2, the simulations qualitatively match experimental data in showing sub-surface temperatures exceeding surface temperatures during thermal runaway, indicating smolder initiates below the surface. As expected, thermal runaway initiates at the surface at higher heat fluxes. One area the simulations do not compare favorably with experimental results is for times to elevated temperatures as an indication of smolder initiation for super-critical incident heat fluxes. The simulation times are significantly shorter than observed in experimental data.

REFERENCES

[1] Childs, K.W., "HEATING 7: Multidimensional, Finite-Difference Heat Conduction Analysis Code System, Versions 7.2i and 7.3," RSICC Report PSR-199, Oak Ridge National Laboratory, Oak Ridge, Tennessee, 1998.

[2] Atreya, A., "Pyrolysis, Ignition and Fire Spread on Horizontal Surfaces of Wood," (PhD Dissertation), Harvard University, Cambridge, MA, 1983.

[3] Babrauskas, V., Ignition Handbook, Fire Science Publishers, Issaquah, WA, 2003.

[4] Bowes, P.C., Self-heating: Evaluating and Controlling the Hazard, Her Majesty's Stationery Office, London, 1984.

[5] Chong, L.V., Shaw, I.R, and Chen, X.D., "Thermal Ignition Kinetics of Wood Sawdust Measured by a Newly Devised Experimental Technique," Process Safety Progress, Vol. 14, No. 4, 1995.

[6] Atreya, A, "Convection Heat Transfer," In The SFPE Handbook of Fire Protection Engineering, 3rd Ed., National Fire Protection Association, Quincy, MA, 2002.